UNIVERSIDADE FEDERAL DO PARANÁ

GUIDO EZEQUIEL ALONSO

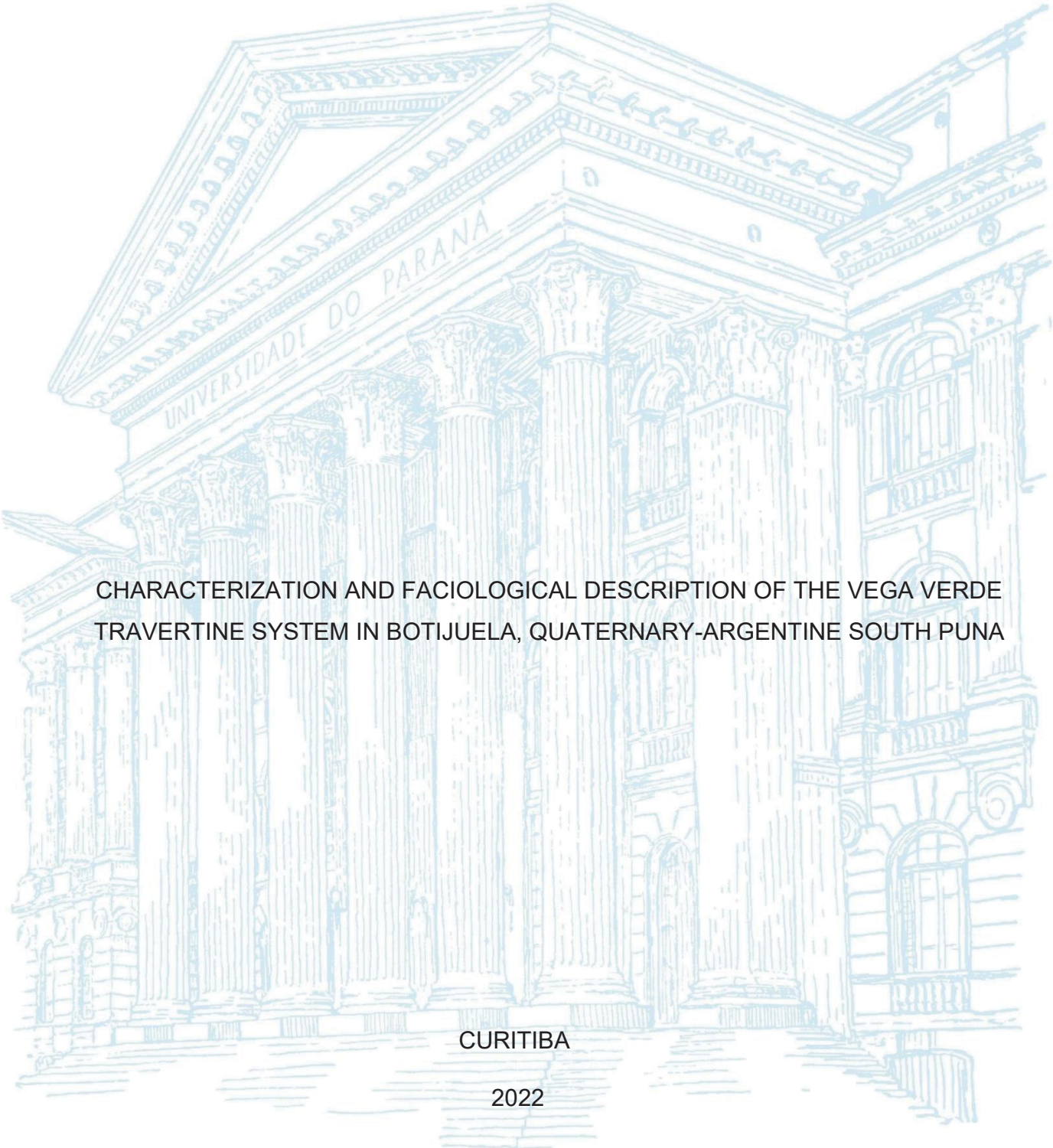

CHARACTERIZATION AND FACIOLOGICAL DESCRIPTION OF THE VEGA VERDE TRAVERTINE SYSTEM IN BOTIJUELA, QUATERNARY-ARGENTINE SOUTH PUNA

CURITIBA

2022

GUIDO EZEQUIEL ALONSO

CHARACTERIZATION AND FACIOLOGICAL DESCRIPTION OF THE VEGA VERDE TRAVERTINE SYSTEM IN BOTIJUELA, QUATERNARY-ARGENTINE SOUTH PUNA.

Dissertação apresentada ao curso de Pós-Graduação em Geologia, Setor de Ciências da Terra, Universidade Federal do Paraná, como requisito parcial à obtenção do título de Mestre em Geologia.

Orientador: Prof. Leonardo Fadel Cury

CURITIBA

2022

FICHA CATALOGRAFICA

DADOS INTERNACIONAIS DE CATALOGAÇÃO NA PUBLICAÇÃO (CIP) UNIVERSIDADE FEDERAL DO PARANÁ
SISTEMA DE BIBLIOTECAS – BIBLIOTECA CIÊNCIA E TECNOLOGIA

Ezequiel Alonso, Guido
Characterization and faciological description of the Vega Verde travertine system in botijuela, Quaternary-Argentine South Puna. / Guido Ezequiel Alonso. – Curitiba, 2022. 1 recurso on-line : PDF.
Dissertação (Mestrado) – Universidade Federal do Paraná, Setor de Ciências da Terra, Programa de Pós-Graduação em Geologia. Orientador: Prof. Dr. Leonardo Fadel Cury.
1. Geologia. 2. Águas. 3. Fatores. 4. Hidrocarbonetos. I. Cury, Leonardo Fadel. II. Universidade Federal do Paraná. Programa de PósGraduação em Geologia. III. Título.

Bibliotecário: Nilson Carlos Vieira Junior CRB-9/1797

MINISTÉRIO DA EDUCAÇÃO
SETOR DE CIENCIAS DA TERRA
UNIVERSIDADE FEDERAL DO PARANÁ
PRÓ-REITORIA DE PESQUISA E PÓS-GRADUAÇÃO
PROGRAMA DE PÓS-GRADUAÇÃO GEOLOGIA
40001016028P5

TERMO DE APROVAÇÃO

Os membros da Banca Examinadora designada pelo Colegiado do Programa de Pós-Graduação GEOLOGIA da Universidade Federal do Paraná foram convocados para realizar a arguição da Dissertação de Mestrado de **GUIDO EZEQUIEL ALONSO** intitulada: **CHARACTERIZATION AND FACIOLOGICAL DESCRIPTION OF THE VEGA VERDE TRAVERTINE SYSTEM IN BOTIJUELA, QUATERNARY-ARGENTINE SOUTH PUNA**, sob orientação do Prof. Dr. LEONARDO FADEL CURY, que após

terem inquirido o aluno e realizada a avaliação do trabalho, são de parecer pela sua APROVAÇÃO no rito de defesa.

A outorga do título de mestre está sujeita à homologação pelo colegiado, ao atendimento de todas as indicações e correções solicitadas pela banca e ao pleno atendimento das demandas regimentais do Programa de Pós-Graduação.

CURITIBA, 04 de Abril de 2022.

Assinatura Eletrônica
18/04/2022 20:01:09.0
LEONARDO FADEL CURY
Presidente da Banca Examinadora

Assinatura Eletrônica
18/04/2022 14:15:16.0
FILIPE GIOVANINI VAREJÃO
Avaliador Externo (32007019)

Assinatura Eletrônica
18/04/2022 13:05:13.0
ANELIZE MANUELA BAHNIUK RUMBELSPERGER
Avaliador Interno (UNIVERSIDADE FEDERAL DO PARANÁ)

DEPARTAMENTO DE GEOLOGIA-CENTRO POLITÉCNICO-UFPR - CURITIBA - Paraná - Brasil
CEP 81531-990 - Tel: (41) 3361-3365 - E-mail:
posgeol@ufpr.br

ACKNOWLEDGEMENTS

To my dad and mom.

I would like to thank my family, my siblings Guillermo, Sol and Pablo for having supported me unconditionally in my decision to move to Brazil to pursue my postgraduate studies at UFPR. To my sisters-in-law Julieta and Griselda as well as my nieces and nephews Joaquin, Amparo and Eva who showed me much affection from a distance and in the difficult stage of doing this in a context of pandemic. To my aunts Teresa and Nora who also collaborated and supported me enormously, as well as my cousins Lucas and Luis who helped me a lot.

To my friends who in a context of pandemic with social isolation gave me a lot of support: Gabriel, Lucia, Ramiro, Andres, Ayelen. Also to Ramiro, Mario, José, Santiago, Mauro M., Valen, Guille, Marcos, Martin, Mauro, Ezequiel, Julian who shared virtual playful moments with me.

To the people at Rilara Hostel who really treated me like family when I arrived here in Curitiba: Matheus, Renata, Andrea and David.

To Dr. Tatiana Stepanenko who supported me throughout this first stage in Brazil, as well as in the realization, revision and writing of this work.

To Dr. Patricio Guillermo Villafañe as well as Dr. Maria Eugenia Farias from PROIMI who put me in contact with the iLAMIR laboratory team.

To my thesis advisor Dr. Leonardo Fadel Cury who shared his knowledge and trusted me to carry out this research in the Puna as well as welcomed me here in Brazil. Also to Dr. Filipe Varejao who taught me many things in the field as well as as help with the revisions of this work. To the geologists Dr. Gustavo Barbosa Athayde and Tereza Filipi, the tour guide Luis Ahumada who collaborated enormously with the field work as well as the local Simón who received us in the Puna. Also, to Dr. Anelize Bahniuk who reviewed and supported this thesis work.

To Dr. Almerio França who solved my doubts regarding the petrography of the system. Fellow project geologists of the Diagenesis project Carolina, Paulo, Larissa who collaborated and helped me in revisions throughout the development of this work.

To the iLamir lab team Rodrigo,Flavia, Inaiara, Ana, Guilherme, Fran, Diego, Keiji, Bruno who helped me enormously in management, sample processing and work.

I would also like to thank the diagenesis project (ANP 20129-3), funded by Shell and iLAMIR for the grant funds and support for this research. To the graduate program

in geology at UFPR for the opportunity to complete graduate school. To the Federative Republic of Brazil, which, as an Argentinean citizen, received me in an excellent manner.

RESUMO

Os travertinos são depósitos não marinhos de carbonato produzidos pela desgaseificação de águas hidrotermais e a influência de fatores bióticos. O interesse econômico e científico em carbonatos não marinhos vem crescendo nos últimos anos porque são considerados como reservatórios de hidrocarbonetos do Presalt do Brasil e de Angola. A expansão do conhecimento destes sistemas permite prever melhor as metas de exploração de potenciais reservatórios de petróleo. Esta pesquisa é a primeira a descrever o sistema de travertino Vega Verde - Botijuela, Argentina Puna do Sul. O sistema foi descrito utilizando abordagens multiescala: megascópico, mesoscópico e microscópico. Em conjunto com a análise mineralógica de abordagem multi-escala com difração de raios X, composição geoquímica de óxidos principais e íons traços com fluorescência de raios X e isótopos estáveis de C e O. Três zonas de deposição no sistema foram reconhecidas com base na distância da fonte, inclinação e características litológicas: proximal, intermediária e distal. A zona proximal é compreendida por um monte cônico bem desenvolvido e uma inclinação de ~15º com a presença de uma moderna crista de fissura com canais e lobbes. A zona intermediária é caracterizada pelo desenvolvimento de um talude com inclinação de 10-20º, placas e canais com piscinas preenchidas por depósitos de carbonato e sedimentos siliciclásticos. A zona distal apresenta uma inclinação de ~10º caracterizada pela presença de vegetação, e mistura de águas, planícies aluviais com desenvolvimento de canais. Mineralogicamente, os depósitos são compostos principalmente de calcita e calcita portadora de Mg. A análise isotópica revela um vasto enriquecimento de δ13C (1,97~10,84) e valores negativos δ12O (-0,67 - -8,91) que em conjunto com a análise Sr e Ba indicaram uma origem hidrotermal para as distintas fácies sedimentares. Na zona proximal, a área é diretamente influenciada pela fonte com um contendo de Fe_2O_3 elevado (~4,3%), Pb-As elevado (~0,5 a 1,7%), e outros metais tais como Zn(~139 ppm). Estas características geoquímicas ocorrem em associação com a presença da facies de geyserites com carbonatos ferruginosos, sílica globular, e calcita fibrosa. Os valores de sílica também mostraram uma concentração considerável na zona proximal (~2%). Na zona distal, as fácies com componentes detríticos dissolvidos em alta alcalinidade atingem valores de Si de ~5-6 % que poderiam estar relacionados a uma fase de Si amorfo. O empobrecimento desses componentes e o incremento do Si em todo o sistema é acompanhado pela crescente influência de processos sedimentares relacionados a depósitos siliciclásticos que aumentam gradualmente de proximal, passando de intermediário para distal na direção da bacia do Salar de Antofalla. Pesquisas futuras, juntamente com dados do reconhecimento Sr e REE, permitirão definir com precisão a origem da água e a influência dos processos orgânicos e inorgânicos no sistema.

Palavras-chave: travertinos. Botijuela. Geyserites. puna sul.

ABSTRACT

Travertines are non-marine carbonate deposits produced by degassing of hydrothermal waters and the influence of biotic factors. The economic and scientific interest in non-marine carbonates have been growing in recent years because they are considered as hydrocarbon reservoirs in the pre-salt plays of Brazil and Angola. Expanding knowledge of these systems allows predicting better exploration targets for potential oil plays. This research is the first research to describe the Vega Verde travertine system- Botijuela, Argentina South Puna. The system was described using multiscale approaches: megascopic, mesoscopic and microscopic. In conjunction with the multi-scale approach mineralogical analysis with X-Ray diffraction, geochemical composition of major oxides and traze ions with X-Ray fluorescence and stable isotopes of C and O. Three deposition zones in the system were recognized based on the distance from the spring, slope, and lithological features: proximal, intermediate, and distal. The proximal zone is comprehended by a well-developed conical mound and a slope of ~15º with the presence of a modern fissure ridge with channels, fans, and lobbes. The intermediate zone is characterized by the development of a slope with 10-20º inclination, sheets and channels with pools filled by carbonate and siliciclastic deposits. The distal zone presents an inclination of ~10º characterized by the presence of vegetation, and mixing of waters, alluvial plains with channels. Mineralogically the deposits are mainly composed of calcite and Mg-bearing calcite. Isotopic analysis reveals a vast enrichment of $\delta^{13}C$ (1.97~10.84) and negative $\delta^{12}O$ values (-0.67 - -8.91) that in conjunction with Sr and Ba analysis indicated a hydrothermal origin for the distinct sedimentary facies. In the proximal zone, the area is directly influenced by the spring by high Fe_2O_3 (~4.3 %), high Pb-As (~0.5 to 1.7%), and other metals such as Zn(~139 ppm). These geochemical characteristics occur in association with the presence of the geyserite facies with ferruginous carbonates, globular silica, and fibrous calcite. Silica values also showed a considerable concentration in the proximal zone (~2%). In the distal zone the facies with detrital components dissolved in high alkalinity reach Si values of ~5-6 % that could be related to an amorphous Si phase. The impoverishment of those components and the increment of Si throughout the system is accompanied by the increasing influence of sedimentary processes related to siliciclastic deposits that gradually increase from proximal, through intermediate to distal in the direction of the Salar de Antofalla basin. Future research together with data from Sr and REE reconnaissance will make it possible to accurately define the origin of the water and the influence of organic and inorganic processes in the system.

Keywords: travertine. Botijuela. geyserites. puna sul.

LIST OF FIGURES

LIST OF TABLES

SUMMARY

1. INITIAL CONSIDERATIONS

To study the etymology of the word “travertine” we have to go back to the past, since the times of the ancient Roman Empire. "Lapis travertinus", “tiburtinus” or “tivertino” were the first names assigned to these materials extracted from Tivoli in Rome. These rocks constituted a precious building material being extracted from quarries located throughout the ancient Roman peninsula and several others in China and Turkey (Pentecost, 2005). For its useful qualities and for economic interest numerous scientists, philosophers and authors have continued throughout history to study travertine. They did so in order to classify the system where these rocks form, to find the most accurate definition for its genesis, and also to know its main components. Actually, the interest of industry and academy in travertine and non-marine carbonates have been growing up because they are considered as hydrocarbon reservoir (Della Porta, 2015; Ronchi & Cruciani 2015, Virgona et al. 2013) in the pre-salt play of Brazil and Angola (Ronchi & Cruciani 2015; Janssens et al.,2020; Shiraishi et al., 2020).

Travertine and tufas are rocks that had many definitions throughout history, among them the one proposed by Emig, (1917); Bates & Jackson (1987); Ridding (1991); Koban & Schweigert (1993); Ford & Pedley (1996); Fouke et al. (2000); Glover & Robertson (2003); Pentecost (2005), Cappezuoli et al., (2014); Kano (2019). This continental carbonate rocks laterally transitions into tufa by water cooling to near ambient temperatures and gradually downward increase of biotic interaction (Ford & Pedley, 1996). The difference between those terms is problematic and could lead to confusion and several research papers were made in order to clarify both terms and find and straightway criteria and definition of them (Ford & Pedley, 1996; Capezzuoli et al. 2014, Kano et al. 2019). Modern authors describe that the biotic/abiotic genesis of travertine is related to the fact that these rocks create situations favorable to the proliferation of benthic microbial communities, a fact that can influence the genesis of a travertine and/or its final shape (Burne & Moore, 1987; Ridding, 2000; Jones & Renault, 2010; Rogerson et al., 2014; Kano et al. 2019, Shiraishi et al., 2020). Geomorphology, tectonics, source of water, sedimentology, geochemistry and influence of microorganisms were used as criteria to describe these open systems that are so sensitive to those factors. On the other hand, the proliferation of terms, types, and facies definitions specific to each travertine system studied by many authors brings with it some difficulties in establishing a common lexicon for all of them.

Modern definitions for travertine and tufas describe them as non-marine carbonates from spring water formed after the process of degassing in water with dissolved Ca^{2+} and CO_2 with biotic and non-biotic factors involved in their formation. Their geochemical classification is based on the origin of CO_2 and also in the origin and the depth at which the fluids circulated in the subsurface (Pentecost, 2005; Crossey et al., 2006; Teboul et al., 2016; Jones & Renault, 2010; Rogerson et al., 2014; Kano et al. 2019, Shiraishi et al., 2020).

1.1. MECHANISM OF PRECIPITATION

The main process involved in the formation of travertine is degassing. In order to understand the importance of this process, we must track the main source of the raw materials that build these rocks which are carried by hydrothermal water. At its

origin, this water has initial high Ca concentrations and high partial pressure of CO_2 (Kano, 2019). The sudden loss of CO_2 (degassing) upon discharge from the hot spring causes the pH to increase and subsequently the $CaCO_3$ precipitates following the mechanism below (1):

$$(1)\ Ca^{2+}_{(aq)} + 2\ HCO^{-}_{(aq)} \leftrightarrow CaCO_{3(s)} + CO_{2(g)} + H_2O_{(l)}$$

Applying the Le-Chatelier principle, a loss of CO_2 in the system will lead to higher consumption of reagents to increase product formation in order to achieve a new equilibrium position, which in this case is achieved by the production of more calcium carbonate. Carbonates are open systems where precipitation and diagenesis are mainly related to temperature, geochemical characteristics of the initial fluid, geological context and microbial communities involved in their development (Della Porta, 2017). Other mechanisms of calcium carbonate precipitation (Pentecost, 2005) through hydrothermal waters are described in (2) (3):

$$(3)\ Ca(OH)_2 + CO_2 \leftrightarrow CaCO_3 + H_2O$$

$$(4)\ Ca(HCO_3)_2 + OH^- \leftrightarrow CaCO_3 + HCO_3^- + H_2O$$

Meteogene and thermogene are two distinct terminologies to refer do travertine acording to the origin of the CO_2 carrier. tufa's are are those in which the carbon dioxide comes from meteoric sources (Capezuoli et al., 2014), while the thermogenic originates from thermal processes in the interior of the earth's crust.

1.2. PETROGRAPHIC COMPONENTS

Tucker (2001) divides the components into four groups: i) non-skeletal grains, ii) skeletal grains, iii) micrite, and iv) cement. The main components found in the studied site are named below. Coated grains is a term used for ooids, pisooids, and also oncoids (Tucker, 2001).

1.2.1. Non skeletal grains

1.2.1.1. Ooids

Ooids are rounded to subrounded particles smaller than 2mm that have concentric lamella that grows around a nucleus (Tucker, 2001). The term superficial ooids is applied to oodis that only have one lamella around their nucleus and composite ooids when many ooids are rounded by other lamellae (Tucker, 2001). Ooids can acquire various shapes beyond rounded or subrounded (Granier & Lapointe, 2022, 2021; Anderson et al., 2018), their shape constitutes an important paleoenvironmental record (Beaupré et al., 2015). The development of a systematic method for the study of the shape and evolution recorded in their plates was proposed by Sipos et al. (2018). Their mineral composition is mainly formed by tangential acicular aragonite and high-Mg calcite but also can be by low-Mg calcite (Tucker,2001), calcareum ooids are normal both in antique and modern sediments (Kimberley, 1983). Ooids coats

could also be ferruginous like the ones exposed in the research of (Dibella et al., 2019) or phosphatic. The origin of ooids is diverse diverse and the relation between pCO_2 and the reason Mg/Ca is important in order to build their mineralogy composition (Tucker, 2001). The exact mechanism of inorganic precipitation is not described yet and the nature of the formation of each individual ooid is still subject to some degree of uncertainty (Tucker, 2001; Flügel 2010).). However, in waters supersaturated with respect to $CaCO_3$ with agitation, sufficient temperature, and incipient degassing, carbonate crystals begin to precipitate around a nucleus (Tucker, 2001). Ooids record their growth in lamellae similarly to trees (Sipos et al., 2018) and these patterns occur by both chemical precipitation (Li & Goldenfeld, 2008) and physical abrasion (Domokos et al. 2014). The presence of mucilaginous layers may coat and permeabilize the ooids, also the organic matter may create a microenvironment where carbonate precipitation occurs (Tucker, 2001), lamellae growth mechanisms possibly biologically mediated given under conditions of $CaCO_3$ supersaturation are also considered (Folk & Lynch, 2001). Formation of ooids is involved at less with the following five requirements: i) presence of nucleus, ii) bottom agitation to move grains, iii) source of supersaturated water, iv) process of water renewal and v) minimal amount of grain degradational process (Flügel, 2010).

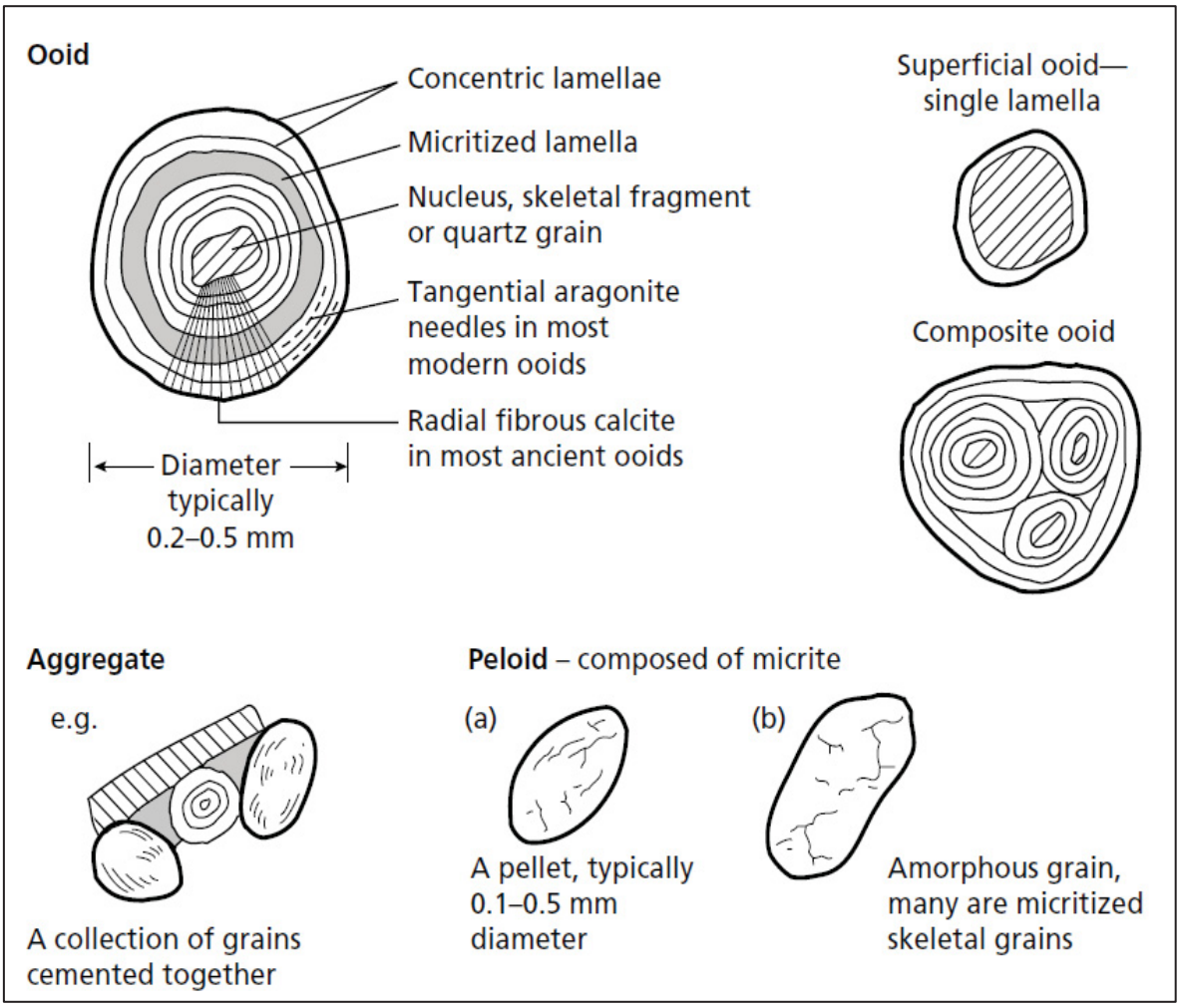

Figure 1.1. Non skeletal coated grains and peloids. From Tucker, (2001)

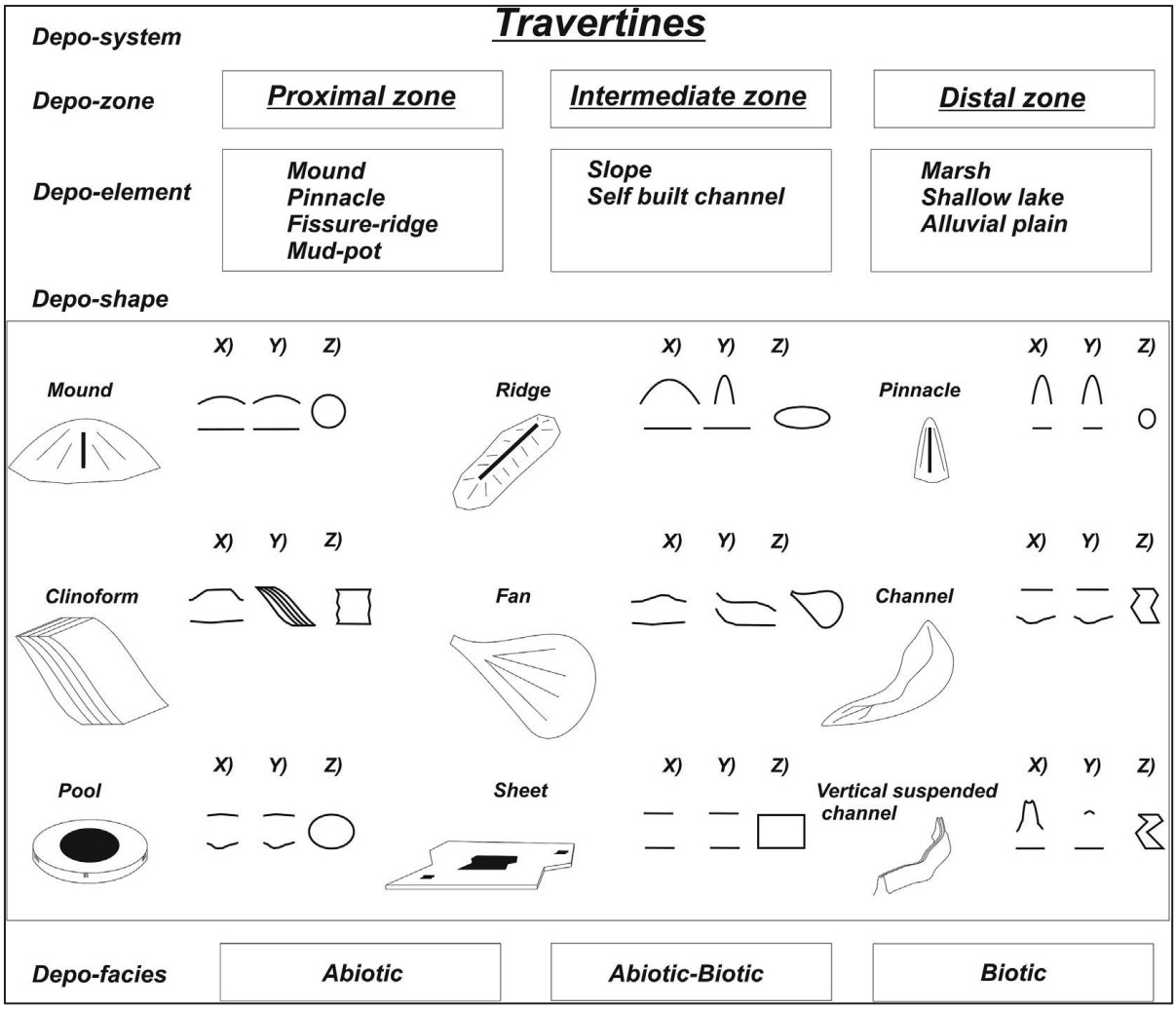

Figure 1.2**:** Travertine system hierarquical classification from Mancini et al. (2019)

1.2.1.2. Pisoids

The term pisoid is considered for ooids larger than 2 mm (Flügel, 2010) and actually they're considered for ooids larger than 2 mm with ooid-like structure formed in continental environment (Middleton et al., 2003; Flügel, 2004; Mei, 2008; Mei and Gao, 2012). On the other hand, ooids larger than 2 mm formed in marine environments are called giant ooids.

1.2.1.3. Peloids

Peloids are "spherical, ellipsoidal or angular grains, composed of microcrystalline carbonate, but with no internal structure" (Tucker, 2001). The term is purely descriptive (Flügel, 2010; Tucker, 2001) and they are mostley composed by carbonates but also could be glauconitic (Van Houten & Purucker, 1984). Peloids are smaller than other carbonate particles like oncoids and ooids (<200μm) (Flügel, 2010). The origin of peloids could be i) biotic (fecal pellets), ii) reworked from mud and grains, iii) product of alteration of grains or iv) formed in situ (Flügel, 2010).

1.2.1.4. Oncoids

Oncoids are coated grains with an irregular cortex that usually overlaps laminae with recognizable biofabric (particularly cyanobacteria) that develop spheroidal and disk plate shapes (Pentecost, 2005). They are also defined as organo-sedimentary structures with non-adherent bodies and concentric lamination (Burne & Moore, 1987). The shape and sphericity of oncoids are related to their nuclei, transport energy, microbiology, and environment, active oncoids are mobile to a certain extent, thus preventing them from cementing to the substrate (Pentecost, 2005). Oncoids are microbialites that are not fixed to the substrate like “microbial balls”(Tucker, 2001). Continental environments described for this structures, lacustrine and fluvial ,are described by Pentecost (2005). Fluvial oncoids occur in moderately gradient hydrologic flux and are subject to occasional water flows necessary to overturn them. They are frequently found in pools separating travertine dams, occasionally being washed down to the dam below and gaining size as they advance, eventually they cease moving and become part of the substratum. Lacustrine oncoids are mainly found at the margins of shallow lakes and usually have a rock or a small shell as a nucleus (Pentecost, 2005), the size of them increases with water depth reflecting water level fluctuations (Shafer & Stapf, 1978; Jones & Wilkinson, 1978).

1.2.1.5. Intraclasts and lithoclasts

Siliclastic materials and carbonate materials from the basin transported and redeposited by water flux or wind could make an important component of some deposits (Tucker, 2001; Capezuoli et al., 2014).

1.2.2. Skeletal grains

Skeletal grains can be divided into "non-algal" and algal. Non-algal grains include all invertebrates such as Mollusca, Arthropoda, Foraminifera, Radiolaria, Porifera, Bryozoa, Cnidaria, Echinodermata, Brachiopoda (Tucker, 2001). Among all the phyla mentioned above, it is particularly important to highlight the arthropods. This taxon, particularly Ostracoda, was recognized in one of the samples from Vega Verde. Algal contribution is an also important framework source to limestones, and therefore travertines, providing them with skeletal carbonate particles or siliceous (Tucker, 2001). In these groups is important to recognize the importance of diatoms, the first eukaryotic algae recognized in travertines (Pentecost, 2005), have a silicon frustule that in some travertines they make up a great proportion of travertine framework components(Pentecost, 2005).

1.2.3. Micrite

Micrite is the abbreviation of “Micro Cristaline Calcite” and it was defined by Folk (1959). They are composed of an aggregate of fine crystals smaller than 4 μm (crypto to microcrystalline) of aragonite to Mg-rich calcite and it is considerate the carbonate rock matrix (Flügel, 2010). During diagenesis, they are transformed into low Mg calcite crystals. Micrite forms at protected, low-energy environments such as lagoons, deep

shelf, abyssal bottoms (Folk, 1962).

1.2.4. Cement

Sparite is the name generally given to carbonate cement and corresponds to calcite crystals larger than 4 um that precipitate in the spaces between the grains of carbonate sediment or in the internal spaces of these particles between the grains of carbonate sediment (Folk, 1962).

1.3. MICROBIAL CONTRIBUTION

Although the travertine deposition is mainly inorganic (CO_2 degassing from water), biological factors such as microbial activity or organic matrix presence, could influence the textural characteristic of sedimentary facies of this carbonate rock. In nature, a variety of microorganisms is known to contribute to carbonate precipitation (MCP) by altering solution chemical equilibrium (producing alkalinity) through different metabolic pathways such as photosynthesis, ureolysis, ammonification, denitrification, sulfate reduction, anaerobic sulfide oxidation, and methane oxidation), and providing nucleation sites for mineral precipitation, particularly due to the presence of extracellular polymeric substances (EPS). An important feature of EPS is its cation-binding ability by its negative functional groups, which depending on the intrinsic physicochemical characteristics, could play a dual role, either promoting carbonate formation (increasing the concentration of metal ions in the microenvironment, which favors the oversaturation state in respect to carbonates) or
inhibiting carbonate precipitation (reduce free cation from solution, which consequently reduces the saturation in respect of calcium carbonate). After EPS are degraded, generally by heterotrophic microorganisms such as sulfate-reducing bacteria, the free Ca^{2+} ions locally reach high concentrations and thus favor precipitation of calcium carbonate when carbonate or bicarbonate is available (Zhang et al 2014; Dupraz et al 2009).

In the process of precipitation of calcium carbonate, it begins as an amorphous material and gradually transforms into a stable crystalline structure. Since the carbonate nucleation and precipitation occur in the organic matrix of the microbial mat, it has been proposed that metastable crystalline intermediates could stabilize their structure by interacting with organic molecules of the matrix, leading to the formation of polymorphic calcium carbonate crystals with characteristic features (spherulites, smooth rhombohedral crystals, dumbells, among others) which has an impact on the texture of the microbial carbonates (Braissant et al 2007; Pentecost, 2005). In addition to this, the calcified microbial structures, like filaments, coccoids, and EPS also contribute to the travertine textural facies (Kano et al 2019).

1.4. ARCHITECTURAL ELEMENTS OF THE TRAVERTINE SYSTEM.

The hierarchical classification of the different elements that compose a travertine system made by Mancini et al., (2019) proposes that each part of the system is associated with particular constructive elements: depo zones, depo elements, depo shapes, depo facies (Fig. 1.2). This classification allows to describe, recognize and

compare the Vega Verde Travertine system with others in the world. Additionally, to the proposal of Mancini et al. (2019), the term "microfabric" to specify the different internal components that each of the present depositional facies content. The terms depositional zone, element and shapes are also modified.

1.5. GEOCHEMISTRY

1.5.1. Major and trace ions composition

Geochemical studies of trace and major elements provide a wide range of data that can be used to understand and particularize the origin of the components, genesis, paleohydrology, paleoenvironment, and the nature of the travertine systems (Pentecost, 2005; Janssen et al.,2020; Claes et al. 2019; Teboul et al.,2016). By Researching for scientific contributions of travertines in all the world Pentecost (2005) made a list of the mean values of the different elements in travertine systems.

1.5.2. Stable isotopes

Isotopes to a specific element that have equal number of protons but a different number of neutrons, with this, they have different masses (Chang, 2011).
Isotopes are present like unstable and stable, the unstable spontaneously emit particles or electromagnetic radiation in a phenomenon called radioactivity. while the stables don't have that property (Chang, 2011). Particularly the stable isotopes, of C and O, are considered a very useful tool for the study of travertines and for geological materials (Pentecost, 2005; Kano, 2019). The fractionation undergone by these stable isotopes is the result of different processes depending on temperature, CO2 source, degree of degassing, and post-depositional alterations including diagenesis (Kano, 2019). Isotopic fractionation or reaction (Kano, 2019) are measured by a factor α of a particular element and it is measured to a respectively standard. For C and O, the standards are Viena Pee Dee Belemnite (VPDB) and Viena Standard Mid Ocean Water (VSMOW) (Pentecost, 2005). The isotopic fractionation can lead to an enrichment or a depletion compared to these two standard values which is identified by the symbol δ. For C exist two isotopes: ^{12}C and ^{13}C and the for the VPDB the value is $\delta^{13}C$ and is calculated as follows:

$$\delta^{13}C=[(^{13}C/^{12}C)\ \text{sample}/(^{13}C/^{12}C)\ \text{standard}] - 1\ (x1000)$$

Positive values of $\delta^{13}C$ mean enrichment and negative means a depletion (Pentecost, 2005). Changes in the isotopic composition across a travertine profile due to changes in temperature, evaporation rate, degassing and pH (Kano,2019; Pentecost, 2005). The degree of change for $\delta 1^{8}O$ is a combination of factors such as distance from the vent, temperature difference, and also water flow. The degree of change for $\delta^{18}C$ depends on the initial pCO_2, pH; and for Kano (2019) the continuous degassing of CO_2 will cause an enrichment of ^{13}C.

1.6. GEOLOGICAL CONTEXT

The Argentinean Puna comprehends a plateau region 3700 m above sea level, located the Catamarca, Salta, and Jujuy provinces, NW Argentina (Fig. 1.3a). The region has limits with the geological provinces of Cordillera Oriental to the east, Cordillera Frontal and Sistema de Famatina to the South and Cordillera Occidental in the West (Ramos, 1999). Alonso et al. (1984) divided the Puna by the El Toro-Olacapato lineament: into North and South Puna (Fig. 1.3a). The Altiplano-Puna plateau is the largest non-collisional orogen on Earth (Oncken et al., 2006) between the Peruvian and Chilean flat slabs (14ºS- 27ºS) at the West margin of South America (Gianni et al., 2019). In this context, Gianni et al. (2019) describe the Southern Puna plateau subduction (SPSS) as a slab shallowing that begins at about ~300 km from the trench that is characterized by a ~200 km wide shallow portion at ~100–120 km that dips between 10 and 12° to the east, within the Altiplano-Puna plateau at the south of the El Toro-Olacapato lineament. The Central Volcanic Zone (CVZ) is a region between 24ºS- 27º30' S (Cahill & Isacks, 1992) that contrasts with the abrupt flat to normal subduction transitions usually described in the Nazca Plate (Scire et al., 2015). For Gianni et al. (2019) beneath the CVZ, the slab segment of the SPSS is ~30 90 km shallower than the rest of the slab. This area has a high concentration of Miocene and younger mafic volcanic centers, which were enhanced by a change in the kinematic conditions of the faults from a compressional regime in the Miocene to an oblique-slip regime with N-S extension component in the late Pliocene (Kraemer et al. 1999; Voss, 2002). The most expressive geological event in the Puna is the Cenozoic orogenic volcanism that intercalates with continental sediments of intermontane endorheic basins, culminating with large evaporitic deposits large salars (Ramos, 1999). Located at the South Puna there are: Rincon salar, Pocitos Salar, Arizaro Salar, Antofalla Salar, and Hombre Muerto Salar among others salars (Alonso & Rojas, 2020). In this context, Gianni et al. (2019) describe the Southern Puna Plateau Subduction as a shallow slab starting around ~300 km from the trench that is characterized by a ~200 km wide shallow portion at ~100–120 km that dips between 10 and 12° to the east, within the Altiplano-Puna plateau at the south of the El Toro-Olacapato lineament.

1.6.1. Antofalla Salar

The Puna is one of the driest regions of the Andes and this condition is related to the tectonic evolution and the regional morphology of the area (Alonso et al. 2006). It shows arid to semiarid climate, average annual temperatures of 4.7ºC-5.3°C (Conhidro, 2016), big Tº variance between day and night (more than 30°C)and annual rainfall reaches a total of 400-500 mm/year in the west and 100-200 mm/year in the east (Cajal, 1998). In this context, the Salar de Antofalla Basin is an example of the Puna local relief (Kraemer et al. 1999),a NNW-SSE striking basin with a 140 km long and 10 km of wide large salar in its center. The Salar de Antofalla is a region located at 3340 m above sea level surrounded by steep slopes and peaks that are thousand of meters above the salar surface (Voss, 2002). The deformation and uplift history of the southern Puna region involving the Salar de Antofalla started in the Paleogene by the Incaic phase at and after that in four different stages: D1, D2, D3, D4 (Kraemer et al. ,1999; Voss, 2002; Carrapa et al. 2005). The Incaic phase (Steinmann, 1929) triggered east and west-vergent thrusting and reverse faulting of basement blocks onto folded Late Eocene strat. The D1 involves E±W to WNW±ESE shortening

accommodated by a significant west-vergent reverse fault system. D2 is characterized by E±W to WNW± ESE shortening reactivating the west-vergent fault system that was active during the deformation interval D1. Additionally, D2 produced new reverse faults and thrusts where basement blocks were thrust towards both east and west onto tilted Tertiary strata. The D3 stage is the Mid-Miocene E±W to WNW±ESE shortening to the eastern part only. In the western part, no significant structural elements indicating compression younger than Early Miocene can be found. The D4 interval comprehends contraction movements and transpressional and transtensional movements of directional faults (Acazoque Fault) that cut older reverse faults. Also the development of monogenetic cones of stratovulcans 5.3 ±0.3 - 3.6 ±0.2 My (million years)(Maro et al. 2017, Báez et al. 2015). The D4 shortening is indicated by reverse faulting and thrusting at the eastern edge of the Salar de Antofalla reducing the basin to its true, narrow, elongate shape giving the region tectonic and sedimentological attributes of an intra-arc environment (Carrapa et al., 2005; Kraemer et al. 1999). The tectonosedimentary and volcanic description of the Antofalla Salar begins in the upper Eocene with Quiñoas Formation following to the Late Oligocene with Chacras Formation (Carrapa et al. 2005; Kraemer et al., 1999). The Early Miocene is represented by the Potrero Grande Formation and the Middle to Late Miocene is represented by the Juncalito Formation. Since the Late Miocene/Early Pleistocene mainly basaltic-andesitic magma erupted from monogenetic centers (Fig. 1.5). The last episode of regional volcanism corresponds to the Cerro Blanco volcano with 5-4 Ky and today the South Puna is under a more quiet tectonic phase as it is indicated by very low seismic activity in comparison with the boundary zones and by young alluvial fans which are generally undeformed (Maro et al., 2017; Báez et al., 2015; Fernández-Turiel et al.,2013; Montero López et al., 2010;).

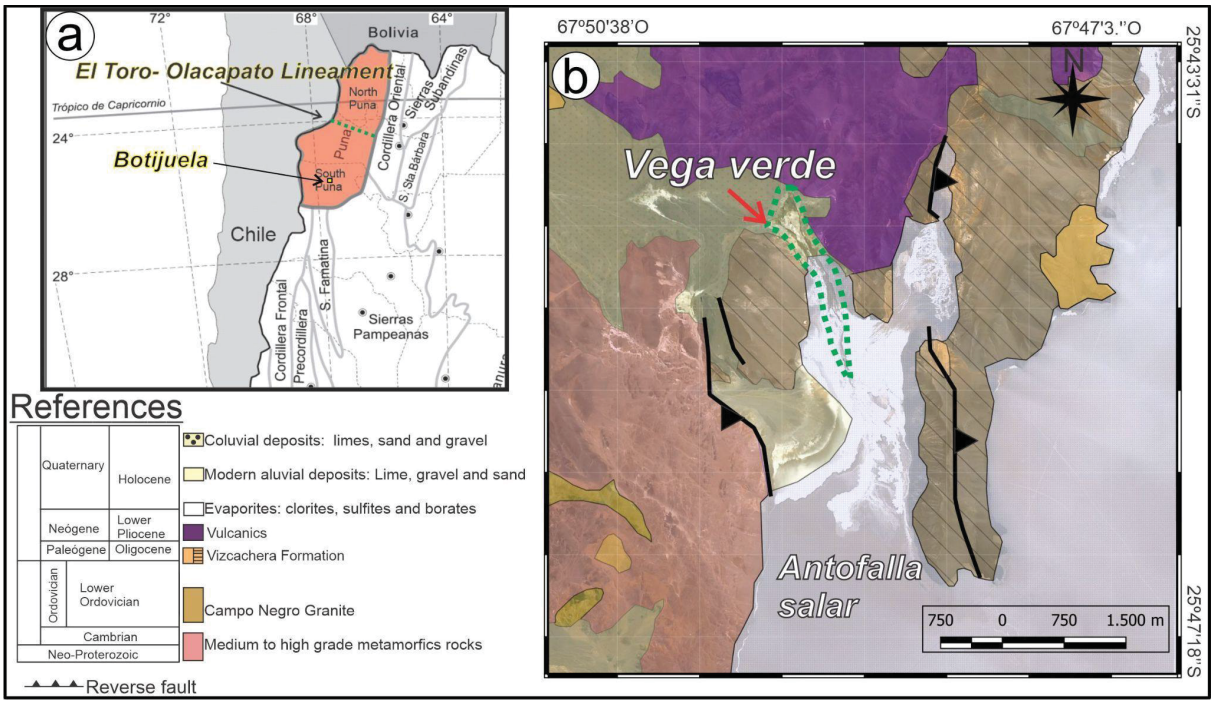

Figure 1.3. Southern Puna in Argentina, modified from Ramos (1999) and Alonso et al. (1984). b) Geological context of Botijuela from Seggiaro (2007).

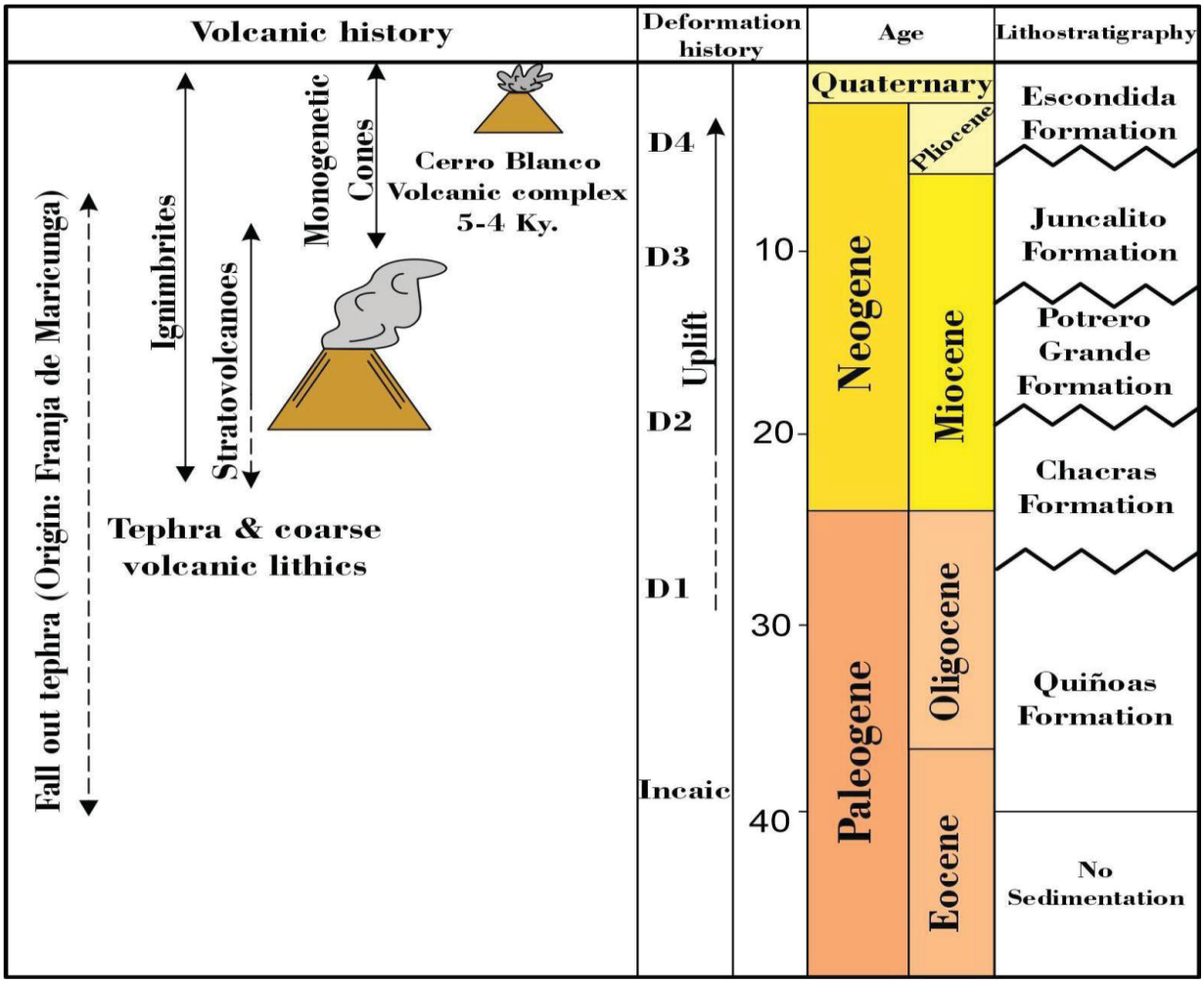

Figure 1.4: Geological history of south Puna

1.6.2. Botijuela

Within the Salar de Antofalla there are several ocurrences of hydrothermal vents and also permanent lakes such as the Salinas Grandes and Olaroz (Alonso & Rojas, 2020). These water bodies brought great scientific interest to the area in recent years, because it is one of the few places in the world where modern microbialites are currently being formed (e.g., Valero-Garces et al., 2000; 2001; Gomez et al., 2008; 2018; Farías, 2009; Farías et al., 2011; 2020; Iturra et al., 2020). Microbialites and travertines, and also other stromatolitic structures were reported by Valero-Garcés et al. (2000; 2001), Iturra et al.(2020), Vignale et al. (2021), Villafañe et al. (2021), who carried out facies analyses for palaeoenvironmental and paleohydrological reconstruction of the system. Among the hydrothermal vents in the area, the Botijuela hot springs located at the western edge of the Salar de Antofalla at 3433 meters above sea level (25º43'32.9”-25º43'32.9"S; 67º50'38.7"- 67º47’3.48’’ W)(Fig. 3). This is a complex hydrothermal system, with remarkable dimensions, where a great diversity of carbonate facies can be recognized in the Vega Verde and Vega Blanca. For Seggiaro (2007) the older rocks of the area are the medium to high-grade metamorphic rocks from the neo-proterozoic to the Cambrian and the Campo Grande Granite from the Lower Ordovician (Fig. 1.3b). An unconformable boundary with the Lower Paleozoic rocks lies the alluvial sediments of the Vizcachera Formation and also Pliocene volcanic rocks. The youngest sediments in the area are represented by alluvial and

colluvial deposits overlying the underlying evaporites of the Salar de Antofalla (Seggiaro, 2007).

1.7. OBJECTIVE

The main goal of this thesis was to recognized the geological and geomorphological features of the Vega Verde travertine system, Botijuela, Argentine Puna. To achieve this objective a multi-proxy and multi-scale approach focoused on facies analysis and geochemical characterization of distinct sectors of the travertine system.

- Evaluate the lithological records
- Analyze three-dimensional architecture of the travertine system.
- Study the relationships between the carbonate deposits and the local tectonic structures.

2. MATERIAL AND METHODS

This research was carried out in field and also in laboratory following a work flux showd in the Fig. 1.5

Bibliographic research: consulting the articles of different authors who have worked both in the region and in similar carbonate systems.

GIS and Remote Sensing: Interpretation of satellite images provided by Google-Earth, Bing satellite, and geological maps provided by SEGEMAR (Servicio Geologico Minero Argentino) and IGN (Instituto Geográfico Nacional de Argentina), with the software SAGAgis, Qgis, GRASSgis to build a cartographic base for the research.

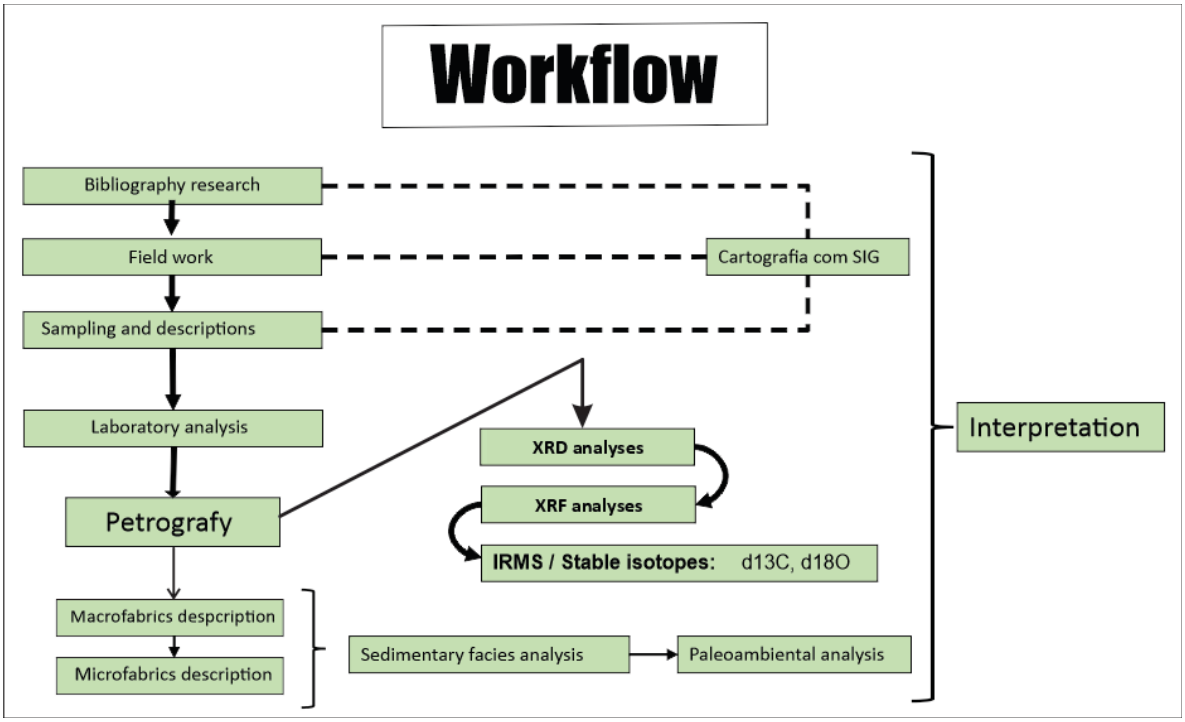

Figure 1.5: Workflux of this thesis

Fieldwork: The fieldwork was carried out during March 2020 when it was identified and described the site and collected the samples. The field activities also included:

- Location and delimitation of the travertine systems of Vega Verde and with GPS and description of their morphologies considering several authors (Dunham, 1962; Pentecost, 2005 and Kano, 2019).

- Systematic collection of samples from each system for further laboratorial macro and microanalyses. A total of 27 samples were collected the letters A through H for each defined geomorphological compartment.

Laboratory Analyses: this step followed a fairly complete analytical flow at iLAMIR installations in the Universidade Federal de Paraná (UFPR), starting with microscope petrography; mineralogical analysis by x-ray diffraction (XRD), chemical analyses by x-ray fluorescence (XRF) and C & O isotopes.

- Macro facies: Polished sections and hand samples were analyzed in Zeiss Discovery V8 binocular magnifier.

- Microfacies: To observe and define the microfacies, estimate porosity, recognize microstructures and identify structures of organic and inorganic origin, 16 thin sections of the samples were described in Zeiss petrographic microscopes, model Imager.A2m were used.

- XRD Analyses: To obtain the mineral fractions present in the samples, 38 powder samples were from the 27 samples collected in the field. Malvern PANalytical Empyrean, with X'Celeratore detector and Cu tube applying in a a scan rate of 0.5 °/ min, under a voltage of 40kv, current of 30mA. The mineral composition and semi- quantitative mineral abundances of the samples were determined using the HighScore software.

- FRX analyses: A total of 38 powder samples were analyzed by the X-ray fluorescence method in order to identify and quantify the presence of 10 main oxides (SiO_2, Al_2O_3, Fe_2O_3, CaO, MgO, K_2O, Na_2O, TiO_2, MnO, and P_2O_5) elements (Sr, Ba, Zr, Rb, S, Nb, Pb, As, Cu, Zn, V,) and REE (Ce, La, Nd, Y). To determine loss on ignition (LOI), the samples were heated to 1000 ° C for 2h in a muffle. The used equipment was the X-ray Fluorescence Spectrometer, from the PANalytical brand, model AXIOS mAX with a rhodium tube. Interpretation of raw data was carried out in the software SuperQ 5.3.

- IRMS / Stable Isotopes: A total of 38 carbonate samples were analysed for C and O stable isotopes in order to know the organic and inorganic influence in the travertines (Burne & Moore, 1987). Mass spectrometer model Delta V Advantage, brand Thermo Fischer Scientific, was used to bulk C and O isotopic composition. The spectrometry is performed on CO_2 released from phosphoric acid digestion of carbonatie powder samples ´online' by reaction with 100%.

- Interpretation of the processes and agents in the systems: By integrating facies and facies associations with the geochemical data, an analysis of the organic and inorganic processes in the outcrops will be done consulting material by Guo & Ridding (1998), Tucker(2001), Penteccost (2005), Flügel, (2010), Fouke et al. (2000), Gandim & Capezzuoli (2014), Teboul et al. (2016), Janssen et al. (2019), Della Porta et al. (2022).

3. RESULTS

Submitted paper in Andean Geology: *"Faciological and geochemical characterization of the Botijuela Travertine System, Central Andes, Argentine."* Still in revision stage at the time of this publication.

TITLE:
Faciological and geochemical characterization of the Botijuela Travertine System, Central Andes, Argentine.

AUTHORS: Alonso, G.E.[1]; Varejão, F.G.[2]; França, A.[1]; Stepanenko, T.[1]; Bahniuk, A.M.[1]; Farias, M.E.[3]; Villafañe, P.G[3] and Cury, L.F. [1]

1. *Instituto LAMIR- Universidade Federal do Paraná.*
2. *Universidade Federal de Ouro Preto.*
3. *Planta Piloto de Procesos Industriales y Microbiologicos Tucumán- CONICET-Argentina.*

ABSTRACT
The economic and scientific interest in non-marine carbonates, particularly travertines, have been growing in recent years because they are considered as hydrocarbon reservoirs in the pre-salt plays of Brazil and Angola. Expanding knowledge of these systems allows predicting better exploration targets for potential oil plays. This research is the first to describe the Vega Verde travertine system- Botijuela, Argentina South Puna. The system was studied using multi-scale approaches: megascopic, mesoscopic and microscopic. In conjunction, mineralogical analysis with X ray diffraction, geochemical composition of major oxides and trace ions with X ray fluorescence and stable isotopes of C and O, were done. Three deposition zones in the system were recognized based on the distance from the spring, slope, and lithological features: proximal, intermediate, and distal. Mineralogically the deposits are mainly composed of calcite and Mg-bearing calcite. Isotopic analysis reveals a vast enrichment of $\delta^{13}C$ (1.97~10.84) and negative $\delta^{12}O$ values (-0.67 - -8.91) that together with Sr and Ba analysis indicated a hydrothermal origin for the distinct sedimentary facies. In the proximal zone, the area is directly influenced by the spring, with high concentration of Fe2O3 (~4.3 %), Pb-As (~0.5 to 1.7%), and other metals such as Zn (~139 ppm) and SiO_2 (~2 %). These geochemical characteristics occur in association with the presence of the geyserite facies with ferruginous carbonates, globular silica and fibrous calcite. In the distal zone detrital components dissolved in high alkalinity reach SiO_2 values of ~5-6 %, that could be related to an amorphous Si phase. The impoverishment of those components and the increment of Si throughout the system is accompanied by the increasing influence of sedimentary processes related to siliciclastic deposits that gradually increase from proximal, through intermediate to distal in the direction of the Salar de Antofalla basin. These results suggest that Vega Verde could be categorized as a hydrothermal-sedimentary travertine system. The origin of the main fluid that build the system could be located in the proximal area denoted
by the geyserite facies presents only in that spot. These facies could be a useful tool for future paleoenvironmental reconstruction in other travertine systems.

Key words: Travertine, geyserite, Botijuela, South Puna

TITULO: Caracterización faciologica y geoquímica del sistema travertino de Botijuela, Andes centrales, Argentina.

RESUMEN
El interés económico y científico por los carbonatos no marinos, en particular los travertinos, ha crecido en los últimos años porque se consideran rocas reservorio de hidrocarburos en los sistemas petroleros del Presalt de Brasil y Angola. La ampliación del conocimiento sobre estas rocas permite predecir mejores objetivos de exploración en tales sistemas. Esta investigación es la primera que describe el sistema travertino de Vega Verde - Botijuela, Puna Sur de Argentina. El sistema fue estudiado utilizando enfoques multiescala: megascópico, mesoscópico y microscópico. En conjunto, se realizaron análisis mineralógicos con difracción de rayos X, composición geoquímica de óxidos principales y elementos traza con fluorescencia de rayos X e isótopos estables de C y O. Se reconocieron tres zonas de deposición en función de la distancia al manantial surgente, la pendiente y las características litológicas: proximal, intermedia y distal. Mineralógicamente los depósitos están compuestos principalmente por calcita y calcita portadora de Mg. Los análisis isotópicos revelan un gran enriquecimiento de $\delta^{13}C$ (1,97~10,84) y valores negativos de $\delta^{12}O$ (-0,67 - -8,91) que, junto con los análisis de Sr y Ba, indican un origen hidrotermal para las distintas facies sedimentarias. En la zona proximal, el área está directamente influenciada por el manantial, con una alta concentración de Fe_2O_3 (~4,3 %), Pb-As (~0,5 a 1,7%), y otros metales como Zn (~139 ppm) y SiO_2 (~2 %). Estas características geoquímicas se dan en asociación con la facies de geiserita que presenta carbonatos ferruginosos, sílice globular y calcita fibrosa. En la zona distal los componentes detríticos disueltos en alta alcalinidad alcanzan valores de SiO_2 de ~5-6 %, que podrían estar relacionados con una fase de Si amorfo. El empobrecimiento de estos componentes y el incremento de Si en todo el sistema se acompaña de la creciente influencia de procesos sedimentarios relacionados con depósitos siliciclásticos que aumentan gradualmente desde la zona proximal, pasando por la intermedia hasta la distal en dirección a la cuenca del Salar de Antofalla. Estos resultados sugieren que Vega Verde podría ser categorizado como un sistema travertino hidrotermal-sedimentario. El origen del fluido principal que construye el sistema podría situarse en la zona proximal denotada por las facies de geiserita presentes sólo en ese lugar. Estas facies podrían ser una herramienta útil para futuras reconstrucciones paleoambientales en otros sistemas travertinos.

Palabras clave: travertino, Botijuela, geiseritas, Puna

I. INTRODUCTION

Travertine and tufa are non-marine carbonates from spring water, formed after the process of degassing in water with dissolved Ca^{2+} and CO_2 with biotic and abiotic factors involved in their formation. Their geochemical classification is based on the origin of CO_2 and also in the origin and the depth at which the fluids circulated in the subsurface (Pentecost, 2005; Teboul *et al.*, 2016; Jones and Renault, 2010; Rogerson *et al.*, 2014; Kano *et al.* 2019, Shiraishi *et al.*, 2020). Travertine and tufa definitions were proposed by many authors through history like Emig, (1917); Bates and Jackson (1987); Riding (1991); Koban and Schweigert (1993); Ford and Pedley (1996); Fouke *et al.* (2000); Glover and Robertson (2003); Pentecost (2005) and the difference between those terms is problematic and could lead to confusion (Ford and Pedley, 1996; Capezzuoli *et al.*, 2014, Kano *et al.*, 2019). In an effort of clarify both terms Capezzuoli *et al.* (2014) made a strict difference between those terms based in diverse features like depositional process, HCO_3^- content, $\delta^{13}C$, water temperature, mineralogy, primary porosity, biological content, depositional morphologies, distinctive lithofacies, hydrological setting and tectonic relation. Normally travertines transitions laterally to tufa in areas where the water has

cooled to near ambient temperatures (Ford and Pedley, 1996) and the biotic factors like (macrophytes,microphytes, microbes, invertebrates and/or vertebrates) that develop in those systems gradually increase (Rainey and Jones, 2009; Capezzuoli *et al.*, 2014, Mancini *et al.*, 2019). Interest of industry and academy in non-marine carbonates have been growing up in the latest years because they are considerate as hydrocarbon reservoir in the Pre-Salt play of Brazil and Angola (Della Porta,2015; Ronchi and Cruciani, 2015, Virgona *et al.*, 2013 Janssens *et al.*,2020; Shiraishi *et al.*, 2020). A large variety of rocks can provide substrate and ion sources for travertines and tufas including igneous rocks and sedimentary rocks (Teboul *et al.*, 2016). Facies and geochemical analyses (trace and major elements and stable and radiogenic isotope proxies), provide a wide range of data that can be used to understand and particularize the origin and the nature of travertine systems (Pentecost, 2005; Janssen *et al.* ,2020; Claes *et al.*, 2019; Teboul *et al.*, 2016), as well as it is used as a tool to understand tectonic-related process (Hancock *et al.*, 1999; Curewitz and Karson, 1997; Mesci *et al.*, 2007).

The travertines of Botijuela are located in the region of South Puna at the west margin of Antofalla Salar in Argentina (Figure 1) (25º45'55'' S/ 67º48'56''O). Outcrop descriptions revealed fossil and modern travertine systems with absence of gushing sources, gaseous phases, presenting significant volume of lithified rocks and mixtures of hot and cold water, and presence of microbial communities. Such characteristics, position Botijuela as an attractive study area that could provide useful interpretations to understand continental carbonate deposition processes in the geological past. As well as trying to establish the relationship between the climate and the geological environment, both ancient and recent, that occurred during the formation of these carbonate systems. It is for the above that the main goal of this work is to describe the Vega Verde travertine system located in Botijuela from a geological, geomorphological, and geochemical approach, classifying and associating facies in order to evaluate the composition, sedimentary structures, and textures. This kind of analysis applied to the study of other continental carbonate systems in the world have been done in numerous scientific contributions (Mors *et al.*, 2022; Shiraishi *et al.*, 2021, Iturra *et al.*, 2021; Della Porta *et al.*,2022, 2017, 2015; Janssen *et al.*, 2019; Teboul *et al.* 2016:) in order to unravel the implications of carbonates in different sedimentary environments.

I.I. Geological context

Argentine Puna comprehends a plateau region, 3700 m above sea level located in the Northwest of Argentina (Figure 2.a). The region has limits with the geological provinces of Cordillera Oriental to the East with a gradual transition to Cordillera Frontal and Sistema de Famatina to the south and Cordillera occidental in the West (Ramos, 1999). Alonso *et al.* (1984) divided the Puna by the El Toro-Olacapato lineament into North and South Puna (Figure 2.a). The Altiplano-Puna plateau is the largest non-collisional orogen on Earth (Alonso *et al., 2006;* Oncken *et al.*, 2006), between the Peruvian and Chilean flat slabs (14º-27º S) at the West margin of South America (Gianni *et al.* 2019). The most expressive geological feature in the Puna region is the Cenozoic orogenic volcanism that intercalates with continental sediments of intermontane endorheic basins, culminating with large evaporitic deposits that constitute large salt flats (Ramos, 1999). Located at the South Puna there are the Rincon, Pocitos, Arizaro, Antofalla, Hombre Muerto, among other salt flats (Alonso and Rojas, 2020). For Seggiaro (2007) the older rocks of the study area are the medium to high-grade metamorphic rocks from the Neoproterozoic to the Cambrian and the Campo Grande Granite from the Lower Ordovician (Figure 2.b). An unconformable boundary with the Lower Paleozoic rocks lies the alluvial sediments of the Vizcachera Formation and also Pliocene volcanic rocks (Figure 2.b). The youngest sediments in the area are represented by alluvial and colluvial deposits overlying the underlying evaporites of the Salar de Antofalla (Seggiaro, 2007).

The Southern Puna plateau subduction (SPSS) was described as a shallow slab subduction that begins at about ~300 km from the trench. It is characterized by a ~200 km wide shallow portion

at ~100– 120 km that dips between 10 and 12° to the east, within the Altiplano-Puna plateau at the south of the El Toro-Olacapato lineament (Gianni *et al.*, 2019). The central volcanic zone (CVZ) is a region between 24ºS- 27º30’ S (Cahill and Isacks, 1992) that contrasts with the abrupt flat to normal subduction transitions usually described in the Nazca Plate (Scire *et al.*, 2015). For Gianni *et al.* (2019) beneath the CVZ, the slab segment of the SPSS is ~30 to 90 km shallower than the rest of the slab. This area has a high concentration of Miocene and younger mafic volcanic centers, which were enhanced by a change in the kinematic conditions of the faults from a compressional regime in the Miocene to an oblique-slip regime of N-S extension in the late Pliocene (Figure 3) (Kraemer *et al.* 1999; Voss, 2002; Carrapa *et al.*, 2005).

I.II. Botijuela

Within the Salar de Antofalla there are several occurrences of hydrothermal vents and also permanent lakes such as the Salinas Grandes and Olaroz (Alonso and Rojas, 2020). These water bodies brought great scientific interest to the area in recent years, because it is one of the few places in the world where modern microbialites are currently being formed (e.g., Valero-Garces *et al.*, 2000; 2001; Gomez *et al.,* 2018; Farías *et al.*, 2009; Farías *et al.*, 2011; 2020; Iturra *et al.*, 2020). Microbialites and travertines, and also other stromatolitic structures were reported by Mors *et al.*, 2022; Valero-Garcés *et al.* (2000; 2001), Iturra *et al.* (2020), Vignale *et al.* (2021), Villafañe *et al.* (2021), who carried out analyses for paleoenvironmental and palaeohydrological reconstruction of the system. Among the hydrothermal vents in the area, the Botijuela hot springs located at the western edge of the Salar de Antofalla at 3433 meters above sea level (25º43'32.9”-25º43'32.9"S; 67º50'38.7"- 67º47’3.48’’ W). Among the travertine systems in the area, Vega Verde is notable for the presence of vegetation and by a relief with both the current and the fossil travertine system in a single profile.

II. MATERIAL AND METHODS

Fieldwork was carried out during March 2020 and comprises tasks of identification and description of the sites and the collection of 27 samples (Table I). The letters A to H were assigned for each compartment according to their morphological features measured in the field based on the criteria of different authors (Mancini *et al.*, 2019; Minissale *et al.*, 2002, Fouke *et al.*, 2000) and the sedimentary facies description following the criteria of Dunham (1962), Envry Klovan (1971), Guo and Riding (1998).

Each one of the 27 samples was sub-sampled in facies using a hand drill and a total of 38 powder samples were extracted and pulverized in agata pot (Table I). X ray diffraction, X ray fluorescence and C and O isotopic analysis were performed in iLAMIR installations at Universidade Federal de Paraná (UFPR). Hand samples were analyzed using a Zeiss Discovery V8 binocular magnifier and a total of 16 thin sections were described in order to observe and define the microfabrics with Zeiss petrographic microscope model Imager A2m.

Mineral fractions were analyzed with Malvern PANalytical Empyrean, with X'Celeratore detector and Cu tube was applying scan rate of 0.5 ° / min, under a voltage of 40kv, current of 30mA. The mineral composition and semi-quantitative mineral abundances of the samples were determined using the HighScore software with semi-quantitative Rietveld analysis to approach the percentual mineral composition. Complementary with this step, carbonate minerals in the samples were calculated from their *d*-spacing in the X-ray diffraction spectra following Zhang *et al.* (2010).

The X ray fluorescence method identified and quantified the presence of 10 main oxides (SiO_2, Al_2O_3, Fe_2O_3, CaO, MgO, K_2O, Na_2O, TiO_2, MnO, and P_2O_5) elements (Sr, Ba, Zr, Rb, S, Nb, Pb, As, Cu, Zn, V,) and rare earth elements (REE) (Ce, La, Nd, Y) by fused tablet with lithium tetraborate / lithium metaborate. The used equipment corresponds to the X ray Fluorescence Spectrometer, from the PANalytical brand, model AXIOS mAX with a rhodium tube. Interpretation of raw data was carried out by the software SuperQ 5.3. To determine loss on

ignition (L.O.I.), the samples were heated to 1000 °C for 2h in a muffle.

For the C and O isotopic analysis the samples were powdered at 325 mesh, submitted to acid digestion with H_3PO_4 at a constant temperature of 72°C, inserted the gas at the injection system GasBench II (Thermo Fischer Scientific), and analyzed in the Delta V Advantage IRMS (Thermo Fischer Scientific). The data processing by the Isodat software, and expressed relative to Vienna Peedee Belemnite (VPDB).

III. GEOLOGICAL FEATURES OF THE DEPOSIT

Based on the distance from the spring, slope and geomorphologic features the Vega Verde travertine system was divided in proximal, intermediate and distal areas (Figure 4, Figure 5). Each area was individualized with its surface, facies features and the process involved in the carbonate precipitation. Proximal area is composed by the compartments A, B, C and D, intermediate area by the compartments E and F and distal area by G and H.

III.I. Proximal area

Smallest area of the system with the steepest slope and the greatest diversity of sedimentary features in the system. Compartments A and B are related to a conical structure (i.e., mound and mound slope). Compartment C is related to a slope that ends with gentle breaks, allowing the recognition of the stacking pattern of the travertine system and compartment D is a fissure ridge in a mound slope that develops fans with channels, pools, and dams (Table II).

III.I.I. Mound

15-m-high conical structure (i.e., mound and mound slope) with 6.3 m of diameter in the upper part and 36 m at the base. The upper part of the (Figure 6.A) is a flat area presenting small-scale pools (1-3 cm) filled with calcite grains with a flat base and convex-up in this area, some small (cm-scale) collapsed conical structures can be observed dispersed. The mound is internally organized of quasi-horizontal layers composed of ferruginous carbonate facies with fibrous calcite, crystal fans, silica globular, and botryoidal mudstones with shrubs disposed parallelly to the laminated bedding (Figure 6.A).

III.I.II. Mound slope

It comprises the edge the mound, displayed in a steep (<45º) presenting collapsed dome structures (Figure 6.A). Small carbonate pools (~3cm) filled with granular calcite and intraclasts are observed associated with the collapsed domes. Botryoidal structures with shrub facies are observed associated with the collapsed domes.

III.I.III. Plateau Slope

Compartment C is a 35m long plateau that surrounds the ancient vent and it is divided into two parts, one close to the vent and the other further away. The nearest part is characterized from bottom to top by i) intercalation of laminated mudstone with fibrous calcite and oncoids, intraclastic rudstones; ii) Crenulated mudstone with oncoids intercalated with laminated mudstone that presents fibrous calcite at the base and intraclastic rudstones at the top. The farthest sector is composed of laminated mudstones with coated bubbles (vugs), shrubs, and oncoidal floatstone facies at the top of the mudstone layers.

III.I.IV. Fissure vent + Slope

Compartment D shows both traces of a fossil system and a still-active one (Figure 6.B). The active system has been individualized into four compartments. i) The first sector corresponds to a travertine mound of spring characterized by an artesian pool with warm water (Figure 6.B) and the proliferation of microbial mats. The facies present in this area are bottom to top: crenulated mudstone, shrubs. ii) The system continues with a flow characterized as a channel developed on a gradient of (>15°) with pools (small ~3cm) rims, walls, and cascades. iii) The

system continues as a slope with deconfinement of the main flow and development of fans and lobes. Pools with rounded and lobular morphologies with calcite fill and shrub facies are present near the rims and walls. iv) The last portion is described as a slope break with carbonate precipitation where runoff features are observed (fine grade calcite precipitation). At the base of the scarp, the development of shrub structures is common.

III.II. Intermediate area

The intermediate area is a gentle slope characterized by the surface shapes of fans and channels. Compartments E and F are composed by siliciclastic materials begin to occur to a greater extent in this area and they develop intercalations with the carbonate rocks (Table III).

III.II.I. Plateau

Compartment E is defined as a plateau (<10°) with the development of small terraces (Figure 7.A). This compartment is represented in profile view, from base to top, by: i) breccia rudstone, at base; ii) interbedded grainstone and crenulated mudstone, at the middle part, and iii) oncoid-rich crenulated mudstone and laminated mudstone with fibrous calcite at top.

III.II.II. Slope

The compartment F is an 81 m long steep area with the development of several steps. At the beginning of this area a 6 m thick mixed siliciclastic carbonate succession was measured (Figure 7.A, B). At the base of the section, intraclastic and volcanic-rich conglomerates with coarse-grained sandstone matrix dominate. The conglomerates constitute the base of a fining-upward succession characterized at the top by interbedded structureless sandstone and crenulated mudstone. The medium portion is dominated by interbeds of crenulated mudstone and thin layers of sandstone, which grades at the top (coarsening-upward succession) to pebbly (basic volcanic and carbonates) sandstones with massive aspects. The upper part of the section is also a coarsening-upward succession, with massive mudstones at the base, grading to medium grained grainstones, interbeds of crenulated mudstone and pebbly sandstone, and conglomerates at the top (paraconglomerate with volcanic and carbonate clasts). The terminal area comprehends an approximately 3-m-thick fining upward succession with siliciclastic-dominated base and carbonate-dominated top. The siliciclastic-dominated lower portion is characterized by sandstones (locally pebbly) with normal grading; sigmoid-shaped lenses of orthoconglomerates with volcanic and carbonate clasts; and horizontally laminated pebbly (angular volcanic clasts) sandstone at the top. The carbonate-dominated upper portion is dominated at base by lower crenulated mudstone with vuggy porosity and dispersed volcanic and carbonate clasts; and a top by upper planar mudstone with fibrous calcite.

III.III. Distal Area

This area includes the travertine system after compartment F and it is composed of the compartments G, H including the development of alluvial plains morphologies like channels and fans (Fig. 7.B). The distal area finishes in the Salar de Antofalla Basin and is characterized by the absence of springs, and the presence of higher energy sedimentary facies (Table IV).

III.III.I. Fans and lenses, rims and pools

It is 210 m long with four slope reliefs separated from each other by flat areas (Figure 7.B). Profile exposition of deposited sedimentary facies is described as 3 m thick succession composed at the base of mudstones that transition to inversely graded gravels. The top of the section is dominated by crenulated mudstones with vuggy porosity and sandstones.

III.III.II. Channels and rims and pools

It is an isolated sloping relief at the terminal portion of the travertine system. It is composed by conglomerates with normal gradation at the base, intercalations of sandstone, mudstone, boundstone with shrubs, and intraclastic rudstone with developing teepee structures at the top.

And finishes in interbedded contact with the Salar de Antofalla basin (Fig, 7.B)

IV. FACIES CHARACTERIZATION AND DISTRIBUTION

The sedimentary facies described are geyserites, autochthonous limestone with fossils, bafflestones, laminated mudstone, crenulated mudstones, grainstones, packstones, rudstones and intraclasts breccias

IV.I. Geyserites

This facies is only present in the mound features in the compartment A. On a mesoscopic scale these facies present massive appearance with globular silica, reddish ferruginous carbonates and development of centimetric bubble morphology (Figure 6.a.i).

IV.II. Autochthonous limestone with shrubs

These rocks are located mainly in the proximal zone in areas close to the vent in the compartments A and B. It occurs as an alternation ~0,5 - 2cm of arborescent structures with laminated reddish or brownish carbonates (Figure 6a i, ii). On a micro scale Internally, it is composed of ~750 μm brownish arborescent structures of prismatic habit that are presented gradually growing radially from a point in common (Figure 8.a). These arborescent structures intercalate with lumpy micrite levels with scattered calcite, ferruginous oxides and carbonates as well as small organic matter. Porosity of these facies is (high Ø = 25-35%) mainly fenestral with development of vugs.

IV.III. Bafflestones

These rocks are mainly located in the slope zones of the proximal and intermediate areas. At hand scale they are characterized by a brownish-whitish color with fragments of botryoidal and oncoid structures <0.7cm of very bad selection that are covered by calcite lamellae. They show a chaotic distribution of these components as well as irregular cavities <1.5cm. At microscale they exhibit fragments of peloids, oncoids, stromatolites, and peloidal micrite that are cemented together by sparite cement (Figure 8.b). Shrubs structures could also be composed of clean sparite growing from a point (Figure 8.c) and were hard enough to stay there after the dissolution process of the organic matter. The porosity (estimated Ø =15-25%) is mainly of the secondary type and has large vugs and channels that may or may not have carbonate infills.

IV.IV. Laminated mudstone

Laminated mudstones exhibit mesoscale laminar textures of 0.5-2mm. These laminae are eventually found in association with ooid and/or oncoids, which interfere with the continuity of the lamination. Near the mound the laminations can occur with a good development of linear continuity grading laterally to mounds, at the rest of the system it shows development of ~5 cm longitudinal and lobular pools structures.

IV.V. Crenulated mudstone

These facies are observed in association with pools where dams are well-developed in all the areas of the system. In mesoscale is presented with a -4.5cm structure characterized by stacked pools and rims that presents this crenulated appearance. At the edges of the pools can develop botryoidal structures and also arborescent <0.5cm. On a micro-scale, these facies present a cyclic heterophasic banded aspect (50-150μm). The lamination is highlighted by the interlamination of dark brownish micrite with oxides, and organic matter that intersperses with covers of microsparite/sparite (Figure 8.d). The corrugated pattern in this scale is shown by the brownish micritic layers with high lateral continuity. Contact with other facies is usually gradual. They may occasionally contain some lithic and peloids fragments as well as stromatolitic crusts and dendrolytes on the edges of the pools.

IV.VI. Sandstones

Sandstones facies start to be present in the intermediate zone and increase in quantity towards

the distal zone. They occur with either normal or inverse grading and are generally intercalated with carbonate facies and showing gradational contact with conglomerates.

IV.VII. Rudstones

At hand sample are present as brownish to white color with oncoids and fragments of other facies. They are present at the end/transition between the proximal and the intermediate area and also in the distal areas. At microscale they are composed of aggregates of peloidal micrite, ooids and oncoids and cemented by sparite isopachous cement (Figure 9.a). Coalescent and coated grains of these particles are common (Figure 9.b). The porosity is medium (Ø 5-15%) and is intraparticle and interparticle.

IV.VIII. Intraclastic breccias.

Intraclastic breccias occur as white to light brown carbonate aggregates with fragments of the that are cemented with microsparite: oncoids, peloids, angular pyroxene lithic fragments and plagioclase and also are recognizable small angular fragments (<2cm) of the other facies. This facies is found in association with channel morphologies at the slopes of the end of the proximal areas and also in the intermediate and distal areas. Caves are sometimes filled by generations of dog tooth calcite developing rhombohedral shapes. Porosity is very low (Ø 5-10%) and is restricted to fracturing. At microscope it exhibits chaotic disposition of the components and also Individual beds display lower, abrupt and irregular contact with the other facies and commonly has reworked fragments of microbialites and oncoids (Figure 9.c).

IV.IX. Grainstones

This facies is mainly located in the intermediate and distal areas. Grainstones generally show a gradual transition to sandstone facies but also it presents abrupt discordances. At thin sections this is composed by poorly-selected oncoids, peloids and detrital fragments of plagioclase and pyroxenes cemented with sparite or microsparite and micritization process in some clasts (Figure 9.d). Porosity is approx. Ø =15% which presents an inter-particular type and also secondary with dissolution generating vugs and fracturing.

IV.X. Packstones

Clastic facies located at the end of the intermediate and in the distal areas. It is composed of allochthonous and intraclastic materials cemented by a dense micritic cement with extremely low porosity (Figure 8.e and f). At the hand scale, it is possible to identify tubular plant marks, but at the micro-scale it is unrecognizable. Diatoms and ostracods fossils are distinguishable in thin sections. The porosity is very low Ø =5% and is strictly restricted to fracturing and some pore dissolution products with a subsequent filling of scalenohedral calcite crystals.

V. MINERALOGICAL AND GEOCHEMICAL COMPOSITION

The isotopic values obtained for the samples are shown in the table V. Sampling spots were held in 7 different positions of the meadow, targeting the recognition of mineralogical, chemical and isotopic distribution, aiming the understand the different patterns in the vent (samples A and B), over the proximal zone (samples C, D), intermediate zone (samples E and F), and the distal zone (samples H). For the analysis, subsamples were selected based on the facies classification, drilling in base and top layers to sight the consistency of the records. Mineralogical analysis by X-ray diffraction shows a very homogeneous pattern in the mineral composition, with predominance of calcite (max 98%, min 52%, mean 79,58%) all over the deposit compartments, and Mg-bearing calcite (max 25%, min 5%, mean 9,73%) consistently observed. D-spacing values show very low molar % content of $MgCO_3$, except only for the samples C1-I; E2; F1. EI with d-spacing values measured of 3.03589 corresponding to 0.23 % of molar $MgCO_3$. Gypsum and anhydrite are observed in some pools placed in the proximal zone sites A, B and C, making no more than 23% of the mineral assemblage (table VI).

Detrital minerals were observed in ~70% of the samples, mainly represented by quartz and plagioclase in the proximal zone, whereas the grainstones, rudstones and breccias of intermediate and distal zones, the lithic fragments including volcanic rock granules together with oncoids and autochthonous carbonate pebbles are frequently.

Results of the main oxides and traces elements are shown in table VII. The chemical composition of the samples suggests that the system is dominantly calcic (CaO 51.05%) with low values of MgO (0.44%). The highest Mg values are found in the samples from compartment C. Values of other major oxides fit within those expected for travertines of thermogenic origin (Pentecost, 2005) except for Fe_2O_3, that shows very high concentration (5.84%) present in the samples located at the mound and mound slope region of the proximal area. Another highly remarkable aspect of the results obtained is the very high As-Pb content (17000 ppm), which is exclusively localized in the proximal area and with a subsequent decrease in the rest of the system (Table VIII). Zn, Ti and Cu values are high in the proximal area (~163 Zn ppm; ~30 Cu ppm respectively) and subsequently decrease in the rest of the system. Among them, Zn exhibits a high ratio with respect to As (R^2 correlation= 0.8). Regarding sulfur content, the samples suggest a higher accumulation in the proximal system (~3000 ppm-) and a much lower accumulation in the intermediate and distal parts (~1500ppm). These values are higher than for an average limestone (~1200 ppm) and fall within those expected for both thermogene and meteogene travertines (Pentecost, 2005). The values of Sr obtained for the samples (~2011 ppm), are high but not as high as those values found (thermogene: 20-14000ppm, meteogene 9->2930 ppm) in Pentecost (2005). Nb contents (-22ppm) are high in compartment A of the system and exceed the values expected for this element in the literature (Pentecost, 2005). Yttrium also shows a behavior similar to Nb, high concentration in the proximal area and below the detection limit towards the intermediate and distal sectors. Nb contents (-22ppm) are high in compartment A of the system and exceed the values expected for this element in the literature (Pentecost, 2005). Y is also highly concentrated in the proximal area and below the detection limit in the intermediate and distal sectors, as well as Nb. V shows a pattern with higher values at the end of the system.

The stable isotopes of C and O anlysis were performed in samples of proximal, intermedaiate and distal zones. Plotting the results together is possible to observe a strong fluctuation and little or no correlation between $\delta^{13}C$ and $\delta^{18}O$ (Figure 10), showing up a consistent pattern with positive $\delta^{13}C$ values spread between 1.65‰ and 10.89‰, and negative $\delta^{18}O$ values between -0.67‰ and -8.91‰. The values fit within the values expected for hydrothermal or thermogenic origin.

VI. DISCUSSION

A well-developed conical mound and a modern fissure ridge are the main source areas for the hydrothermal fluids. It's remarkable that the FRX analysis of the mound samples (e.g., A2-III) located there shows the highest contents of all metals and trace elements in the whole system. Although there is another pulse of element enrichment in compartment D, no other sample shows values as high as those. In addition, these values showed a tendency to an impoverishment compared to the rest of the samples. The value of certain elements in each sample may increase either by their mobility or by the contribution of allochthonous terrigenous components. The proximal area is characterized by the exclusive occurrence of vertical and lateral association of bafflestones, autochthonal limestone with fossils and crenulated mudstone with pool and rims that develop botryoidal features and shrubs. All geochemical, mineralogical, and petrographic results collected so far suggest that the proximal zone, particularly the mound, and mound slopes have a distinct and exclusive geochemical

signal. This set of geochemical, sedimentological, and geomorphological results suggest that mound samples and its surroundings constitute the point where the main source of hydrothermal water of the travertine system is located. We suggest that this main source could be represented by an antique geyser that developed a regular mound system.

The geometry of the travertines facies association is controlled by different factors: local topographic gradient, the location, and morphology of the hydrothermal vents, the rate, and chemistry of thermal water discharge which in turn are influenced by the substrate rocks, the tectonic, and the climate regime (Della Porta *et al.*, 2017). Fractures in the bedrock allow rising hydrothermal hot waters to build travertines throughout the fissure ridges (Ford and Pedley, 1996; Hancock *et al.*,1999; Guo and Riding, 1999,1998,1994). Travertine system migration through fissures is normal, and it was previously reported in other travertine systems over the world like Therma San Giovanni (Brogi *et al.*, 2010), Futamata (Shiraishi *et al.* 2020). The travertine mounds are the subaerial expression of a travertine pipe (Hillaire-Marcel, 1986; Della Porta, 2017) and near areas of volcanic activity, hydrothermal vents occur associated with sill complexes (Hansen, 2006; Hansen *et al.*, 2008; Grove, 2013). Hancock *et al.* (1999) suggest that mounds and cones occur when fissures underlie softer sediments. In the holes of these mounds self-sealing happens by the rapid deposition of carbonates resulting in the migration of the vent building complex deposits (Pentecost, 2005). The existence of the new vent for the migration of the travertine system to the Antofalla Basin could be related to the complex fissure-ridge inherited from the travertine systems developed in volcanic areas together with the self-sealing action typically of those carbonate deposits.

VI.I. Magnesium

Magnesium and Ca content in the system are within the parameters presented in the literature (Pentecost, 2005; Cappezuoli *et al.* 2014). It is important to note that Mg-bearing calcite is pure calcite that underwent a late replacement of Ca by Mg, when that replacement reaches a value >4,2% molar of $MgCO_3$ it is considered magnesian calcite (Pentecost, 2005). The almost exclusive presence of calcite is suggestive in changes of Mg concentration and temperature, below 30ºC and in low Mg content only calcite is formed (Folk, 1994; Fouke *et al.*, 2000) and high magnesian travertines are rarely encountered (Pentecost, 2005). The contents of Mg-bearing calcite in the system vary greatly (Table V). Analysis of the d-spacing using the Zhang *et al.* (2010) method shows that only three samples: C1-1, E2, and F1.E1 correspond to a value of 0,23% mol of $MgCO_3$, which are indicative of those data are near the normal mean values for the thermogene travertine systems (Pentecost, 2005). Comparison of these data with petrographic descriptions suggests that the facies with higher Mg-bearing calcite, and in very particular cases with $MgCO_3$-bearing calcite, are related to rudstone facies with presence of oncoids in the C compartment at the proximal area.

VI.II. Strontium

As has been previously reported, aragonite transformation into calcite via meteoric water circulation leads to precipitate calcite with lower Sr content further down the profile (Pentecost, 2005; Dickinson, 1990), with Sr: Ca ratios of <0.001 (Pentecost, 2005) (Table IX). This mechanism could be caused by a dynamic calcite dissolution and re-precipitation processes that will lead to successive less Sr in the recrystallized Ca (Pentecost, 2005). The values of the Vega Verde system reflect a much bigger Sr: Ca ratio (higher than 0.001) but not as big as expected in aragonite (0.011) shown in bibliography (Pentecost, 2005) (Table IX). This situation suggests that calcites are not the product of aragonite dissolution or that in any case the initial Sr content in the system may be too low to apply this parameter. Regarding the Ba,

its values fit into the mean for travertines(~64ppm) with a high concentration at the A compartment in the proximal area (~88ppm). The graphic with log Sr/ log Ba (Figure 11) shows a clear carbonate source from granites and mafic (Teboul *et al.*, 2016).

VI.III. C and O isotopes

The highest values of $^{13}\delta C$ are in the C and D compartments. Degassing process together Downstream changes of $^{13}\delta C$ in Vega Verde show a trend to an impoverishment. This is apparently contradictory with the fact that, whereas as the flow progresses downstream the remaining liquid would be increasingly enriched in $^{13}\delta C$ due to the successive degassing and crystallization of calcite (Kano *et al.*, 2019). High positive $^{13}\delta C$ and slightly negative ^{18}O values suggest a hydrothermal source for the travertines (Kano *et al.*, 2019).

VI.IV. Arsenium, Iron and trace elements

The proximal area of the Vega Verde travertine system shows a marked enrichment in As, Pb, Fe_2O_3 and trace elements compared to the intermediate and distal areas. Results suggest a decrease of these elements after the compartment A, and an already noticeable impoverishment since the beginning of the intermediate area of the system (Figure 11). The presence of As (5000 to 17000 ppm) and Pb (up to 4850 ppm) is almost exclusively concentrated on the mound. The values obtained are by far higher compared to the travertine average (Pb 2-228 ppm; As150->1600 ppm) (Pentecost, 2005) and only comparable to that at Carlsbad (As~ 27000 ppm) by Clarke (1916). Arsenic is present in hot spring deposits (Lindgren, 1933) and is highly associated with ferrihydrite (Smedley and Kinniburg, 2001; Mitsunobu *et al.* 2013). The mound samples (e.g., A2-III) particularly exhibits very high As and Pb associated with the occurrence of Fe, Cu, Zn, Nb, Y. In general, much of the iron present in travertines is autochthonous and it is precipitated when groundwaters containing ferrous ions enter in contact with the atmosphere (Pentecost, 2005). The presence of iron oxides near the vent area, as well as ferrihydrite, are common in Japanese thermal springs (Takashima 2008; 2010). Iron oxides could also be considered as cement for travertines formed during meteoric diagenesis (Della Porta 2017). Regarding Y and Nb, the highest accumulation was observed in the mound samples (A and B compartments) and also higher values in the proximal area compared to the intermediate and distal ones. However, Rb exhibits an inverse pattern showing a higher accumulation towards the end of the system, this could be due to the high mobility of Rb that can be transported in the detritus (Figure 11). The distribution patterns of REE in spring deposits are a good source of information regarding the interaction of fluids that provide ions for the travertine systems (Bisse et al, 2022; Franchi and Frisia, 2020; Uysal *et al.*, 2009). The content of Eu and the presence of anomalies in travertine rocks are related to the origin and the history of the rock/fluid interactions (Bisse *et al.*, 2022). In addition, analysis of the anomalies in the Ce content is a useful tool to differentiate organic and inorganic fabric. Data of Eu and Ce in the system are below the 55ppm so it is not possible to carry out the anomalies analyses.

VI.V. Silica

The content of silica near the vent is manifested by the presence of globular silica that intercalates with calcite precipitation. Siliceous sinters are common in the hot springs of the Yellowstone Park as well as mixtures of travertine and silica (Pentecost, 2005). Hot water under high pressure is capable of dissolving a large quantity of silica as orthosilicic acid $Si(OH)_4$ and hydrothermal silica is deposited by evaporation in circumneutral pH and low Ca content (Pentecost, 2005). As regards the other areas, the intermediate and distal, the values of SiO_2 % are much higher than in the proximal (~2.6% in proximal and ~4.66% in distal). Transport and

deposition are important sedimentary processes and silica values obtained might be high in these two areas because of the content of lithic fragments. Content of a higher amount of allochthonous components raises the values of silica up to 14% (e.g., sample F1.D-I), this value is related to the quartz and plagioclases facies described by petrography and detected in the DRX analyses.

VII. CONCLUSION

The sedimentology, geomorphology, petrography, and geochemistry of the Vega Verde system were addressed. This set of data suggests that the development of this system is strongly linked to hydrothermalism. As we move away from the main source, the influence of different sedimentary events that generate deposits of mixed character starts to take on greater relevance. Authors like Gandin and Cappezuoli (2014), Mancini *et al.* (2019), and Minissale (2002) have discussed the tendency of the travertine system to have more siliciclastic facies at the intermediate and distal areas. As an additional appreciation, these systems are very open and susceptible to tectonic and chemical changes so, many times the springs that provide the water to build the carbonate system can be activated or deactivated. Although the Vega Verde travertines present characteristic facies for each depositional geomorphological compartment, the great variability of facies may overlap laterally and these only facies assembly would not allow to build and define a precise facies model for similar systems.

Among the set of results, we obtained from the analyzed data, we found different and diverse targets but undoubtedly one of the most important is the distinction and recognition of the geyserite facies that constitutes the remnant in the record of the main hydrothermal source. This important sector was recognized both in geomorphology, sedimentology and geochemistry. The geyserite facies are unique in the travertine system and geochemically they are marked by a strong imprint that is denoted by the high concentration of metals and arsenic that were stored in this sector. With this in account we suggest that geyserites facies could bring potential proxies to paleoenvironmental reconstruction in other fossil systems.

The behavior of silica in the system is under study. The origin of the Si-rich solution in the spring could be related both to the volcanic area and to the dissolution of the high content of siliciclastic formations that lies under the travertine system as exposed in the distal area. Its precipitation in the hydrothermal vent nearby the spring and then post-precipitation in distal zones may be related to pH changes in the fluid as well as to other inorganic and organic factors.

No data were found that allow us to establish defined limits for where a tufa system begins, so we prefer to keep the term of this system as a hydrothermal sedimentary travertine system. Future researches together with data from Sr and REE reconnaissance, will make it possible to accurately define the origin of the water and the influence of organic and inorganic processes.

VIII. ACKNOWLEDGEMENTS

The authos would like to thanks the Diagenesis Project ANP 20257-2 sponsored by Shell do Brasil; all the LAMIR Institute technicians for the support; to Professor Gustavo Barbosa Athayde and MSc Tereza Filpi, and Luis Ahumada, who collaborated enormously with the field work. At last but not least, all our respect for Don Simón, representing the communities of the original people that until nowadays maintain the Andean culture in the altiplano of Antofalla.

IX. REFERENCES

Alonso, R. N. and Rojas, W. 2020. Originate and evolution of the Central Andes: deserts, salars, lakes, and volcanoes. Microbial Ecosystems in Central Andes Extreme Environments.(Farías, M.E.; editor) Springer: 3-19. Cham.

Alonso, R.N.; Viramonte, J. and Gutierrez, R. 1984 Puna Austral – Bases para el subprovincialismo Geológico de la Puna Argentina. In Congreso Geológico Argentino, No. 9, Actas 1: 43-63. Buenos Aires.

Alonso, R.N.; Bookhagen, B.; Carrapa, B.; Coutand, I.; Haschke, M.; Hilley, G.E., Schoenbohm, L.; Sobel, E.; Strecker,M.; Trauth, M. and Villanueva, A. 2006. Tectonics, Climate, and Landscape Evolution of the Southern Central Andes: the Argentine Puna Plateau and Adjacent Regions between 22 and 30°S. The Andes. Active Subduction Orogeny (Oncken, O.; Chong, G.; Franz, G.; Giese, P.; Gotze, H.J.; Ramos, V. A.; Strecker, M.R.; Wigger, P; editors). Springer: 265-283. Berlin.

Bates, R. L. and Jackson, J. A. 1987. Glossary of geology. American Geological Institute: 788 p. Falls Church, Virginia.

Bisse, S. B.; Ekoko, B. E.; Gerber, J.; Ekomane, E. and Franchi, F. 2022. Influence of biotic vs abiotic processes on the genesis of non-marine carbonates along the Cameroon Volcanic Line (Cameroon) and palaeofluid provenance. The Depositional Record, 8(1): 102-126.

Brogi, A.; Capezzuoli, E.; Aqué, R.; Blanca, M.; and Voltaggio, M. 2010. Studying travertines for neotectonics investigations: Middle–Late Pleistocene syn-tectonic travertine deposition at Serre di Rapolano (Northern Apennines, Italy). International Journal of Earth Sciences, 99(6): 1383-1398.

Cahill, T. and Isacks, B. L. 1992. Seismicity and shape of the subducted Nazca plate. Journal of Geophysical Research: Solid Earth, 97(B12): 17503-17529.

Capezzuoli, E.; Gandin, A.; and Pedley, M. 2014. Decoding tufa and travertine (fresh water carbonates) in the sedimentary record: the state of the art. Sedimentology, 61(1): 1-21.

Carrapa, B.; Adelmann, D.; Hilley, G. E.; Mortimer, E.; Sobel, E. R. and Strecker, M. R. 2005. Oligocene range uplift and development of plateau morphology in the southern central Andes. Tectonics, 24(4): 210-234.

Claes, H.; Huysmans, M.; Soete, J.; Dirix, K.; Vassilieva, E.; Marques Erthal, M.; Vandewijngaerde, W.; Hamaekers, H.; Aratman, C.; Özkul, M.; Swennen, R. 2019. Elemental geochemistry to complement stable isotope data of fossil travertine: Importance of digestion method and statistics. Sediment. Geol. 386: 118–131.

Clarke, R. W. 1916. The data of geochemistry 3d edition. US Geological Survey Bulletin, 616: 821 p.

Curewitz, D. and Karson, J. A. 1997. Structural settings of hydrothermal outflow: Fracture permeability maintained by fault propagation and interaction. Journal of Volcanology and Geothermal Research, 79(3-4): 149-168.

Della Porta, G.; Capezzuoli, E. and De Bernardo, A. 2017. Facies character and depositional

architecture of hydrothermal travertine slope aprons (Pleistocene, Acquasanta Terme, Central Italy). Marine and Petroleum Geology, 87: 171-187.

Della Porta, G.; Hoppert, M.; Hallmann, C.; Schneider, D. and Reitner, J. 2021. The influence of microbial mats on travertine precipitation in active hydrothermal systems (Central Italy). The Depositional Record, 8(1): 165-209.

Della Porta, G., 2015. Carbonate build-ups in lacustrine, hydrothermal and fluvial settings: Comparing depositional geometry, fabric types and geochemical signature. In Microbial carbonates in space and time: Implications for global exploration and production (Bosence, D. W. J.; Gibbons, K. A.; Le Heron, D. P.; Morgan, W. A.; Pritchard, T. and Vining, B. A.; editors). Geological Society Special Publications 2015, v. 418: 17–68. London

Dickson, J.A.D. 1990. Carbonate mineralogy and chemistry. In Carbonate Sedimentology (Tucker, M.E. and Wright, V.P.; editors). Blackwell scientific publications: 284–313. Oxford.

Dunham, R. J. 1962. Classification of carbonate rocks according to depositional textures. In Classification of carbonate rocks 1(Ham, W.E. editor). Memoriam American Association Petroleum Geology: 108-121. Tulsa.

Emig, W. H. (1917). Travertine deposits of Oklahoma. Oklahoma Geological Survey.

Emig, W.H. 1917. The travertine deposits of the Arbuckle Mountains, Oklahoma, with reference to plants agencies concerned in their formation. Bulletin Oklahoma Geolical Survey(29): 1-76.

Embry, A. F. and Klovan, J. E. 1971. A late Devonian reef tract on northeastern Banks Island, NWT. Bulletin of Canadian petroleum geology 19(4): 730-781.

Farías, M. E., 2020. Microbial Ecosystems in Central Andes Extreme Environments: Biofilms, Microbial Mats, Microbialites and Endoevaporites. Springer: 298 p. Switzerland

Farías, M. E., Poiré, D. G., Arrouy, M. J., and Albarracín, V. H. (2011). Modern stromatolite ecosystems at alkaline and hypersaline high-altitude lakes in the Argentinean Puna. In Stromatolites: Interaction of Microbes with Sediments Cellular Origin, Life in Extreme Habitats and Astrobiology (Tewari, V. and Seckbach, J.; editors). Springer Netherlands: 427-441. Dordrecht.

Farías, M.E.; Fernandez-Zennof, V.; Flores, R.; Ordoñez, O. and Estevez, C. 2009. Impact of solar radiation on bacterioplankton in Laguna Vilama, an hypersaline Andean Saline Lake (4,650 m). Special issue on the high lakes project and other high-altitude lakes. Journal of Geophysical Research: Biogeoscienses (G2)114.

Folk, R. 1994. Interaction between bacteria, nanobacteria, and mineral precipitation in hot springs of central Italy. Géographie physique et Quaternaire 48(3): 233-246.

Folk, R. L. (1962). Spectral subdivision of limestone types. In Classification of carbonate rocks (Ham, W.E. editor). Memoriam American Association Petroleum Geology: 62-84. Tulsa.

Ford, T. D. and Pedley, H. M. 1996. A review of tufa and travertine deposits of the world. Earth-Science Reviews 41(3-4):117-175.

Fouke, B. W.; Farmer, J. D.; Des Marais, D. J.; Pratt, L.; Sturchio N. C.; Burns, P. C.; and Discipulo, M. K. 2000. Depositional facies and aqueous-solid geochemistry of travertine-depositing hot springs (Angel Terrace, Mammoth Hot Springs, Yellowstone National Park, USA). Journal of Sedimentary Research 70(3): 565-585.

Franchi, F. and Frisia, S. 2020. Crystallization pathways in the Great Artesian Basin (Australia) spring mound carbonates: Implications for life signatures on Earth and beyond. Sedimentology 67(5): 2561-2595.

Gandin, A., and Capezzuoli, E. (2014). Travertine: distinctive depositional fabrics of carbonates from thermal spring systems. Sedimentology 61(1): 264-290.

Gianni, G. M.; García, H. P.; Pesce, A.; Lupari, M.; González, M. and Giambiagi, L. 2020. Oligocene to present shallow subduction beneath the southern Puna plateau. Tectonophysics 780: 228402.

Glover, C., and Robertson, A. H. 2003. Origin of tufa (cool-water carbonate) and related terraces in the Antalya area, SW Turkey. Geological journal 38(3-4): 329-358.

Gomez, F. J.; Mlewski, C.; Boidi, F. J.; Farías, M. E. and Gérard, E. 2018. Calcium carbonate precipitation in diatom-rich microbial mats: the Laguna Negra hypersaline lake, Catamarca, Argentina. Journal of Sedimentary Research 88(6): 727-742.

Grove, C. 2013. Submarine hydrothermal vent complexes in the Paleocene of the Faroe-Shetland Basin: Insights from three-dimensional seismic and petrographical data. Geology 41(1): 71-74.

Guo, L. I. and Riding, R. 1999. Rapid facies changes in Holocene fissure ridge hot spring travertines, Rapolano Terme, Italy. Sedimentology 46(6):1145-1158.

Guo, L. I. and Riding, R. 1998. Hot-spring travertine facies and sequences, Late Pleistocene, Rapolano Terme, Italy. Sedimentology 45(1): 163-180.

Guo, L. I. and Riding, R. 1994. Origin and diagenesis of Quaternary travertine shrub fabrics, Rapolano Terme, central Italy. Sedimentology 41(3): 499-520.

Hancock, P. L.; Chalmers, R. M. L.; Altunel, E. R. H. A. N. and Çakir, Z. 1999. Travitonics: using travertines in active fault studies. Journal of Structural Geology 21(8-9): 903-916.

Hansen, D. M. 2006. The morphology of intrusion-related vent structures and their implications for constraining the timing of intrusive events along the NE Atlantic margin. Journal of the Geological Society *163*(5): 789-800.

Hansen, D. M.; Redfern, J.; Federici, F.; Di Biase, D. and Bertozzi, G. 2008. Miocene igneous activity in the Northern Subbasin, offshore Senegal, NW Africa. Marine and Petroleum Geology 25(1): 1-15.

Hillaire-Marcel, C.; Carro, O. and Casanova, J. 1986. 14C and Th/U dating of Pleistocene and Holocene stromatolites from East African paleolakes. Quaternary Research *25*(3): 312-239.

Iturra, A. J. P., Mors, A., Astini, R. A., and Gómez, F. J. (2020). Travertinos fósiles de la terma Los Hornos, Puna Austral de Catamarca. Revista de la Asociación Geológica Argentina 77(4):

571-590.

Janssens, N.; Capezzuoli, E.; Claes, H.; Muchez, P.; Yu, T. L.; Shen, C. C. and Swennen, R. 2020. Fossil travertine system and its paleo fluid provenance, migration and evolution through time: Example from the geothermal area of Acquasanta Terme Central Italy. Sedimentary Geology 398: 105580.

Jones, B. and Renaut, R. W. 2010. Calcareous spring deposits in continental settings. Developments in Sedimentology 61:177-224.

Kano, A.; Okumura, T.; Takashima, C. and Shiraishi, F. 2019. Geomicrobiological Properties and Processes of Travertine Vol. 176. Springer Geology: 181 p. Singapore.

Koban, C. G. and Schweigert, G. 1993. Microbial origin of travertine fabrics—two examples from southern Germany (Pleistocene Stuttgart travertines and Miocene Riedöschingen travertine). Facies 29(1): 251-263.

Kraemer, B.; Adelmann, D.; Alten, M.; Schnurr, W.; Erpenstein, K.; Kiefer, E.; Van Den Bogaard, P. and Go, K. 1999. Incorporation of the Paleogene foreland into the Neo-gene Puna plateau: the Salar de Antofalla area, NW Argentina. Journal of South American Earth Sciences 12 (2): 157-182.

Lindgren, W. (1933). Mineral Deposits. McGraw-Hill Book Company: 930 p. New York and London.

Mancini, A.; Capezzuoli, E.; Erthal, M. and Swennen, R. 2019. Hierarchical approach to define travertine depositional systems: 3D conceptual morphological model and possible applications. Marine and Petroleum Geology 103: 549-563.

Maro, G.; Caffe, P. J. and Báez, W. 2017. Volcanismo monogenético máfico cenozoico de la Puna. In Ciencias de la Tierra y Recursos Naturales del NOA. Relatorio del XX Congreso Geológico Argentino San Miguel de Tucumán, Vol. 2017: 548-577. San Miguel de Tucumán.

Minissale, A.; Kerrick, D.M.; Magro, G.; Murrell, M.T.; Paladini, M.; Rihs, S.; Sturchio, N.C.; Tassi, F. and Vaselli, O. 2002. Geochemistry of Quaternary travertines in the region north of Rome (Italy): structural, hydrologic and paleoclimatic implications. Earth and Planet Science Letters 203: 709–728.

Mitsunobu, S.; Muramatsu, C.; Watanabe, K. and Sakata, M. 2013. Behavior of antimony (V) during the transformation of ferrihydrite and its environmental implications. Environmental Science and Technology 47(17): 9660-9667.

Montero López, M. C.; Hongn, F.; Affonso Brod, J.; Seggiaro, R.; Marrett, R. and Sudo, M. 2010. Magmatismo ácido del mioceno superior-cuaternario en el área de Cerro Blanco-La Hoyada, Puna Austral. Revista de la Asociación Geológica Argentina 67(3): 329-348.

Mors, R. A.; Gomez, F. J.; Astini, R. A.; Celestian, A. J. and Corsetti, F. A. 2022. Assessing the origin of pisoids within a travertine system in the border of Puna Plateau, Argentina. Sedimentology 69(3): 1252-1275.

Oncken, O.; Hindle, D.; Kley, J.; Elger, K.; Victor, P. and Schemmann, K. 2006. Deformation of the central Andean upper plate system-Facts, fiction, and constraints for plateau models. In

The Andes (Oncken, O; Chong, G.; Franz, G.; Giese, P.; Götze, H-J.; Ramos, V.A.; Strecker, M.R.; Wigger, P.; editors). Springer: 3-27). Berlin, Heidelberg.

Pentecost, A., 2005. Travertine. Springer-Verlag: 446 p. London.

Rainey, D. K. and Jones, B. 2009. Abiotic versus biotic controls on the development of the Fairmont Hot Springs carbonate deposit, British Columbia, Canada. Sedimentology 56(6): 1832-1857.

Ramos, V. A. 1999. Las provincias geológicas del territorio argentino. Geología Argentina 29(3): 41-96.

Riding, R. 1991. Classification of microbial carbonates. In Calcareous algae and stromatolites (Ridding, R. editor). Springer: 21-51. Berlin, Heidelberg.

Rogerson, M.; Pedley, H. M.; Kelham, A. and Wadhawan, J. D. 2014. Linking mineralization process and sedimentary product in terrestrial carbonates using a solution thermodynamic approach. Earth Surface Dynamics 2(1): 197-216.

Ronchi, P. and Cruciani, F. 2015. Continental carbonates as a hydrocarbon reservoir, an analog case study from the travertine of Saturnia, Italy. American Association of Petroleum Geologists. Bulletin 99(4): 711-734.

Scire, A.; Biryol, C. B.; Zandt, G. and Beck, S. 2015. Imaging the Nazca slab and surrounding mantle to 700 km depth beneath the central Andes (18 S to 28 S). Geodynamics of a Cordilleran Orogenic System: The Central Andes of Argentina and Northern Chile: Geological Society of America Memoir 212: 23-41.

Seggiaro, R. E.; Becchio, R.; Pereyra, F. X. and Martínez, L. 2007. Hoja Geológica 2569-IV Antofalla. Programa Nacional de Cartas Geológicas 1:250.000. SEGEMAR, boletín 343. Buenos Aires.

Shiraishi, F.; Morikawa, A.; Kuroshima, K.; Amekawa, S.; Yu, T. L.; Shen, C. C.; Kakizaki, Y.; Kano, A.; Asada, J. and Bahniuk, A. M. 2020. Genesis and diagenesis of travertine, Futamata hot spring, Japan. Sedimentary Geology 405: 105706.

Takashima, C. and Kano, A. 2008. Microbial processes forming daily lamination in a stromatolitic travertine. Sedimentary Geology, 208(3-4), 114-119.

Takashima, C.; Okumura, T.; Hori, M. and Kano, A. 2010. Geochemical characteristics of carbonate hot-springs in Japan Bulletin of the Graduate School of Social and Cultural Studies Kyushu University, I6: 65–72.

Teboul, P.A.; Durlet, C.; Gaucher, E.C.; Virgone, A.; Girard, J.P.; Curie, J.; Lopez, B. and Camoin, G. F. 2016. Origins of elements building travertine and tufa: new perspectives provided by isotopic and geochemical tracers. Sedimentary Geology 334: 97–114.

Tucker, M. E. (Ed.). (2001). Sedimentary petrology: an introduction to the origin of the Sedimentary Rocks. Blackwell Science: 262 p. Malden, Massachusetts.

Uysal, I. T.; Feng, Y. X.; Zhao, J. X.; Isik, V.; Nuriel, P. and Golding, S. D. 2009. Hydrothermal CO_2 degassing in seismically active zones during the late Quaternary. Chemical Geology

265(3-4): 442-454.

Valero-Garcés, B.L.; Delgado-Huertas, A.; Ratto, N., Navas, A. and Edwards, L. 2000. Paleohydrology of Andean saline lakes from sedimentological and isotopic records, northwestern Argentina. Journal of Paleolimnology 24: 343– 359.

Valero-Garcés, B.L.; Arenas, C. and Delgado-Huertas, A. 2001. Depositional environments of quaternary lacustrine travertines and stromatolites from high-altitude Andean lakes, northwestern Argentina. Canadian Journal of Earth Science 38: 1263 - 1283.

Villafañe, P. G.; Lencina, A. I.; Soria, M.; Saona, L. A.; Gómez, F. J.; Alonso, G. E. and Farías, M. E. 2021. Los oncoides de Las Quinoas: un nuevo depósito de microbialitos en el salar de Antofalla (Catamarca, Argentina). Andean geology, 48(2): 281-302.

Virgone, A.; Broucke, O.; Held, A. E.; Lopez, B.; Seard, C.; Camoin, G.; Swennen, R.; Foubert, A.; Rouchy, J.M.; Pabian-Gouheneche, C. and Guo, L. 2013. Continental carbonates reservoirs: the importance of analogues to understand presalt discoveries. In Microbial Carbonates in Space and Time: Implications for Global Exploration and Production. International Petroleum Technology Conference. IPTC-17013-MS. Beijing.

Voss, R. 2002. Cenozoic stratigraphy of the southern Salar de Antofalla region, northwestern Argentina. Revista geológica de Chile 29(2): 167-189.

Zhang, F.; Xu, H.; Konishi, H. and Roden, E. E. 2010. A relationship between d spacing value and composition in the calcite disordered dolomite solid-solution series. American Mineralogist, 95(11-12), 1650-1656.

X. FIGURES CAPTIONS

Figure 1: The road to the work area starts at Ruta Nacional 40 in Catamarca. Between the cities of San Fernando and Hualfin take Ruta Provincial 43 and drive to the north until you reach the town of Antofagasta de La Sierra. From there take the provincial route Nº 44 and then take a rural road that crosses from SE-NW the Salar de Antofalla. Botijuela is in the W margin of Antofalla Salar
Figure 2: a) Puna location and its North and south division. b) Geological context of Botijuela.
Figure 3: Geological history of Botijuela modified from Carrapa *et al.* 2005
Figure 4: a) Samples location. B) Vega Verde schematic picture of compartments and sample's location.
Figure 5: Vega Verde profile showing the different compartments and geomorphological features: M= mound, MS= Mound slope, S= Slope, FL= Fans and lobes, P= plateau, AP= Aluvial plains.
Figure 6: Proximal area. A) Mound with location of A, B, C. Ai) Geyserite. Bi) Autochtonous limestone with fossils, Bii) Bafflestone and crenulated mudstone, Ci) rudstone. B) Compartment D. Di) Intraclast Breccia, Dii) Crenulated mudstone
Figure 7: A) Intermediate area with compartments E and F. Ei) Grainstone , Fi) Rudstone. B) Distal area. Hi, Hii) Packstone.
Figure 8: Petrographic features I. a) Micritic shrubs, filaments and oxides develop in the vent area. b) Stromatolites structure "cauliflower" growing up in cycles and different accretion levels of the pools c) sparitic shrubs growing up after micrite laminae d) Micritic shrubs, stromatolites in a crenulated mudstone e) Packstone with clasts of volcanics. f) Packstone with ostracods and peloidal micrite.
Figure 9: Petrographic features II a) oncoids cemented by sparite isopachous cement. b) Coalescent and coated oncoids. c) Intraclast breccia and dog tooth crystal with euhedral shapes filling up a cave. d) Grainstone composed by bad selection of angular oncoids and fragments cemented by sparite.
Figure 10: Crossplot of ^{13}C and ^{18}O values of the samples normalized with VPDB.
Figure 11: a) Log Sr/Ba and geochemical data showing hypogene origin for (Calcite aragonite travertine and tufa (CATT). b) Stacked chart plot showing high concentration of Fe, As -Pb at the proximal area samples. c) Stacked chart plot showing high concentration of Nb, Y at the proximal area and high concentration of Rb in the intermediate and distal areas.

XI. TABLE CAPTIONS

Table I: Location in X and Y of the samples collected in the field trip
Table II: Proximal area
Table III: Intermediate area
Table IV: Distal area
Table V: Stable isotopes of C and O
Table VI: Mineralogical composition obtained in XRD
Table VII: Main oxides composition obtained by XRF
Table VIII: Trace elements composition
Table IX: Sr/Ca relation.

TABLES

Table I

Sample	UTM	X	Y	Altitude	Amostras	Sub facies
A	UTM 19 J	618,054	7,152,320	3512	A1 I	shrubs (autochtonous limestone)
					A1 II	mudstone
					A2 I	mudstone
					A2 II	shrubs
					A2 III	mudstone
					A3 I	Bafflestone
					A3 II	Mudstone + shrubs
					A4 I	shrubs
B	UTM 19 J	618.058	7152307	3508	B1 I	Mudstone + shrubs
					B2 I	Botryoids (Bafflestone)
					B2 II	Mudstone + shrubs
					B3 I	Mudstone
					B3 II	Rudstone breccia
C	UTM 19 J	618,058	7,152,307	3504	C1 gral. I	Rudstone + oncoids
					C1 base I	Rudstone + oncoids
					C1 topo I	Rudstone breccia
					C2 base I	Rudstone + oncoids
					C2 base II	Mudstone
					C2 topo I	Rudstone + oncoids
					C2 Topo II	Rudstone
					C2 Topo III	Mudstone
D	UTM 19 J	618,048	7,152,254	3495	D1 I	Rudstone breccia red
					D1 II	Rudstone breccia white
					D2 I	Rudstone with gypsum lamellas
					D3 I	White calcite infill
					D3 II	Black calcite infill
					D4 I	Crenulated mudstone
					D5 I	Rudstone breccia
E	UTM 19 J	618,091	7,152,199	3469	E I	Mudstone + oncoids
					E II	shrubs
F	UTM 19 J	618,133	7,152,133	3454	F1.A I	Packstone
					F1. B I	Grainstone
					F1. C I	Rudstone
					F1. D I	Grainstone
					F1. E I	grainstone + packstone
					F2. A	grainstone + packstone
H	UTM 19 J	618,337	7,151,356	3397	H I	grainstone + packstone
					H II	calcite+yeso

Table II : Proximal area

Depositional	Compartment	Geomorphology	Surface	Facies	Microfabrics	Processes of carbonate	General observations	
Proximal	A	mound	Rim and pools	bafflestones,geyserites	Shrubs, lamination	desgassing in the vent,	cristal fans, silica	active water flux between
			Mound	geyserites	Shrubs	desgassing in the vent	globular.	
	B	Mound slope <45°	Rim and pools	crenulated mudstone,geyserites, rudstone	Oncoids, shrubs, lamination	desgassing in the vent, bacterial, water flux	negative plains of precipitation what suggest a high precipitation rate. bafflestones suggest sub aerial depositti on in an evaporite	
			mound	rudstone, bafflestones	Om, Shs,Cb, Ml	desgassing, bacterial, water flux		
	C	Slope 15° close to the vent	channels	Laminated mudstone.	Oncoids and coated grains, lamination	desgassing in rapid and slow flux, erosion and	paper thin raft, cristal fans	
			channels	crenulated mudstone, laminated				
		Slope 15°	Channels	rudstones, bafflestones	Oncoids, lamination.	desgassing.	bubbles, vugg porosity	
	D	Mound	Mound	Crenulated mudstone.	Shrubs, lamination.	bacterial, desgassing	Longitudinal and rounded pools. Shrubs structures suggest sub aerial conditions.	
		Mound slope <15°	channel	crenulated mudstones.		bacterial, desgassing in		
		fans and lobbes	Rim and pools	crenulated mudstone.	Oncoids, lamination, shrubs	bacterial, desgassing in rapid and slow flux plus transport and		
			Channels	rudstone, bafflestones				

Table III: Intermediate area

Depositional	Compartment	Geomorphology		Surface	Facies	Microfabrics	Processes of carbonate	General observations	
Intermediate	E	Plateau <10°		Sheet	Grainstone, crenulated mudstone, laminated mudstone	Lamination, dog tooth calcite, peloidal micrite	Disolution in vadose area, bacterial, slow and rapid flux	calcite veins infill	
	F	Slope	proximal: fans and lobbes	channels	sandstones, intraclast breccia, crenulated mudstones	Oncoids, lamination, peloidal micrite, dog tooth calcite	desgassing in rapid and slow flux plus transport and erosion. Detrites flux		field observations and facies suggest an intense hidrotermalism
			intermediate	channels & rim and pools	crenulated mudstones, sandstones	Oncoids, lamination	desgassing in rapid and slow flux plus transport and erosion.		
					Grainstones, crenulated mudstones, intraclast breccia	Oncoids, lamination, breccia.	desgassing in rapid and slow flux plus transport and erosion. Detrites flux	grainstones massives and laminated	
			distal	channel	sandstones, grainstones	Lamination, breccia	Detrites flux		
				rims and pools	crenulated mudstones	Lamination, oncoids	desgassing in rapid and slow flux	vuggy porosite	
				channels & rim and pools	laminated mudstone			fibrous calcite, bubbles, calcite veins	

Table IV: Distal area

Deposition	Compartment	Geomorphology	Surface	Facies	Microfabrics	Processes of carbonate	General
Distal	G	Alluvial plain	Fans & rim and pools	laminated mudstones, crenulated mudstones ,	Lamination, oncoids, breccia	Desgassing in slow and desgassing in slow and	sandstones
	H	Alluvial plain	Channels & rim	conglomerates, packstone,	Lamination, oncoids,	desgassing.	tepee structures,

Table V: Stable isotopes results normalized with VPDB.

Sample	δ¹³C (‰ VPDB)	δ18O (‰ VPDB)	Sample	δ¹³C (‰ VPDB)	δ18O (‰ VPDB)
A1 I	3.57	-4.70	C2 top II	10.71	-2.33
A1 II	4.11	-6.58	C2 top III	8.39	-0.67
A2 I	2.99	-4.74	D1 I	10.00	-3.96
A2 II	3.34	-7.45	D1 II	10.89	-2.50
A2 III	02.04	-8.91	D2 I	3.58	-5.01
A3 I	4.73	-4.93	D3 I	2.95	-5.90
A3 II	4.32	-5.17	D3 II	2.42	-5.58
A4 I	4.23	-3.01	D4 I	1.97	-7.43
B1 I	3.74	-0.75	D5 I	8.91	-4.27
B2 I	9.65	-5.02	E I	5.18	-4.28
B2 II	6.70	-7.40	E II	4.22	-4.10
B3 I	7.46	-5.78	F1.A I	02.05	-6.08
B3 II	10.37	-5.17	F1. B I	1.69	-5.23
C1 gral. I	7.99	-1.91	F1. C I	1.65	-4.94
C1 base I	8.30	-3.38	F1. D I	2.46	-5.99
C1 top I	8.90	-2.74	F1. E I	2.91	-5.78
C2 base I	7.28	-4.83	F2. A	6.34	-3.78
C2 base II	9.20	-4.44	H I	3.71	-5.59
C2 top I	9.36	-4.68	H II	3.57	-6.78

Table VI: X-ray diffraction results.

Samples	D spacing	Calcite	Bearing Mg Calcite	Gyspsum	Quartz	Others	Samples	D spacing	Calcite	Bearing Mg Calcite	Gyspsum	Quartz	Others
A1 I	3.03774	98.00%			2.00%		C2 Topo II	3.03954	64.60%	9.10%	18.20%	2.00%	6.00%
A1 II	3.03854	92.00%	8.00%				C2 Topo III	3.04089	89.00%	5.00%		5.00%	1.00%
A2 I	3.03901	87.00%	13.00%				D1 I	3.03878	81.20%	9.90%		3.00%	5.90%
A2 II	303,889	89.00%	10.00%		1.00%		D1 II	3.03830	55.00%	25.00%			20.00%
A2 III	3.03785	76.00%	13.00%			11.00%	D2 I	3.03776	89.90%	9.10%		2.00%	
A3 I	3.04004	76.00%	6.00%	17.00%	1.00%		D3 I	3.03804	92.00%	5.00%		2.00%	1.00%
A3 II	3.03853	92.00%	8.00%				D3 II	3.03794	75.00%	11.00%			14.00%
A4 I	3.03862	55.00%	21.00%	23.00%	1.00%		D4 I	3.03807	94.00%	6.00%			
B1 I	3.03818	88.00%	12.00%				D5 I	3.03650	81.00%	8.00%		2.00%	9.00%
B2 I	3.03963	81.00%	7.00%	8.00%		4.00%	E I	3.03653	92.00%	8.00%			
B2 II	3.04017	66.00%	7.00%		27.00%		E II	3.03589	89.00%	10.00%			1.00%
B3 I	3.04023	77.20%	7.90%	14.90%			F1.A I	3.03709	81.00%	7.00%			12.00%
B3 II	3.03990	83.20%	11.90%		5.00%		F1. B I	3.03736	52.00%	5.00%		43.00%	
C1 gral. I	3.03720	73.00%	13.00%		3.00%	12.00%	F1. C I	3.03803	88.00%	12.00%			
C1 base I	3.03589	82.00%	11.00%			7.00%	F1. D I	3.03653	65.00%	5.00%		19.00%	12.00%
C1 topo I	3.03988	86.00%	12.00%		2.00%		F1. E I	3.03589	79.00%	7.00%		4.00%	10.00%
C2 base I	3.03871	92.00%	8.00%				F2. A	3.03709	88.00%	7.00%		4.00%	1.00%
C2 base II	3.03971	58.00%	12.00%			30.00%	H I	3.03736	62.00%	15.00%		19.00%	4.00%
C2 topo I	3.03844	60.00%	10.00%	21.00%	1.00%	8.00%	H II	3.03803	95.00%	5.00%			

Table VII: Main oxides composition

Sample ID	CaO (%)	MgO (%)	SiO2 (%)	Al2O3 (%)	Fe2O3 (%)	Na2O (%)	K2O (%)	TiO2 (%)	MnO (%)	P2O5 (%)	LOI(%)	Total (%)
A1 I	53.33	0.22	0.51	0.10	2.51	0.07	0.02	0.01	0.46	0.01	41.60	99.57
A1 II	50.73	0.34	2.39	0.52	3.51	0.17	0.10	0.04	0.40	0.02	40.13	99.30
A2 I	50.65	0.30	1.63	0.33	5.00	0.11	0.06	0.02	0.44	0.02	39.95	99.53
A2 II	50.92	0.32	1.83	0.36	3.48	0.15	0.07	0.02	0.43	0.02	40.50	99.06
A2 III	40.87	0.55	3.74	1.03	17.65	0.14	0.15	0.06	0.21	0.06	33.97	100.48
A3 I	50.15	0.33	1.57	0.37	3.85	0.14	0.07	0.03	0.74	0.07	39.67	97.97
A3 II	50.34	0.32	1.50	0.30	4.54	0.06	0.06	0.02	0.48	0.08	40.17	98.79
A4 I	48.95	0.30	1.37	0.27	7.74	0.00	0.04	0.02	0.60	0.01	40.02	100.42
B1 I	52.69	0.21	0.26	0.04	4.30	0.00	0.01	0.01	0.30	< 0,01	41.29	99.88
B2 I	52.24	0.47	1.94	0.40	0.62	0.27	0.09	0.03	0.14	0.01	40.65	98.03
B2 II	52.03	0.40	1.67	0.42	1.02	0.26	0.09	0.02	0.22	0.03	41.15	98.34
B3 I	53.05	0.35	1.18	0.28	0.92	0.18	0.06	0.02	0.17	0.02	41.95	98.99
B3 II	50.14	0.47	5.10	1.10	0.67	0.30	0.21	0.05	0.11	0.19	40.13	99.27
C1 gral. I	53.06	0.49	2.76	0.42	0.28	0.17	0.09	0.03	0.09	0.01	41.73	99.66
C1 base I	52.39	0.40	3.16	0.76	0.81	0.18	0.12	0.04	0.14	0.02	41.30	99.80
C1 topo I	50.93	0.56	4.85	0.69	0.41	0.23	0.14	0.03	0.10	0.01	40.47	99.08
C2 base I	51.98	0.63	2.43	0.24	0.30	0.26	0.07	0.02	0.07	0.01	42.16	98.96
C2 base II	50.86	0.64	3.53	0.16	0.29	0.50	0.10	0.01	0.07	0.01	41.64	98.83
C2 topo I	49.53	1.27	5.03	0.61	0.33	0.28	0.13	0.03	0.11	< 0,01	39.81	98.32
C2 Topo II	50.01	0.74	5.56	1.17	0.48	0.33	0.21	0.06	0.06	0.01	39.55	98.96
C2 Topo III	50.30	0.65	5.17	1.09	0.70	0.23	0.22	0.06	0.14	0.07	40.22	99.32
D1 I	50.59	0.60	3.74	0.50	1.16	0.24	0.12	0.03	0.10	0.02	40.49	98.54
D1 II	51.07	0.60	4.62	1.09	0.42	0.31	0.18	0.06	0.07	0.03	40.58	99.53
D2 I	54.04	0.29	0.96	0.22	0.83	0.05	0.03	0.01	0.22	0.01	42.90	99.97
D3 I	54.02	0.39	0.73	0.12	0.15	0.12	0.04	0.02	0.00	0.03	42.76	98.82
D3 II	53.94	0.36	0.69	0.08	0.20	0.14	0.05	0.02	0.14	0.04	42.67	98.82
D4 I	53.65	0.36	0.87	0.07	1.31	0.14	0.07	0.02	0.28	0.05	42.63	99.79
D5 I	47.96	0.74	6.53	1.61	1.24	0.33	0.30	0.09	0.15	0.08	38.91	98.61
E I	53.68	0.28	1.46	0.31	0.56	0.13	0.07	0.03	0.15	0.05	42.30	99.34
E II	53.17	0.24	0.99	0.07	1.53	0.07	0.05	0.02	0.31	0.04	42.26	99.10
F1.A I	51.65	0.22	3.98	0.61	0.41	0.66	0.15	0.04	0.05	0.05	41.69	99.71
F1. B I	50.50	0.32	4.99	0.88	0.63	0.53	0.19	0.05	0.13	0.04	40.84	99.40
F1. C I	53.50	0.43	1.16	0.06	0.30	0.17	0.05	0.02	0.04	0.05	43.29	99.39
F1. D I	42.98	0.39	14.91	3.39	0.90	0.68	0.44	0.16	0.04	0.05	34.62	98.73
F1. E I	48.51	0.46	7.80	1.49	0.68	0.34	0.21	0.09	0.09	0.06	39.07	99.07
F2. A	49.83	0.53	5.77	1.39	0.80	0.28	0.21	0.11	0.02	0.05	39.15	98.51
H I	50.68	0.40	5.03	1.20	0.40	0.30	0.19	0.06	0.01	0.03	40.23	98.90
H II	54.95	0.33	0.47	< 0.01	0.03	0.07	0.01	0.01	0.01	0.02	43.22	99.41

Table VIII: Trace elements composition

Sample ID	Ba (ppm)	Ce (ppm)	Cu (ppm)	La (ppm)	Nb (ppm)	Nd (ppm)	s-Pb (ppm)	Rb (ppm)	S (ppm)	Sr (ppm)	V (ppm)	Y (ppm)	Zn (ppm)	Zr (ppm)
A1 I	52	< 55	14	< 41	9	< 52	3131	< 4	2114	1818	11	7	111	18
A1 II	82	< 55	20	< 41	< 3	< 52	3866	< 4	3203	2000	19	< 5	151	18
A2 I	86	< 55	34	< 41	13	< 52	5367	6	2610	1889	8	6	139	22
A2 II	93	< 55	19	< 41	< 3	< 52	3699	< 4	3558	2089	22	6	123	21
A2 III	82	< 55	26	< 41	42	< 52	16996	< 4	2041	723	15	39	348	37
A3 I	129	< 55	30	< 41	12	< 52	4520	36	3262	1874	< 7	1	157	21
A3 II	98	< 55	82	< 41	32	< 52	5069	149	2089	1346	< 7	< 5	132	30
A4 I	85	< 55	22	< 41	26	< 52	8457	< 4	1089	1063	17	19	196	26
B1 I	49	< 55	18	< 41	25	< 52	4852	< 4	1641	1161	8	10	110	25
B2 I	65	< 55	6	< 41	< 3	< 52	703	< 4	7264	3685	7	2	25	14
B2 II	61	< 55	19	< 41	< 3	< 52	1123	< 4	5716	3321	20	< 5	45	16
B3 I	56	< 55	11	< 41	< 3	< 52	897	< 4	4330	2716	7	7	43	15
B3 II	77	< 55	12	< 41	< 3	< 52	381	18	4619	2754	10	< 5	29	18
C1 gral. I	64	< 55	8	< 41	< 3	< 52	193	< 4	2621	2531	< 7	< 5	19	17
C1 base I	63	< 55	6	< 41	3	< 52	501	11	2386	1773	< 7	< 5	24	25
C1 topo I	61	< 55	6	< 41	< 3	< 52	289	5	3214	3045	8	< 5	19	18
C2 base I	53	< 55	8	< 41	< 3	< 52	310	16	3581	3952	9	< 5	14	9
C2 base II	67	< 55	7	< 41	< 3	< 52	362	7	4544	5260	< 7	< 5	12	< 6
C2 topo I	77	< 55	4	< 41	< 3	< 52	118	< 4	4901	6875	18	< 5	14	< 6
C2 Topo II	83	< 55	5	< 41	< 3	< 52	120	< 4	3987	3594	< 7	9	17	13
C2 Topo III	87	< 55	18	44	6	< 52	341	10	2431	1759	16	< 5	25	22
D1 I	90	< 55	22	< 41	< 3	< 52	935	18	4874	3374	9	< 5	27	10
D1 II	76	< 55	10	< 41	6	< 52	145	26	2808	2040	< 7	< 5	19	24
D2 I	50	< 55	21	< 41	14	< 52	820	52	1695	1238	12	< 5	44	22
D3 I	26	< 55	10	< 41	6	< 52	121	236	2595	1425	9	< 5	12	21
D3 II	45	< 55	87	48	11	< 52	155	321	2716	1446	18	< 5	196	17
D4 I	69	< 55	29	< 41	23	< 52	1264	272	854	729	17	< 5	67	25
D5 I	94	< 55	20	< 41	< 3	< 52	462	359	3722	2200	16	< 5	41	28
E I	47	< 55	15	< 41	16	< 52	361	209	1777	915	9	< 5	33	21
E II	68	< 55	18	44	16	< 52	1409	336	965	614	10	< 5	59	21
F1.A I	29	< 55	11	< 41	16	< 52	47	359	1041	458	18	< 5	30	30
F1. B I	48	< 55	15	< 41	19	< 52	82	300	1796	615	32	< 5	43	33
F1. C I	29	< 55	13	< 41	< 3	< 52	92	281	1599	1335	< 7	< 5	25	18
F1. D I	101	< 55	43	< 41	23	< 52	100	223	834	486	34	< 5	52	42
F1. E I	64	< 55	11	< 41	16	< 52	143	329	1334	950	< 7	< 5	40	34
F2. A	49	< 55	75	< 41	10	< 52	249	281	1973	1052	28	< 5	23	31
H I	38	< 55	13	< 41	13	< 52	100	158	2263	1163	24	< 5	43	31
H II	< 20	< 55	8	< 41	12	< 52	94	204	2155	1179	9	< 5	24	18

Table IX: Sr/Ca relation of the samples.

Samples	Sr/Ca	Samples	Sr/Ca
A1 I	0.004770	C2 Topo II	0.010056
A1 II	0.005517	C2 Topo III	0.004893
A2 I	0.005219	D1 I	0.009332
A2 II	0.005741	D1 II	0.005590
A2 III	0.002475	D2 I	0.003206
A3 I	0.005229	D3 I	0.003691
A3 II	0.003741	D3 II	0.003751
A4 I	0.003039	D4 I	0.001901
B1 I	0.003083	D5 I	0.006419
B2 I	0.009871	E I	0.002385
B2 II	0.008932	E II	0.001616
B3 I	0.007164	F1.A I	0.001241
B3 II	0.007686	F1. B I	0.001704
C1 gral. I	0.006675	F1. C I	0.003492
C1 base I	0.004736	F1. D I	0.001582
C1 topo I	0.008366	F1. E I	0.002740
C2 base I	0.010639	F2. A	0.002954
C2 base II	0.014472	H I	0.003211
C2 topo I	0.019423	H II	0.003002

FIGURES

Figure 1

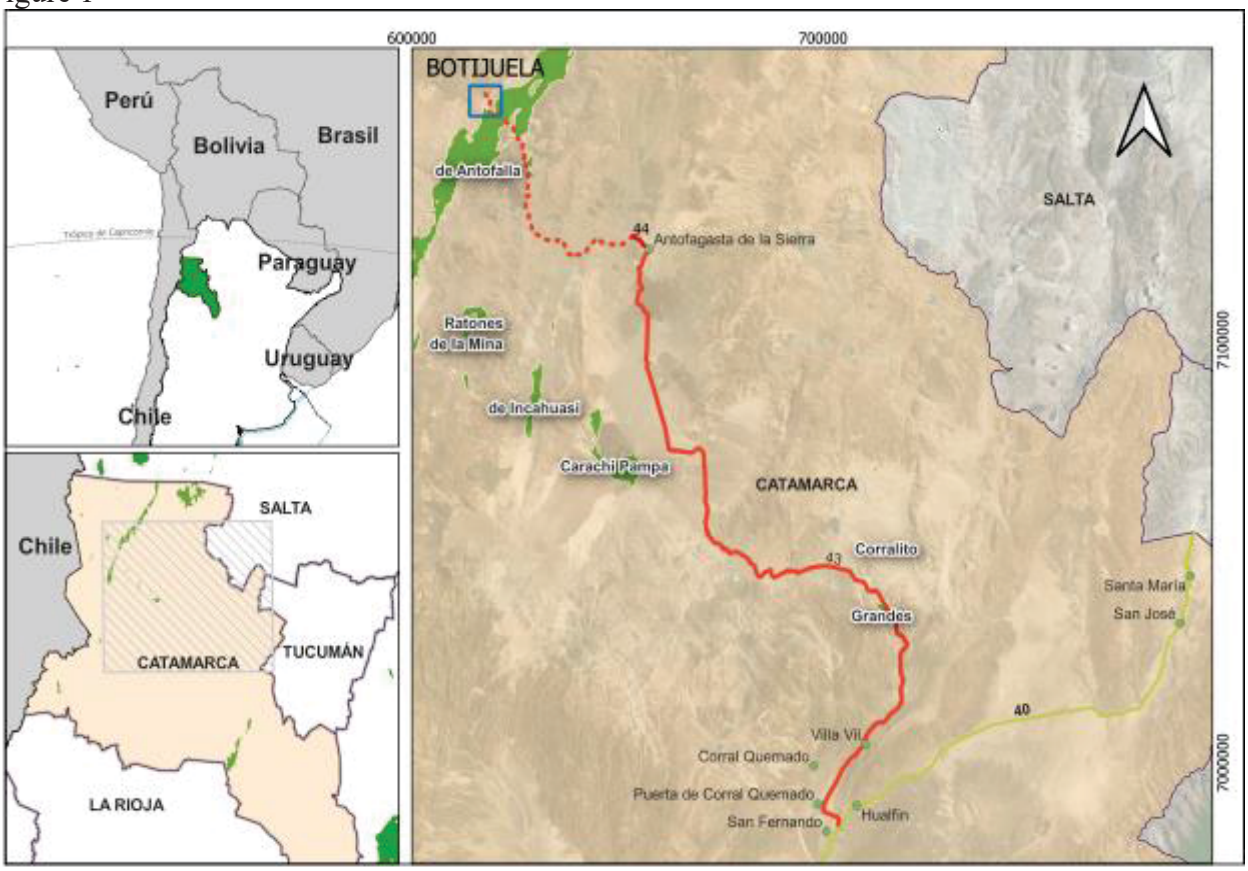

Figure 2

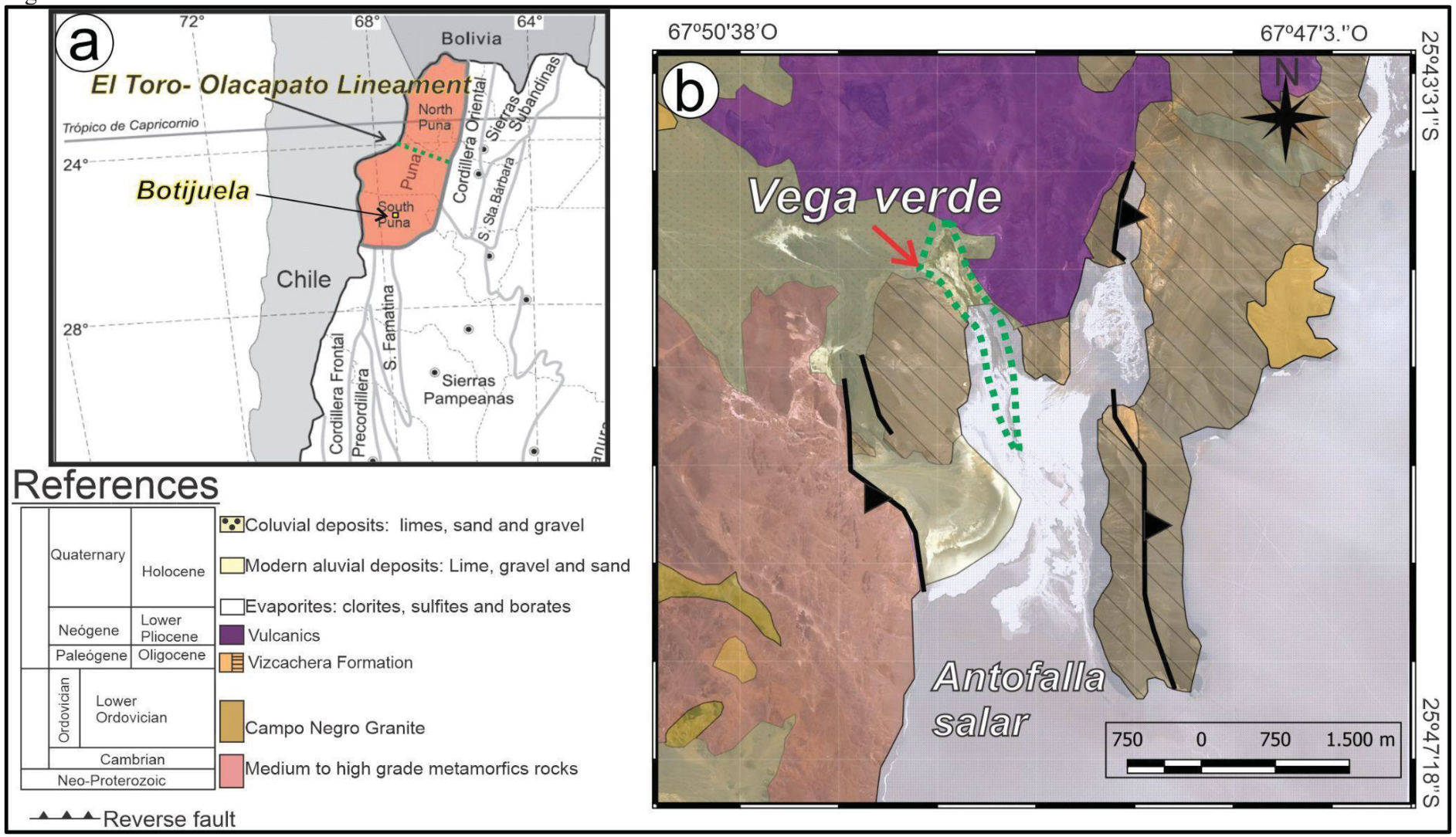
a
72°
68°
64°
Bolivia
El Toro- Olacapato Lineament
Trópico de Capricornio
24°
Botijuela
North Puna
South Puna
Puna
Cordillera Oriental
Sierras Subandinas
S. Sta Bárbara
Chile
28°
Cordillera Frontal
Precordillera
S. Famatina
Sierras Pampeanas
b
67°50'38'O
67°47'3.''O
25°43'31''S
25°47'18''S
N
Vega verde
Antofalla salar
750 0 750 1.500 m
References
Quaternary
Holocene
Neógene
Lower Pliocene
Paleógene
Oligocene
Ordovician
Lower Ordovician
Cambrian
Neo-Proterozoic
Coluvial deposits: limes, sand and gravel
Modern aluvial deposits: Lime, gravel and sand
Evaporites: clorites, sulfites and borates
Vulcanics
Vizcachera Formation
Campo Negro Granite
Medium to high grade metamorfics rocks
Reverse fault

Figure 3

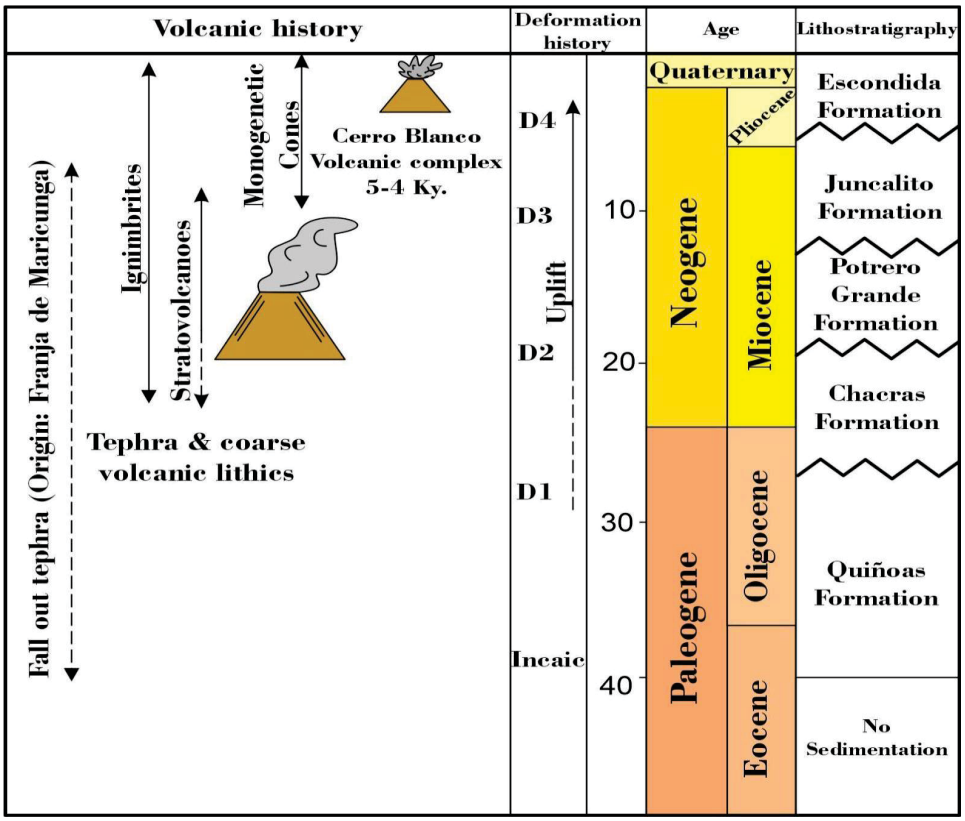

Figure 4

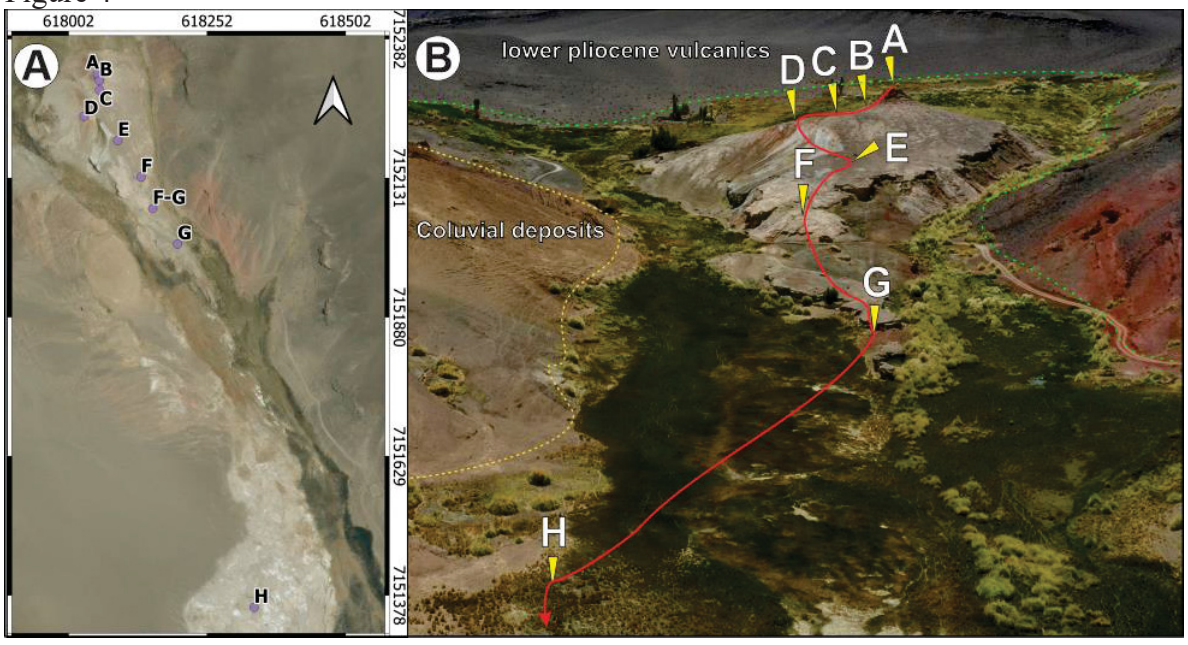

Figure 5

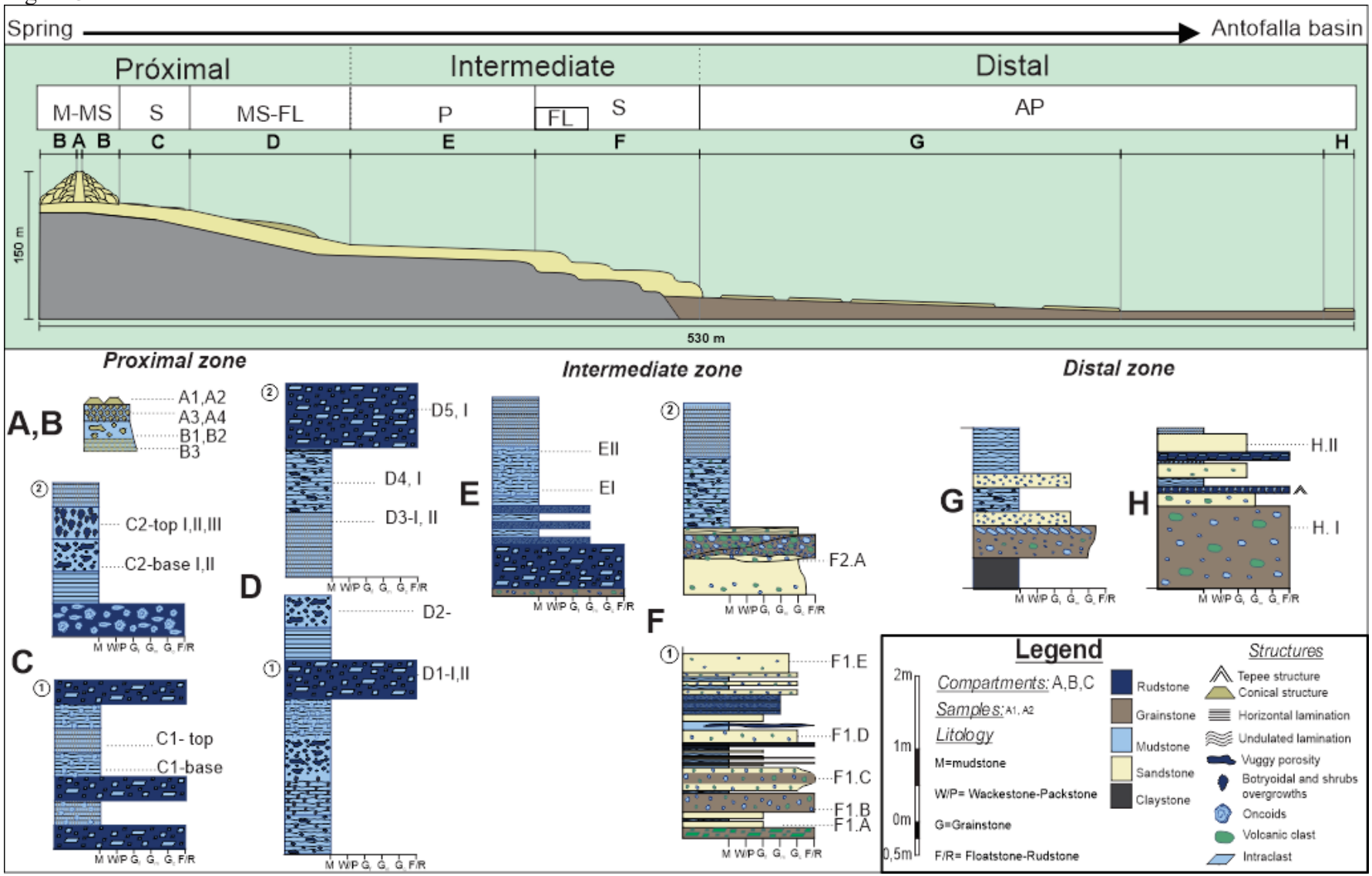
Spring
Antofalla basin
Próximal
Intermediate
Distal
M-MS
S
MS-FL
P
FL
S
AP
B A B
C
D
E
F
G
H
150 m
530 m
Proximal zone
Intermediate zone
Distal zone
A,B
A1,A2
A3,A4
B1,B2
B3
C2-top I,II,III
C2-base I,II
C
C1- top
C1-base
D
D5, I
D4, I
D3-I, II
D2-
D1-I,II
E
EII
EI
F
F2.A
F1.E
F1.D
F1.C
F1.B
F1.A
G
H
H.II
H. I
M W/P G, G, G, F/R
Legend
Compartments: A,B,C
Samples: A1, A2
Litology
M=mudstone
W/P= Wackestone-Packstone
G=Grainstone
F/R= Floatstone-Rudstone
2m
1m
0m
0,5m
Rudstone
Grainstone
Mudstone
Sandstone
Claystone
Structures
Tepee structure
Conical structure
Horizontal lamination
Undulated lamination
Vuggy porosity
Botryoidal and shrubs overgrowths
Oncoids
Volcanic clast
Intraclast

Figura 6

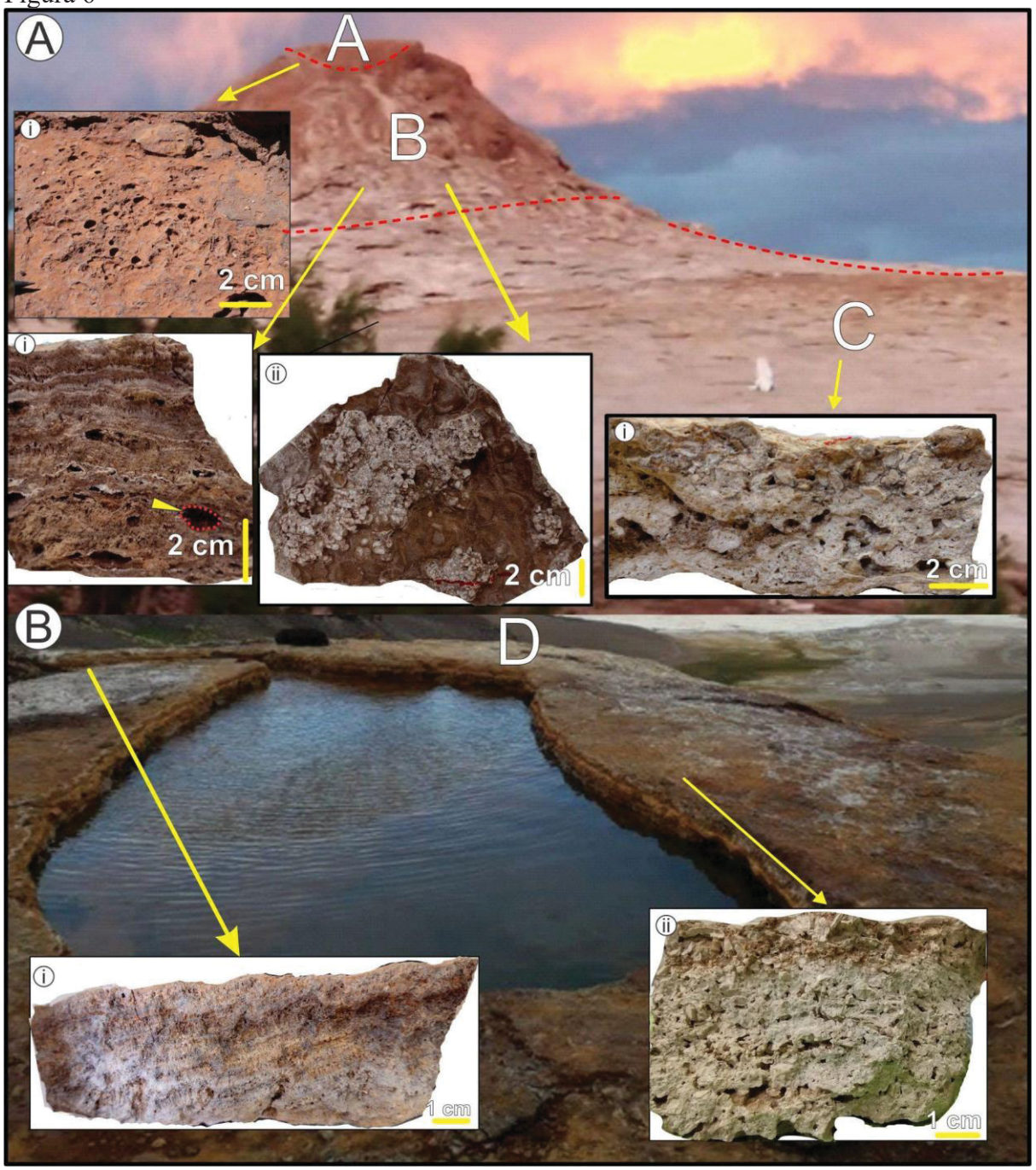

Figure 7

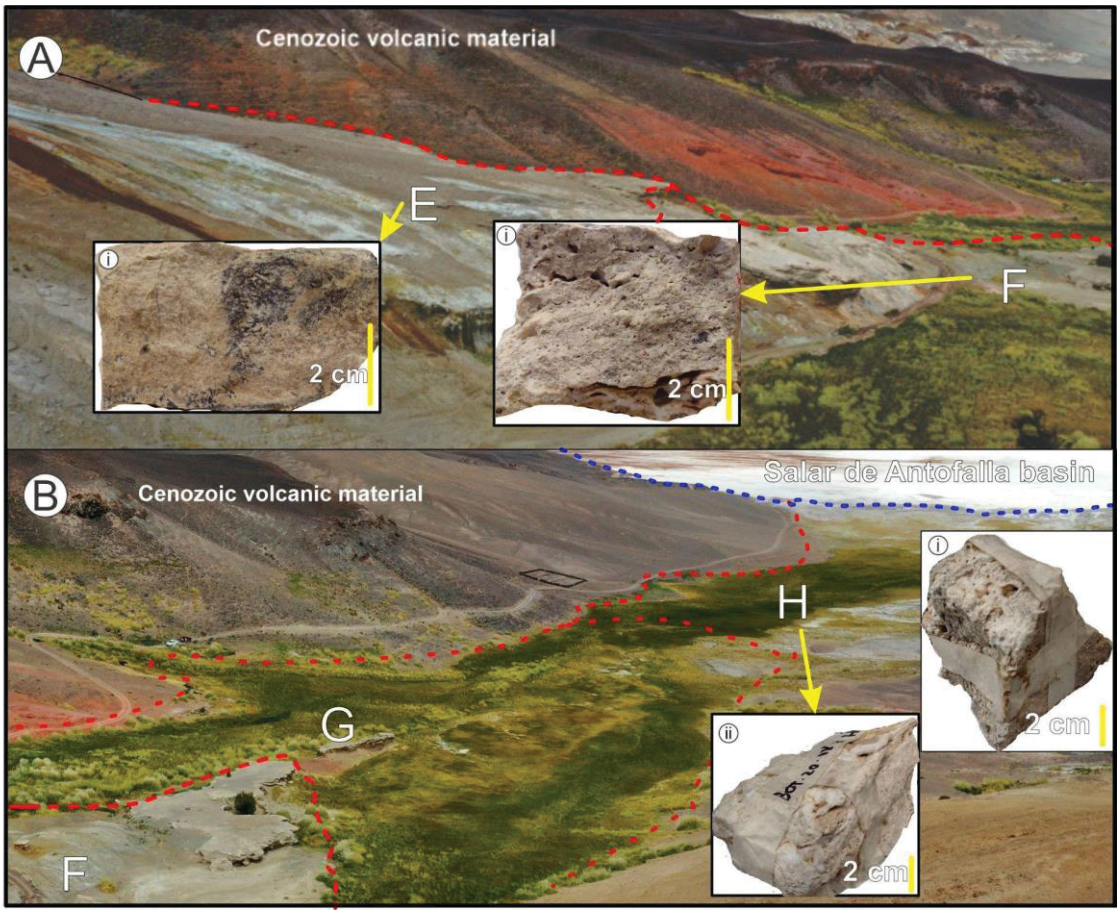
A
Cenozoic volcanic material
E
F
2 cm
2 cm
B
Cenozoic volcanic material
Salar de Antofalla basin
H
G
F
2 cm
2 cm

Figure 8

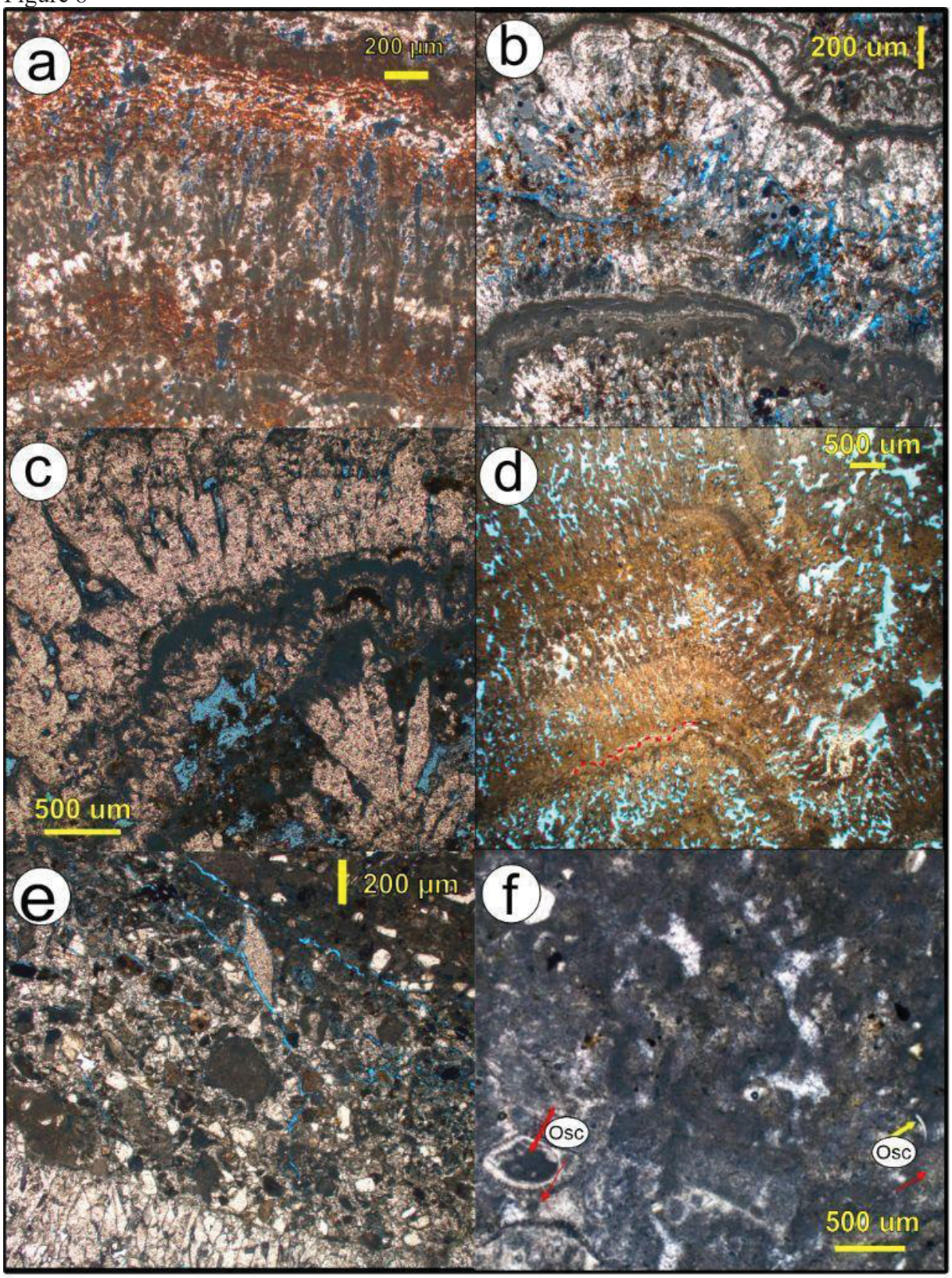

Figure 9

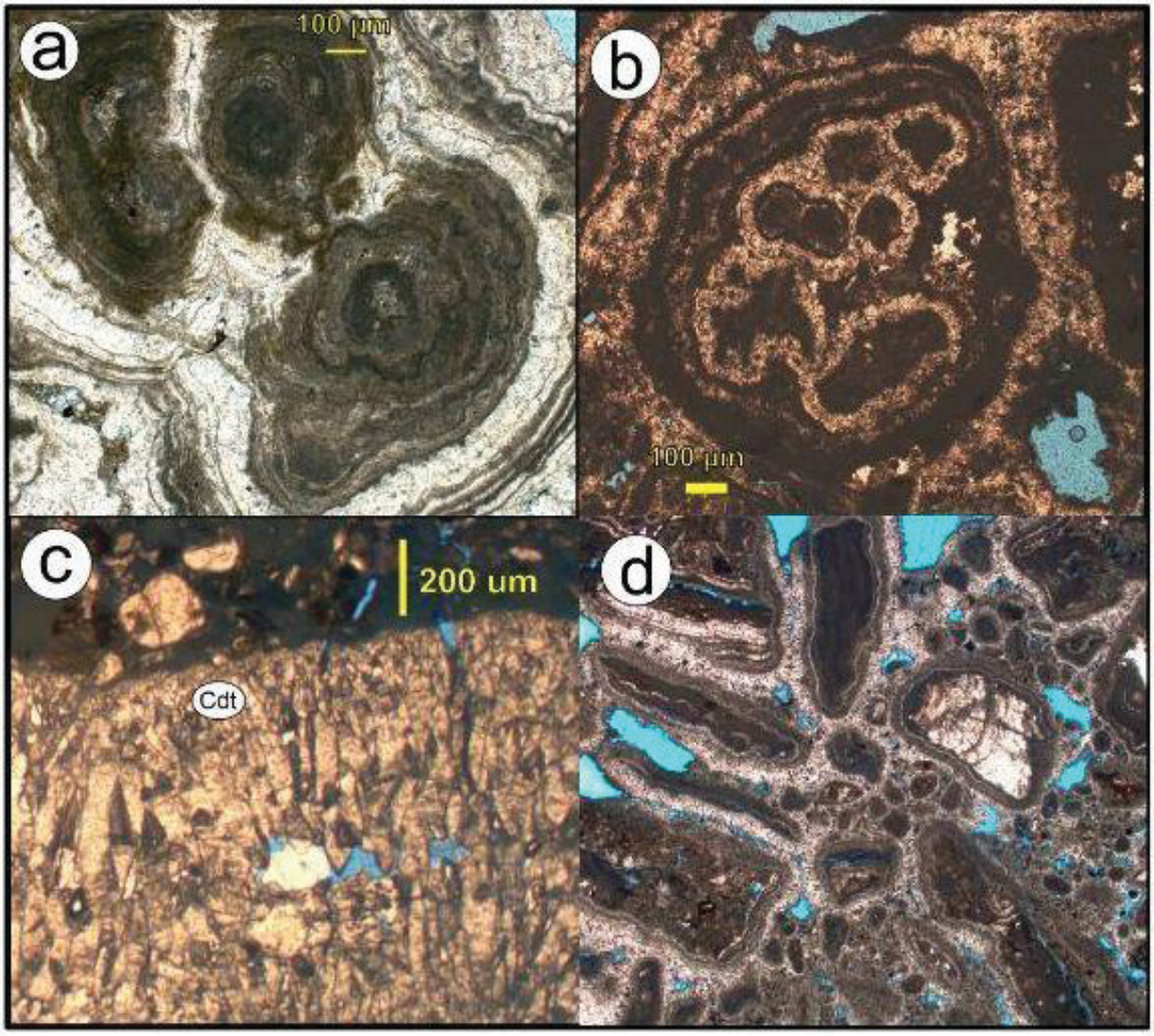

Figure 10

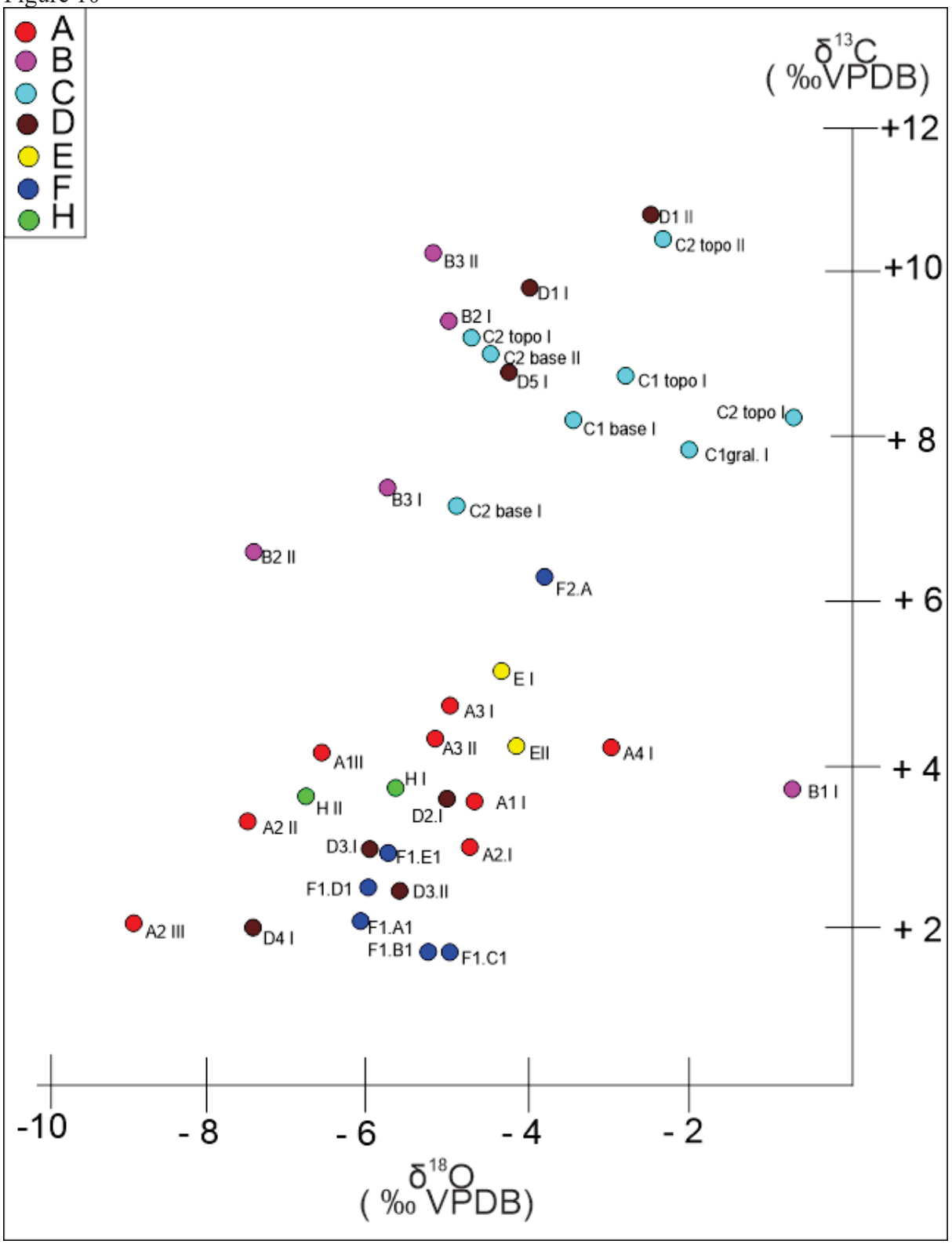
A
B
C
D
E
F
H
δ13C
(‰VPDB)
+12
+10
+ 8
+ 6
+ 4
+ 2
D1 II
C2 topo II
B3 II
D1 I
B2 I
C2 topo I
C2 base II
D5 I
C1 topo I
C2 topo I
C1 base I
C1gral. I
B3 I
C2 base I
B2 II
F2.A
E I
A3 I
A3 II
EII
A4 I
A1III
H I
H II
A1 I
D2.I
A2 II
D3.I
F1.E1
A2.I
F1.D1
D3.II
A2 III
D4 I
F1.A1
F1.B1
F1.C1
B1 I
-10
- 8
- 6
- 4
- 2
δ18O
(‰ VPDB)

Figure 11

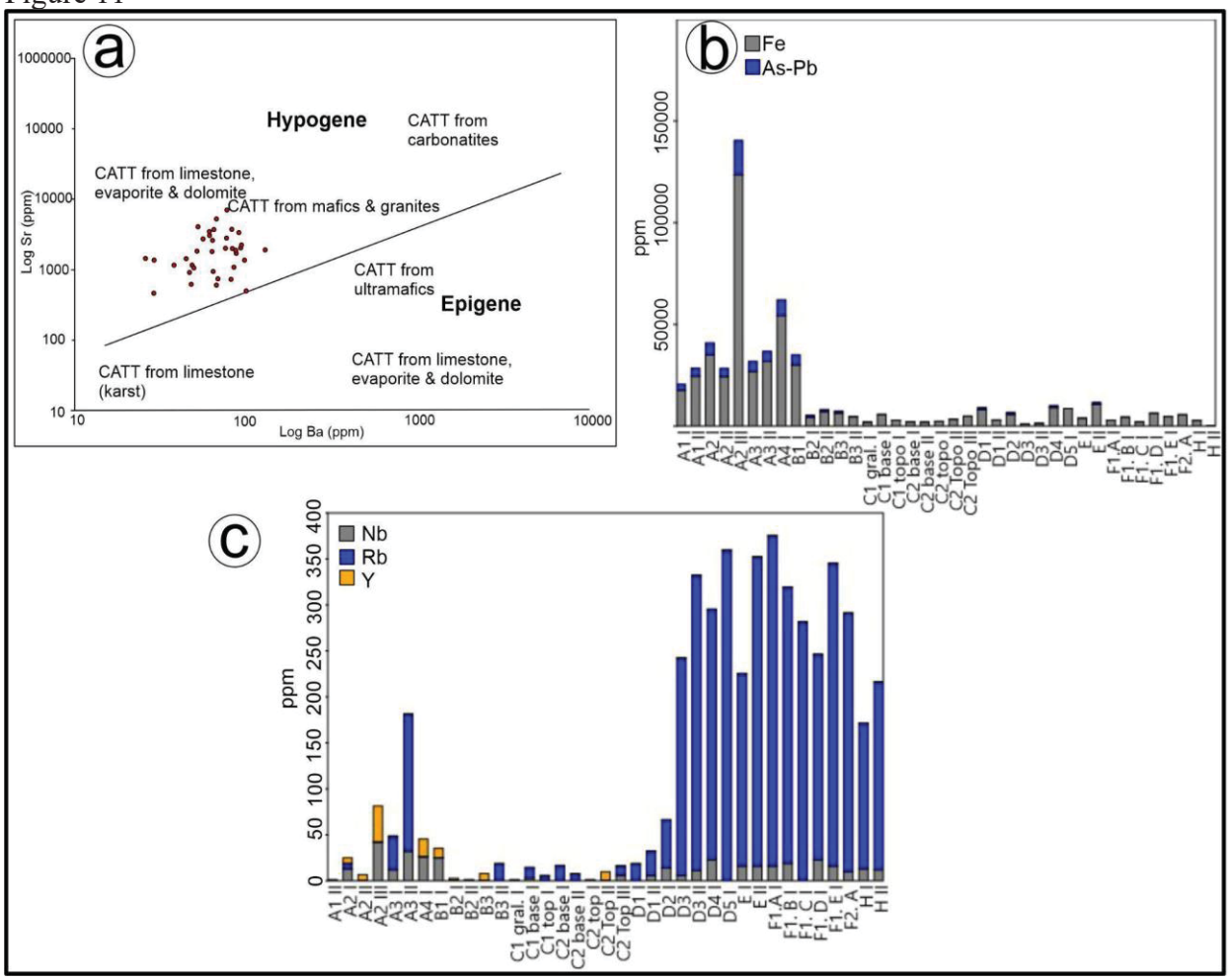
a
1000000
10000
1000
100
10
Log Sr (ppm)
10000
10
100
1000
10000
Log Ba (ppm)
Hypogene
CATT from carbonatites
CATT from limestone, evaporite & dolomite
CATT from mafics & granites
CATT from ultramafics
Epigene
CATT from limestone (karst)
CATT from limestone, evaporite & dolomite
b
Fe
As-Pb
ppm
150000
100000
50000
A1 II
A1 I
A2 I
A2 II
A2 III
A3 I
A3 II
A4 I
B1 I
B2 I
B2 II
B3 I
B3 II
C1 gral. I
C1 base I
C1 topo I
C2 base I
C2 base II
C2 topo I
C2 Topo II
C2 Topo III
D1 I
D1 II
D2 I
D3 I
D3 II
D4 I
D5 I
E I
E II
F1.A I
F1. B I
F1. C I
F1. D I
F1. E I
F2. A
H I
H II
c
Nb
Rb
Y
ppm
400
350
300
250
200
150
100
50
0
A1 II
A2 I
A2 II
A2 III
A3 I
A3 II
A4 I
B1 I
B2 I
B2 II
B3 I
B3 II
C1 gral. I
C1 base I
C1 top I
C2 base I
C2 base II
C2 top I
C2 Top II
C2 Top III
D1 I
D1 II
D2 I
D3 I
D3 II
D4 I
D5 I
E I
E II
F1.A I
F1. B I
F1. C I
F1. D I
F1. E I
F2. A
H I
H II

4. CONCLUSIONS

8 different geomorphologycal compartments from A to H was defined based in the slope and its sedimentary features. Facies recognized in the system are: geyserites, autochtonous limestone with fossils, bafflestone, rudstone, grainstone, rudstone, laminated mudstones and crenulated mudstones. Isotopical data of C and O and Sr / Ba relation revealed a hydrothermal origin. Composition data shows a pattern where certain group of elements are concentrated in the mound and other in the distal area. Mineralogical data shows that the system is main composed by calcite and Mg- bearing calcite.

The sedimentology, geomorphology, petrography, and geochemistry of the Vega Verde system were addressed. This set of data suggests that the development of this system is strongly linked to hydrothermalism. As we move away from the main source, the influence of different sedimentary events that generate deposits of mixed character starts to take on greater relevance. Authors like Gandin and Cappezuoli (2014), Mancini et al. (2019), and Minissale (2002) have discussed the tendency of the travertine system to have more siliciclastic facies at the intermediate and distal areas. As an additional appreciation, these systems are very open and susceptible to tectonic and chemical changes so, many times the springs that provide the water to build the carbonate system can be activated or deactivated. Although the Vega Verde travertines present characteristic facies for each depositional geomorphological compartment, the great variability of facies may overlap laterally and these only facies assembly would not allow to build and define a precise facies model for similar systems.

Among the set of results, we obtained from the analyzed data, we found different and diverse targets but undoubtedly one of the most important is the distinction and recognition of the geyserite facies that constitutes the remnant in the record of the main hydrothermal source. This important sector was recognized both in geomorphology, sedimentology and geochemistry. The geyserite facies are unique in the travertine system and geochemically they are marked by a strong imprint that is denoted by the high concentration of metals and arsenic that were stored in this sector. With this in account we suggest that geyserites facies could bring potential proxies to paleoenvironmental reconstruction in other fossil systems.

The behavior of silica in the system is under study. The origin of the Si-rich solution in the spring could be related both to the volcanic area and to the dissolution of the high content of siliciclastic formations that lies under the travertine system as exposed in the distal area. Its precipitation in the hydrothermal vent nearby the spring and then post-precipitation in distal zones may be related to pH changes in the fluid as well as to other inorganic and organic factors.

No data were found that allow us to establish defined limits for where a tufa system begins, so we prefer to keep the term of this system as a hydrothermal sedimentary travertine system. Future researches together with data from Sr and REE reconnaissance, will make it possible to accurately define the origin of the water and the influence of organic and inorganic processes.

5. REFERENCES

ALONSO, R. N.; ROJAS, W. Origin and Evolution of the Central Andes: Deserts, Salars, Lakes, and Volcanoes. **Microbial Ecosystems in Central Andes Extreme Environments**. p.3–19, 2020. Springer International Publishing.

ALONSO, R. N.; GUTIÉRREZ, R.; VIRAMONTE, J. Puna Austral—bases para el subprovincialismo geológico de la Puna Argentina: Asociación Geológica Argentina, **9th Congreso Geológico Argentino**, Bariloche, , p. 43-63,1984. *Actas*, vol. 1.

ALONSO, R. N.; BOOKHAGEN, B.; CARRAPA, B.; et al. Tectonics, Climate, and Landscape Evolution of the Southern Central Andes: the Argentine Puna Plateau and Adjacent Regions between 22 and 30°S. **The Andes**, n. January 2006, p. 265–283, 2006.

BÁEZ, W.; ARNOSIO, M.; CHIODI, A.; et al. Estratigrafia y evolucion del complejo volcanico Cerro Balnco Puna austral Argentina. **Revista mexicana de ciencias geologicas**, v. 32, n. 1, p. 29–49, 2015. Disponível em: <http://www.scielo.org.mx/scielo.php?pid=S1026-87742015000100004&script=sci_arttext&tlng=pt>. .

BATES, R. L.; JACKSON, J. A. **Glossary of geology: American geological institute**. Falls Church, Virginia: American Geological Institute, 1987.

BISSE, S. B.; EKOKO, B. E.; GERBER, J.; EKOMANE, E.; FRANCHI, F. Influence of biotic vs abiotic processes on the genesis of non-marine carbonates along the Cameroon Volcanic Line (Cameroon) and palaeofluid provenance. **Depositional Record**, v. 8, n. 1, p. 102–126, 2022.

BRAISSANT, O.; DECHO, A. W.; DUPRAZ, C.; et al. Exopolymeric substances of sulfate-reducing bacteria: Interactions with calcium at alkaline pH and implication for formation of carbonate minerals. **Geobiology**, v. 5, n. 4, p. 401–411, 2007.

BROGI, A.; CAPEZZUOLI, E.; AQUÉ, R.; BRANCA, M.; VOLTAGGIO, M. Studying travertines for neotectonics investigations: Middle-Late Pleistocene syn-tectonic travertine deposition at Serre di Rapolano (Northern Apennines, Italy). **International Journal of Earth Sciences**, v. 99, n. 6, p. 1383–1398, 2010.

CAHILL, T.; ISACKS, B. L. Seismicity and shape of the subducted Nazca Plate. **Journal of Geophysical Research**, v. 97, n. B12, 1992.

CAPEZZUOLI, E.; GANDIN, A.; PEDLEY, M. Decoding tufa and travertine (fresh water carbonates) in the sedimentary record: The state of the art. **Sedimentology**, v. 61, n. 1, p. 1–21, 2014.

CARRAPA, B.; ADELMANN, D.; HILLEY, G. E.; et al. Oligocene range uplift

and development of plateau morphology in the southern central Andes. **Tectonics**, v. 24, n. 4, p. 1–19, 2005.

CHAFETZ, H. S.; GUIDRY, S. A. Bacterial shrubs, crystal shrubs, and ray-crystal shrubs: bacterial vs. abiotic precipitation. **Sedimentary Geology**, v. 126, n. 1–4, p. 57–74, 1999. Disponível em: <https://www.sciencedirect.com/science/article/pii/S0037073899000329?casa_token=l3VbAbiO9dsAAAAA:eq0_0_liZREEurYI5YbMu9lndCxZ4e_qPwFhlQWxQU5437dgIBigUdBYmmqdoyhnpqDX8VODuuk>. Acesso em: 24/6/2022.

CHAFETZ, H. S.; RUSH, P. F.; UTECH, N. M. Microenvironmental Controls on Mineralogy and Habitof CaCO3 Precipitates An Example from an Active Travertine System.pdf. **Sedimentology**, 1991.

CHANG, R. *Fundamentos de química*. McGraw-Hill. 1174pp. Mexico 2011

CLAES, H.; HUYSMANS, M.; SOETE, J.; et al. Elemental geochemistry to complement stable isotope data of fossil travertine: Importance of digestion method and statistics. **Sedimentary Geology**, v. 386, p. 118–131, 2019. Elsevier B.V. Disponível em: <https://doi.org/10.1016/j.sedgeo.2019.04.002>.

CLARKE, R. W. The data of geochemistry 3d edition. **Bolletin of USA geological survey**. p.821, 1916. Disponível em: <https://scholar.google.com/scholar?hl=es&as_sdt=0%2C5&q=CLARKE%2C+R.+W.+The+data+of+geochemistry+3d+edition.+US+Geological+Survey+Bulletin%2C+616p%2C+821.+1916&btnG=>. Acesso em: 24/6/2022.

DELLA PORTA, G.; HOPPERT, M.; HALLMANN, C.; SCHNEIDER, D.; REITNER, J. The influence of microbial mats on travertine precipitation in active hydrothermal systems (Central Italy). **Depositional Record**, v. 8, n. 1, p. 165–209, 2022.

DELLA PORTA, G.; CAPEZZUOLI, E.; DE BERNARDO, A. Facies character and depositional architecture of hydrothermal travertine slope aprons (Pleistocene, Acquasanta Terme, Central Italy). **Marine and Petroleum Geology**, v. 87, p. 171–187, 2017. Elsevier Ltd. Disponível em: <http://dx.doi.org/10.1016/j.marpetgeo.2017.03.014>.

DELLA PORTA, G. Carbonate build-ups in lacustrine, hydrothermal and fluvial settings: Comparing depositional geometry, fabric types and geochemical signature. **Geological Society Special Publication**, v. 418, n. 1, p. 17–68, 2015.

DUNHAM, R. J. Classification of Carbonate Rocks According to Depositional Textures. Classification of Carbonate Rocks--A Symposium. **Memorials of American Asociation of Petroleum Geologist**,1 . p.108–121, 1962. Tulsa, Oklahoma. . Disponível em: <https://archives.datapages.com/data/specpubs/carbona2/data/a038/a038/0001/0100/0108.html>. Acesso em: 24/6/2022.

DUPRAZ, C.; REID, R. P.; BRAISSANT, O.; et al. Processes of carbonate precipitation in modern microbial mats. **Earth-Science Reviews**, v. 96, n. 3, p. 141–162, 2009. Elsevier.

EMIG, W. H. The travertine deposits of the Arbuckle Mountains Oklahoma, with reference to the plant agencies concerned in their formation. **Bulletin Oklahoma Geological Survey**, v. 29, p. 9–75, 1917. Disponível em: <https://scholar.google.com/scholar?hl=es&as_sdt=0%2C5&q=Emig%2C+W.+H.+%281917%29.+Travertine+deposits+of+Oklahoma.+Oklahoma+Geological+Survey.&btnG=>. Acesso em: 24/6/2022.

EMBRY, A. F.; KLOVAN, E. J. The Upper Devonian stratigraphy of northeastern Banlts Island has. **Bulletin of Canadian Petroleum Geology**, v. 19, n. 4, p. 730–781, 1971.
FARÍAS, M. E.; POIRÉ, D. G.; ARROUY, M. J.; ALBARRACIN, V. H. Modern Stromatolite Ecosystems at Alkaline and Hypersaline High-Altitude Lakes in the Argentinean Puna. , p. 427–441, 2011.

FOLK, R. L. Interaction Between Bacteria, Nannobacteria, and Mineral Precipitation in Hot Springs of Central Italy. **Géographie physique et Quaternaire**, v. 48, n. 3, p. 233–246, 2007. Disponível em: <https://www.erudit.org/en/journals/gpq/1900-v1-n1-gpq1907/033005ar/abstract/>. Acesso em: 24/6/2022.

FOLK, R. L. Interaction Between Bacteria, Nannobacteria, and Mineral Precipitation in Hot Springs of Central Italy. **Géographie physique et Quaternaire**, v. 48, n. 3, p. 233–246, 2007. Disponível em: <https://www.erudit.org/en/journals/gpq/1900-v1-n1-gpq1907/033005ar/abstract/>. Acesso em: 24/6/2022.

FLÜGEL, E. **Microfacies of Carbonate Rocks**. Berlin: Springer, 2010.

FOLK, R. L. Interaction Between Bacteria, Nannobacteria, and Mineral Precipitation in Hot Springs of Central Italy. **Géographie physique et Quaternaire**, v. 48, n. 3, p. 233–246, 2007. Disponível em: <https://www.erudit.org/en/journals/gpq/1900-v1-n1-gpq1907/033005ar/abstract/>. Acesso em: 24/6/2022.

FOLK, R. L. Spectral subdivision of limestone types. (W. E. Ham, Org.)**Bulletin of the American Association of Petroleum Geologists**, 1. jan. 1962. American Association of Petroleum Geologists.

FORD, T. D.; PEDLEY, H. M. A review of tufa and travertine deposits of the world. **Earth-Science Reviews**, v. 41, n. 3–4, p. 117–175, 1996.

FOUKE, B. W.; FARMER, J. D.; DES MARAIS, D. J.; et al. Depositional facies and aqueous-solid geochemistry of travertine-depositing hot springs (Angel Terrace, Mammoth Hot Springs, Yellowstone National Park, U.S.A.). **Journal of Sedimentary Research**, v. 70, n. 3, p. 565–585, 2000.

FRANCHI, F.; FRISIA, S. Crystallization pathways in the Great Artesian Basin (Australia) spring mound carbonates: Implications for life signatures on Earth and beyond. **Sedimentology**, v. 67, n. 5, p. 2561–2595, 2020. Blackwell Publishing Ltd.

GANDIN, A.; CAPEZZUOLI, E. Travertine: Distinctive depositional fabrics of carbonates from thermal spring systems. (M. Pedley, Org.)**Sedimentology**, v. 61, n. 1, p. 264–290, 2014. Disponível em: <https://onlinelibrary.wiley.com/doi/10.1111/sed.12087>. .

GIANNI, G. M.; GARCÍA, H. P. A.; PESCE, A.; et al. Oligocene to present shallow subduction beneath the southern Puna plateau. **Tectonophysics**, v. 780, n. January, p. 228402, 2020. Elsevier. Disponível em: <https://doi.org/10.1016/j.tecto.2020.228402>. .

GLOVER, C.; ROBERTSON, A. H. F. Origin of tufa (cool-water carbonate) and related terraces in the Antalya area, SW Turkey. **Geological Journal**, v. 38, n. 3–4, p. 329–358, 2003. John Wiley & Sons, Ltd. Disponível em: <https://onlinelibrary.wiley.com/doi/full/10.1002/gj.959>. Acesso em: 24/6/2022.

GOMEZ, F. J.; MLEWSKI, C.; BOIDI, F. J.; FAŕIAS, M. E.; ǴERARD, E. Calcium carbonate precipitation in diatom-rich microbial mats: The laguna negra hypersaline lake, catamarca, Argentina. **Journal of Sedimentary Research**, v. 88, n. 6, p. 727–742, 2018.

GROVE, C. Submarine hydrothermal vent complexes in the Paleocene of the Faroe-Shetland Basin: Insights from three-dimensional seismic and petrographical data. **Geology**, v. 41, n. 1, p. 71–74, 2013. Disponível em: <https://pubs.geoscienceworld.org/gsa/geology/article-abstract/41/1/71/131050?casa_token=NC6fW9Ol5sAAAAAA:0XDchspKUTlxpys8IMfIs61GXLnKJ5VBTRzMqwT9qtIoBsJ-6tdu5Gc3v64Md4gIVIf0I9X6Zg>. Acesso em: 24/6/2022.

GUO, L.; RIDING, R. Hot-spring travertine facies and sequences, Late Pleistocene, Rapolano Terme, Italy. **Sedimentology**, v. 45, n. 1, p. 163–180, 1998.

GUO, L.; RIDING, R. Rapid facies changes in Holocene fissure ridge hot spring travertines, Rapolano Terme, Italy. **Sedimentology**, v. 46, n. 6, p. 1145–1158, 1999.

GUO, L.; RIDING, R. Origin and diagenesis of Quaternary travertine shrub fabrics, Rapolano Terme, central Italy. **Sedimentology**, v. 41, n. 3, p. 499–520, 1994.

HANCOCK, P. L.; CHALMERS, R. M. L.; ALTUNEL, E.; ÇAKIR, Z. Travitonics: Using travertines in active fault studies. **Journal of Structural Geology**, v. 21, n. 8–9, p. 903–916, 1999. Disponível em: <https://www.sciencedirect.com/science/article/pii/S0191814199000619?casa_token=6goqbGXPCssAAAAA:pH3TciUaGcr3A5uJgpOMuVW3WkC1U_uGpYR0

D5S1SeoTEKx7gZys2ycNfgXy0fXnKYby8Ssmqnw>. Acesso em: 24/6/2022.

HANSEN, D. M.; REDFERN, J.; FEDERICI, F.; DI BIASE, D.; BERTOZZI, G. Miocene igneous activity in the Northern Subbasin, offshore Senegal, NW Africa. **Marine and Petroleum Geology**, v. 25, n. 1, p. 1–15, 2008. Disponível em: <https://www.sciencedirect.com/science/article/pii/S0264817207000529?casa_token=_kPRnSnFX-UAAAAA:m1xj51Df0J4EAA475R2Xs5DvHehpBR_k8P2U5MKqHamymESM1xuabYlvA3ciY2PucrGnzYvII3o>. Acesso em: 24/6/2022.

HANSEN, D. M. The morphology of intrusion-related vent structures and their implications for constraining the timing of intrusive events along the NE Atlantic margin. **Journal of the Geological Society**, v. 163, n. 5, p. 789–800, 2006.

HANSEN, D. M. The morphology of intrusion-related vent structures and their implications for constraining the timing of intrusive events along the NE Atlantic margin. **Journal of the Geological Society**, v. 163, n. 5, p. 789–800, 2006.

JANSSENS, N.; CAPEZZUOLI, E.; CLAES, H.; et al. Fossil travertine system and its palaeofluid provenance, migration and evolution through time: Example from the geothermal area of Acquasanta Terme (Central Italy). **Sedimentary Geology**, v. 398, p. 105580, 2020. Elsevier B.V. Disponível em: <https://doi.org/10.1016/j.sedgeo.2019.105580>.

JONES, B.; RENAUT, R. W. **Chapter 4 Calcareous Spring Deposits in Continental Settings**. Elsevier, 2010.

JONES, F. G.; WILKINSON, B. H. Structure and growth of lacustrine pisoliths from Recent Michigan marl lakes. **Journal of Sedimentary Research**, v. 48, n. 4, p. 1103–1110, 1978. GeoScienceWorld. Disponível em: <http://pubs.geoscienceworld.org/sepm/jsedres/article-pdf/48/4/1103/2807505/1103.pdf>. Acesso em: 24/6/2022.

JONES, B. Review of calcium carbonate polymorph precipitation in spring systems. **Sedimentary Geology**, v. 353, p. 64–75, 2017. Elsevier B.V. Disponível em: <http://dx.doi.org/10.1016/j.sedgeo.2017.03.006>.

KANO, A.; OKUMURA, T.; TAKASHIMA, C.; SHIRAISHI, F. **Geomicrobiological Properties and Processes of Travertine With a Focus on Japanese Sites**. 2019.

KANO, A.; OKUMURA, T.; TAKASHIMA, C.; SHIRAISHI, F. **Geomicrobiological Properties and Processes of Travertine With a Focus on Japanese Sites**. 2019.

KITANO, Y. Geochemistry of calcareous deposits found in hot springs. **J.Earth Sci., Nagoya Univ.**, v. 11, p. 68–100, 1963. Disponível em: <https://ci.nii.ac.jp/naid/110000016869/>. Acesso em: 24/6/2022.

KOBAN, C. G.; SCHWEIGERT, G. Microbial origin of travertine fabrics-two examples from Southern Germany (Pleistocene stuttgart travertines and miocene riedöschingen Travertine). **Facies**, v. 29, n. 1, p. 251–263, 1993. Springer-Verlag.

KRAEMER, B.; ADELMANN, D.; ALTEN, M.; et al. Incorporation of the Paleogene foreland into the Neogene Puna plateau: The Salar de Antofalla area, NW Argentina. **Journal of South American Earth Sciences**, v. 12, n. 2, p. 157–182, 1999.

LINDGREN, W. Mineral Deposits, McGraw-Hill Book Company. **Inc. New York**, 1933.

MANCINI, A.; CAPEZZUOLI, E.; ERTHAL, M.; SWENNEN, R. Hierarchical approach to define travertine depositional systems: 3D conceptual morphological model and possible applications. **Marine and Petroleum Geology**, v. 103, n. March, p. 549–563, 2019. Elsevier. Disponível em: <https://doi.org/10.1016/j.marpetgeo.2019.02.021>. .

MARO, G.; CAFFE, P. J. Volcanismo monogenético máfico cenozoico de la puna. In: C. M. Muruaga; P. Grosse (Orgs.); **Relatorio del XX Congreso Geologico Argentino**. p.548–577, 2017. San Miguel de Tucumán.

MCKEE, E.; GUTSCHICK, R. History of the Redwall Limestone of northern Arizona. , 1969. Disponível em: <https://pubs.geoscienceworld.org/gsa/books/book/119/chapter/3788672/History-of-the-Redwall-Limestone-of-Northern>. Acesso em: 24/6/2022.

MINISSALE, A.; KERRICK, D. M.; MAGRO, G.; et al. Geochemistry of Quaternary travertines in the region north of Rome (Italy): Structural, hydrologic and paleoclimatic implications. **Earth and Planetary Science Letters**, v. 203, n. 2, p. 709–728, 2002.

MITSUNOBU, S.; HAMANURA, N.; KATAOKA, T.; SHIRAISHI, F. Arsenic attenuation in geothermal streamwater coupled with biogenic arsenic(III) oxidation. **Applied Geochemistry**, v. 35, p. 154–160, 2013. Elsevier Ltd. Disponível em: <http://dx.doi.org/10.1016/j.apgeochem.2013.04.005>. .

MONTERO LÓPEZ, M. C.; HONGN, F.; BROD, J. A.; et al. Magmatismo ácido del mioceno superiorcuaternario en el área de cerro blancola hoyada, Puna austral. **Revista de la Asociacion Geologica Argentina**, v. 67, n. 3, p. 329–348, 2010. Disponível em: <http://www.scielo.org.ar/pdf/raga/v67n3/v67n3a03.pdf>. Acesso em: 24/6/2022.

NICOLLI, H. B.; SURIANO, J. M.; GOMEZ PERAL, M. A.; FERPOZZI, L. H.; BALEANI, O. A. Groundwater contamination with arsenic and other trace elements in an area of the pampa, province of Córdoba, Argentina. **Environmental Geology and Water Sciences**, v. 14, n. 1, p. 3–16, 1989. Disponível em: <https://doi.org/10.1007/BF01740581>. .

OKUMURA, M.; KITANO, Y. Coprecipitation of alkali metal ions with calcium carbonate. **Geochimica et Cosmochimica Acta**, v. 50, n. 1, p. 49–58, 1986. Disponível em: <https://ui.adsabs.harvard.edu/abs/1986GeCoA..50...49O/abstract>. Acesso em: 24/6/2022.

ONCKEN, O.; HINDLE, D.; KLEY, J.; et al. Deformation of the Central Andean Upper Plate System — Facts, Fiction, and Constraints for Plateau Models. **The Andes**, p. 3–27, 2006. Springer, Berlin, Heidelberg. Disponível em: <https://link.spring

PENTECOST, A. **Travertine**. London: Springer International Publishing, 2005.

PENTECOST, A.; VILES, H. A Review and Reassessment of Travertine Classification. **Géographie physique et Quaternaire**, v. 48, n. 3, p. 305–314, 1994.

PENTECOST, A. The origin and development of the travertines and associated thermal waters at Matlock Bath, Derbyshire. **Proceedings of the Geologists' Association**, v. 110, n. 3, p. 217–232, 1999. Disponível em: <https://www.sciencedirect.com/science/article/pii/S0016787899800728>. Acesso em: 24/6/2022.

PENTECOST, A.; VILES, H. A Review and Reassessment of Travertine Classification. **Géographie physique et Quaternaire**, v. 48, n. 3, p. 305–314, 1994.

RAMOS, V. A. Las Provincias Geológicas del Territorio Argentino. **Geología Argentina**, v. 29, n. 24, p. 41–96, 1999.

RAINEY, D. K.; JONES, B. Abiotic versus biotic controls on the development of the Fairmont Hot Springs carbonate deposit, British Columbia, Canada. **Sedimentology**, v. 56, n. 6, p. 1832–1857, 2009.

RIDING, R. **Calcareous Algae and Stromatolites**. Berlin, Heidelberg: Springer Berlin Heidelberg, 1991.

ROGERSON, M.; PEDLEY, H. M.; KELHAM, A.; WADHAWAN, J. D. Linking mineralisation process and sedimentary product in terrestrial carbonates using a solution thermodynamic approach. **Earth Surface Dynamics**, v. 2, n. 1, p. 197–216, 2014. Disponível em: <https://esurf.copernicus.org/articles/2/197/2014/>.

RONCHI, P.; CRUCIANI, F. Continental carbonates as a hydrocarbon reservoir, an analog case study from the travertine of Saturnia, Italy. **AAPG Bulletin**, v. 99, n. 04, p. 711–734, 2015. Disponível em: <http://search.datapages.com/data/doi/10.1306/10021414026>. .

SAONA ACUÑA, L. A.; SORIA, M. N.; VILLAFAÑE, P. G.; STEPANENKO, T.;

FARÍAS, M. E. Arsenic and Its Biological Role: From Early Earth to Current Andean Microbial Ecosystems. **Microbial Ecosystems in Central Andes Extreme Environments**. p.275–284, 2020. Cham: Springer International Publishing. Disponível em: <http://link.springer.com/10.1007/978-3-030-36192-1_19>. Acesso em: 24/6/2022.

SCIRE, A.; BIRYOL, C. B.; ZANDT, G.; BECK, S. Imaging the Nazca slab and surrounding mantle to 700 km depth beneath the central Andes (18°S to 28°S). **Memoir of the Geological Society of America**. v. 212, p.23–41, 2015. Geological Society of America. Disponível em: <https://books.google.com/books?hl=es&lr=&id=RxUJBgAAQBAJ&oi=fnd&pg=PA23&dq=Scire,+A.,+Biryol,+C.+B.,+Zandt,+G.,+%26+Beck,+S.+(2015).+Imaging+the+Nazca+slab+and+surrounding+mantle+to+700+km+depth+beneath+the+central+Andes+(18+S+to+28+S).+Geodynamics+of+a+Cordilleran+Orogenic+System:+The+Central+Andes+of+Argentina+and+Northern+Chile:&ots=nJ0u7jh0Z8&sig=zh4XocAzbyF54HDNN_qvj-q7V1o>. Acesso em: 24/6/2022.

SCHÄFER, A.; STAPF, K. R. G. Permian Saar-Nahe Basin and Recent Lake Constance (Germany): Two Environments of Lacustrine Algal Carbonates. **Modern and Ancient Lake Sediments**. p.83–107, 1978. Wiley. Disponível em: <https://onlinelibrary.wiley.com/doi/10.1002/9781444303698.ch5>. Acesso em: 24/6/2022.

SHIRAISHI, F.; MORIKAWA, A.; KUROSHIMA, K.; et al. Genesis and diagenesis of travertine, Futamata hot spring, Japan. **Sedimentary Geology**, v. 405, p. 105706, 2020. Elsevier B.V. Disponível em: <https://doi.org/10.1016/j.sedgeo.2020.105706>. .

SMEDLEY, P. L.; KINNIBURGH, D. G. A review of the source, behaviour and distribution of arsenic in natural waters. **Applied Geochemistry**, v. 17, n. 5, p. 517–568, 2002. Disponível em: <https://linkinghub.elsevier.com/retrieve/pii/S0883292702000185>. .

SUAREZ-GONZALEZ, P.; BENITO, M. I.; QUIJADA, I. E.; MAS, R.; CAMPOS-SOTO, S. 'Trapping and binding': A review of the factors controlling the development of fossil agglutinated microbialites and their distribution in space and time. **Earth-Science Reviews**, v. 194, p. 182–215, 2019. Disponível em: <https://www.sciencedirect.com/science/article/pii/S0012825218307293?casa_token=-sVsZI5z76kAAAAA:YNIwnEBUa37qkna6fqHlNkE9R7tWLdGYrrAxPsNx_BKG_YkeftiTuA9OEZhJBNc26BbPseDVDYU>. Acesso em: 24/6/2022.

TAKASHIMA, C.; KANO, A. Microbial processes forming daily lamination in a stromatolitic travertine. **Sedimentary Geology**, v. 208, n. 3–4, p. 114–119, 2008. Disponível em: <https://www.sciencedirect.com/science/article/pii/S003707380800122X?casa_token=V9o6zipm6m8AAAAA:q4UBDx13ROwQ-841LB_Fo5vtkpsBdPp2fdhnyvDuezn63OsSWrTcCnpl6wUG5oO2kXxr0pBoQcw>. Acesso em: 24/6/2022.

TAKASHIMA, C.; OKUMURA, T.; HORI, M.; KANO, A. Geochemical characteristics of carbonate hot-springs in Japan. , 2010. Disponível em: <https://catalog.lib.kyushu-u.ac.jp/ja/recordID/17112/?repository=yes>. Acesso em: 24/6/2022.

TEBOUL, P.-A.; DURLET, C.; GAUCHER, E. C.; et al. Origins of elements building travertine and tufa: New perspectives provided by isotopic and geochemical tracers. **Sedimentary Geology**, v. 334, p. 97–114, 2016. Elsevier B.V. Disponível em: <http://dx.doi.org/10.1016/j.sedgeo.2016.01.004>. .

TUCKER, M. E. An introduction to the origin of sedimentary rocks. **Sedimentary Petrology**, p. 260, 2001. Disponível em: <https://books.google.com/books?hl=es&lr=&id=SecSEAAAQBAJ&oi=fnd&pg=PR7&dq=Tucker,+M.+E.+(Ed.).+(2001).+Sedimentary+petrology:+an+introduction+to+the+origin+of+sedimentary+rocks.+John+Wiley+%26+Sons.&ots=Sut0KUWKue&sig=WGfw-pV5Raiz1FA2MvCKCb20vns>. Acesso em: 24/6/2022.

TURI, B. Stable isotope geochemistry of travertines. **The Terrestrial Environment, B**. p.207–238, 1986. Elsevier. Disponível em: <https://pascal-francis.inist.fr/vibad/index.php?action=getRecordDetail&idt=8146504>. Acesso em: 24/6/2022.

UYSAL, I. T.; FENG, Y.; ZHAO, J.; et al. Hydrothermal CO2 degassing in seismically active zones during the late Quaternary. **Chemical Geology**, v. 265, n. 3–4, p. 442–454, 2009. Disponível em: <https://www.sciencedirect.com/science/article/pii/S0009254109002332?casa_token=IiiuFMM2fqwAAAAA:VK3l94LSOwIhS_blwabmEcHVysfZEcOahotNNouaaJS9syMboAzJZSOqk5iJFPmcjoxb6gvow4Y>. Acesso em: 24/6/2022.

VALERO-GARCÉS, B. L.; ARENAS, C.; DELGADO-HUERTAS, A. Depositional environments of Quaternary lacustrine travertines and stromatolites from high-altitude Andean lakes, northwestern Argentina. **Canadian Journal of Earth Sciences**, v. 38, n. 8, p. 1263–1283, 2001. Disponível em: <http://www.nrc.ca/cgi-bin/cisti/journals/rp/rp2_abst_e?cjes_e01-014_38_ns_nf_cjes38-01>. .

VALERO-GARCÉS, B.; DELGADO-HUERTAS, A.; RATTO, N.; NAVAS, A.; EDWARDS, L. Paleohydrology of Andean saline lakes from sedimentological and isotopic records, Northwestern Argentina. **Journal of Paleolimnology**, v. 24, n. 3, p. 343–359, 2000.

VAN EVERDINGEN, R. O.; SHAKUR, M. A.; KROUSE, H. R. Role of corrosion by H2SO4 fallout in cave development in a travertine deposit - Evidence from sulfur and oxygen isotopes. **Chemical Geology**, v. 49, n. 1–3, p. 205–211, 1985. Disponível em: <https://www.sciencedirect.com/science/article/pii/0009254185901561>. Acesso em: 24/6/2022.

VILLAFAÑE, P. G.; LENCINA, A. I.; SORIA, M.; et al. Las Quínoas oncoids: a

new deposit of microbialites in the Salar de Antofalla (Catamarca, Argentina). **Andean Geology**, v. 48, n. 2, p. 281, 2021. Disponível em: <http://www.andeangeology.cl/index.php/revista1/article/view/V48n2-3292>. .

VIRGONE, A.; BROUCKE, O.; HELD, A.-E.; et al. Continental Carbonates Reservoirs: The Importance of Analogues to Understand Presalt Discoveries. All Days. **Anais...** . v. 6, p.4439–4447, 2013. IPTC. Disponível em: <https://onepetro.org/IPTCONF/proceedings/12IPTC/All-12IPTC/Beijing, China/155050>. .

VOSS, R. Cenozoic stratigraphy of the southern Salar de Antofalla region, northwestern Argentina. **Revista geológica de Chile**, v. 29, n. 2, 2002. Disponível em: <https://www.scielo.cl/scielo.php?pid=S0716-02082002000200002&script=sci_arttext&tlng=en>. Acesso em: 24/6/2022.

ZHANG, M.; WANG, H. Organic wastes as carbon sources to promote sulfate reducing bacterial activity for biological remediation of acid mine drainage. **Minerals Engineering**, v. 69, p. 81–90, 2014. Disponível em: <https://www.sciencedirect.com/science/article/pii/S0892687514002404?casa_token=8O2SEIaRbcYAAAAA:u1RgRx25rgmmvkdW7vnu0LzOxrUFKDwsjo-GP8WIMGLZCKs1V9PEL-SDbRI_gDaqvUUwJDlpMwM>. Acesso em: 24/6/2022.

ZHANG, F.; XU, H.; KONISHI, H.; RODEN, E. E. A relationship between d104 value and composition in the calcite-disordered dolomite solid-solution series. **American Mineralogist**, v. 95, n. 11–12, p. 1650–1656, 2010. Disponível em: <https://www.degruyter.com/document/doi/10.2138/am.2010.3414/html>. .